Wedge-Shaped Amphiphilic Sulfonate Molecules: Phase Behavior, Ion Conductivity and Membrane Preparation

Von der Fakultät für Mathematik, Informatik und Naturwissenschaften der RWTH Aachen University zur Erlangung des akademischen Grades eines Doktors der Naturwissenschaften genehmigte Dissertation

vorgelegt von

Master of Science

Heng ZHANG

aus Chongqing, Volksrepublik China

Berichter: Universitätsprofessor Dr. rer. nat. Martin Möller

Universitätsprofessor Dr. rer. nat. Ulrich Simon

Tag der mündlichen Prüfung: 23. Oktober 2013

Die vorliegende Arbeit wurde in der Zeit von 08. 2009 bis 08. 2013 am Lehrstuhl für Makromolekulare Chemie der Rheinisch-Westfälischen Technischen Hochschule Aachen angefertigt. Herr Prof. Dr. Martin Möller danke ich für die Übernahme der wissenschaftlichen Betreuung dieser Promotionsarbeit.

To my parents

Contents

Summary

This dissertation describes the synthesis, phase behavior and ion-conductive properties of various wedge-shaped amphiphilic sulfonate molecules including lithium/sodium/potassium/cesium 2,3,4-tris(11'-acryloyloxyundecyl-1'-oxy)benzene-sulfonates (A-Li, A-Na, A-K and A-Cs), and sodium 4'-[3",4",5"-tris(11'"-methacryloyloxyundecyl-1'"-oxy)benzoyloxy]azobenzene-4-sulfonate (Azo-Na). It is pursued that via supramolecular self-assembly these molecules are able to create ionic channels of different geometry depending on the molecular geometry and environmental conditions. The introduction of polymerizable groups is intended to allow in the second step the covalent incorporation of these channels into a polymer matrix by means of polymerization reaction.

In **Chapter 1**, the structure and properties of a perfluorinated sulfonic acid ionomer membrane: Nafion is described. It is shown that the formation of ionic channel is crucial for the unique conducting properties of this kind of membranes. Supramolecular assembly is then discussed as a way to construct a well-defined channel structure. From the literature review the aims and the research plan of this thesis are deduced. In **Chapter 2**, the synthesis of A-Li, A-Na, A-K and A-Cs is reported. ^{1}H and ^{13}C NMR spectroscopy as well as elemental analysis are employed to characterize these molecules and show their high purity.

In **Chapter 3**, the relation between the structure and conducting properties of A-Na is studied as a function of relative humidity (RH). This compound is able to self-assemble at ambient conditions into a disordered columnar (Col_{hd}) structure with an ionic channel along the axis of the cylinder. Upon increase of RH up to 55%, the columnar structure remains but a minor water uptake and a slight swelling of the cylinders are observed, which results, however, in a significant enhancement of the ion conductivity by 4 orders of magnitude. Further water uptake by increasing

humidity leads to a dramatic change of the mesophase structure whereby bicontinuous cubic phases (Cub_{bi}) are formed. The $Col_{hd} \rightarrow Cub_{bi}$ transition is accompanied by an additional substantial increase of conductivity due to the formation of an interconnected network of ionic channels. The obtained results are discussed in the context of studies of Nafion membranes which are believed to present ionic channel structures. **Chapter 4** reports the study on the orientation of the Col_{hd} phase formed by A-Na. The columns of A-Na are oriented preferentially in plane (homogeneous or planar orientation) on both hydrophilic and hydrophobic substrates. Anodized aluminium oxide (AAO) porous substrate with an average pore diameter of 25 nm is used to achieve a homeotropic orientation of the columnar phase. It is shown by X-ray scattering measurements that the supramolecular columns in the pores of AAO substrate are oriented parallel to the pore wall, i.e. perpendicular to the substrate plane, and this orientation even spreads to the whole sample out of the pores. It is further demonstrated that the oriented sample has a higher conductivity than that of a non-oriented one. In **Chapter 5**, membranes are prepared via photo-polymerization of A-Na under different relative humidity. The phase structure, water uptake, ion conductivity before and after the polymerization are studied. It is found that the polymerization does not change significantly the phase structure of the material at different humidity conditions. Interestingly, in comparison with the monomer sample, the membranes prepared by polymerization at RH=100% condition exhibits a higher ion conductivity, but the membranes polymerized at RH≤55% conditions are much less conductive. This is in good agreement with the results of the water uptake measurements. In **Chapter 6**, the four salts with different counterions, namely A-Li, A-Na, A-K, and A-Cs are studied regarding their phase behavior and ion conductivity. The real-time X-ray measurements are carried out to reveal the detailed phase transitions. A-Li and A-Cs are isotropic at room temperature, meanwhile A-Na and A-K form a disordered hexagonal columnar mesophase. By

cooling, A-Li and A-Cs undergo a transition from isotropic to lamellar phases at -11 ℃ and -7 ℃, respectively. And A-Na and A-K are transformed from the hexagonal columnar to a centered rectangular columnar both at -10 ℃. Models of molecular packing in different mesophases are proposed based on the X-ray data. Furthermore, the conductivity of the sulfonates is determined at room temperature as a function of humidity. It is found that the salts, which form a columnar phase, show much higher water uptake ability, which results also in much higher ion conductivity.

In **Chapter 7**, the synthesis, phase behavior and ion conductivity of a new methacrylated wedge-shaped sulfonate molecule, sodium 4'-[3",4",5"-tris(11'"-meth-acryloylundecyl-1'"-oxy)benzoyl]azobenzene-4-sulfonate (Azo-Na), are described. It is found that Azo-Na forms an orthorhombic crystalline phase at low temperature, and by heating it is transformed into a disordered hexagonal columnar (Col_{hd}) phase. The formation of the Col_{hd} mesophase is also observed by water uptake of Azo-Na at RH=100%. In this case, according to the X-ray scattering data, very thick supramolecular columns with a diameter of 12.5 nm are formed, and the center of the columns is filled with water molecules. According to gravimetry analysis, at RH=100%, Azo-Na uptakes 15.3 water molecules per sulfonate group. At 25 ℃, the dry sample shows a very low conductivity of 7.32×10^{-6} μS/cm, but at RH=100%, the conductivity increases to 102.9 μS/cm.

In **Chapter 8**, two partially deuterated wedge-shaped amphiphilc sulfonate molecules, namely sodium and potassium 2,3,4-tris(n-butyl-d9-octyloxy)benzene-sulfonates, are synthesized. The whole synthesis procedure of these compounds consists of 8 steps. All intermediate and final products are characterized by means of ^{1}H NMR and ^{13}C NMR spectroscopy. These compounds will be studied in future by solid state deuterium NMR to elucidate the packing of alkyl groups in different mesophases.

List of Abbreviations

Materials

Abbreviation	Full Wording
A-Cs	Cesium 2,3,4-tris(11'- acryloyloxyundecyl-1'-oxy)benzenesulfonate
A-K	Potassium 2,3,4-tris(11'- acryloyloxyundecyl-1'-oxy)benzenesulfonate
A-Li	Lithium 2,3,4-tris(11'- acryloyloxyundecyl-1'-oxy)benzenesulfonate
A-Na	Sodium 2,3,4-tris(11'- acryloyloxyundecyl-1'-oxy)benzenesulfonate
A-Na-100	A-Na at RH=100% and room temperature
A-Na-Dry	A-Na in the dry state
AAO	Anodized aluminum oxide
Azo-Na	4'-[3",4",5"-tris(11"'-methacryloyloxyundecyl-1"'-oxy)benzoyloxy]-azo-benzene-4-sulfonate
D-K	Potassium 2,3,4-tris(n-butyl-d9-octyloxy)benzenesulfonate
D-Na	Sodium 2,3,4-tris(n-butyl-d9-octyloxy)benzenesulfonate
DMSO	Dimethyl sulfoxide
DOBOB-CE	3,4,5-tris[4-(11-methacryloyl-undecyl-1-oxy)benzyloxy]-benzoic acid (2), 2 - methyl - (1,4,7,10,13 - penta - oxabenzo - cyclopentadecane) - 3,4,5-tris[4-(11-methacryloyl-undecyl-1-oxy)benzyloxy]benzoate
ITO	Indium tin oxide
PTFE	Polytetrafluoroethene
Poly-A-Na-100	Polymerized A-Na at RH=100% state and room temperature
Poly-A-Na-55	Polymerized A-Na at RH=55% state and room temperature
Poly-A-Na-Dry	Polymerized A-Na at dry state and room temperature

Devices and Institutes

Abbreviation	Full Wording
AFM	Atomic force microscopy
BNL	Brookhaven National Laboratory
CCD	Charge-coupled device
DESY	Deutsches Elektronen-Synchrotron
DSC	Differential scanning calorimetry
ESRF	European Synchrotron Radiation Facility
FTIR	Fourier transform infrared spectroscopy
GISAXS	Grazing incidence small angle X-ray scattering
GIXS	Grazing incidence X-ray scattering
HASYLAB	Hamburger Synchrotronstrahlungslabor
ITME	Institute of Electronic Materials Technology Warszawa. Poland
NMR	Nuclear magnetic resonance
NSLS	National Synchrotron Light Source
POM	Polarizing optical microscopy
SAXS	Small angle X-ray scattering
SEM	Transmission electron microscopy
TEM	Scanning electron microscopy
UV-Vis	Ultraviolet visible
WAXS	Wide angle X-ray scattering

Phase structure

Abbreviation	Full Wording
Col_{cr}	Columnar centered rectangular
Col_{h}	Columnar hexagonal
Col_{hd}	Columnar hexagonal disordered
Cr	Crystalline
Cub_{bi}	Bicontinuous cubic
D	Diamond
G	Gyroid
Iso	Isotropic
Lam	Lamellar

Other general abbreviations

Abbreviation	Full Wording
AC	Alternative circuit
DC	Direct circuit
EW	Equivalent weight
Eq.	Equation
FETs	Field effect transistors
LEDs	Light emitting diodes
PEMFCs	Proton exchange membrane fuel cells
RH	Relative humidity

Chapter 1

Introduction and Objectives of the Thesis

1.1. Nafion Membranes

1.1.1 General information of Nafion membranes

Biological membranes establish the fundamental barrier within or around a cell in organs. They contain highly selective channels or pores consisting of reversibly self-organized aggregates of functional proteins to regulate the permeation of nutrients and osmolytes [1]. A supreme challenge in synthetic materials design lies in mimicking such behavior in order to prepare functional membranes with characteristics of native protein-assisted ion transport. Indeed, highly selective membranes can significantly improve industrial and laboratory praxis because the energy- and labor-intensive purification methods will be replaced in this case by facile isothermal membrane processes [2].

A well-known example of synthetic ion-selective membranes is the perfluorinated sulfonic acid ionomer membranes, e.g. Nafion. Nafion was developed by Walther Grot *et al* in the E.I. DuPont Company in the late 1960s, and has recently drawn great attentions as a proton conductor for proton exchange membrane fuel cells (PEMFCs) because of its unique ionic property, excellent thermal and mechanical stability [3]. Nafion is produced by copolymerization of a perfluorinated vinyl ether comonomer with tetrafluoroethylene, resulting in the chemical structure given below.

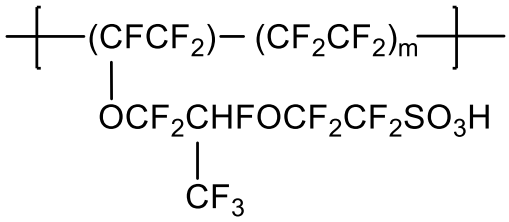

Figure 1. The chemical structure of Nafion.

Due to the insoluble Teflon backbones, Nafion cannot form a true solution. Hence, it is very hard to determine the molecular weight of Nafion using conventional methods such as light scattering and gel permeation chromatography. Although some estimations are made that presume the molecular weight to be the range of 10^5-10^6 Da [3,4].

Instead, the equivalent weight (EW) and membrane thickness are used to describe and distinguish the most commercially available Nafion membranes. An example is Nafion 117, referring to a membrane having 1100 EW and a nominal thickness of 0.007 inch. The EW is the number of grams of dry Nafion per mole of sulfonic acid groups when the material is in the acid form, and it can be determined by acid-base titration, analysis of atomic sulfur, FT-IR spectroscopy, and etc. Another structural value of Nafion is *m*, presenting the number of CF_2 units separating the sulfonic side chains (see Figure 1). The relationship between EW and *m* is:

$$EW = 100 \times m + 446 \qquad \text{Eq. (1)}$$

Thus, for instance, the side chains are separated by around 14 CF_2 units in Nafion 117 membrane [3].

Nafion's unique properties include high conductivity and selectivity of cations [5], good mechanical strength [6,7], good chemical resistance [8-10], board operating temperature range [9,11], and etc. A lot of work has been done and tried to relate the structure and their ionic properties, and these features are believed as a result of incorporating perfluorovinyl ether groups terminated with sulfonate groups onto a Teflon backbone. Since 1980s, there has been a thrust to the structural study of Nafion from the improvement of chlor-alkali cell technology [12]. But up to now, the accurate structure of Nafion is still not well understood. The difficulty stems from inconsistent solubility and crystalline structure among its various derivatives. Little information of Nafion can be provided while using common structural-analysis

approaches including SEM, TEM and AFM. Fortunately, it is found the peak shifts on the X-ray diffractograms while Nafion is being hydrated. Thus the X-ray study and the corresponding simulations dominated the structural study of Nafion.

1.1.2 Structural models of Nafion membranes

In SAXS diffractograms of Nafion, as described in the following models, only one scattering maximum and an upturn at low angles are shown (see Figure 2). Most models are therefore based on the investigation of the position and the shifting of the scattering maximum to integrate the structural scales and changes. This introduction is not meant to list a very large number of publications dealing with Nafion structure models. The focus is on the following selected models, which have addressed the most fundamental aspects of the structure that are relevant to the work of this thesis.

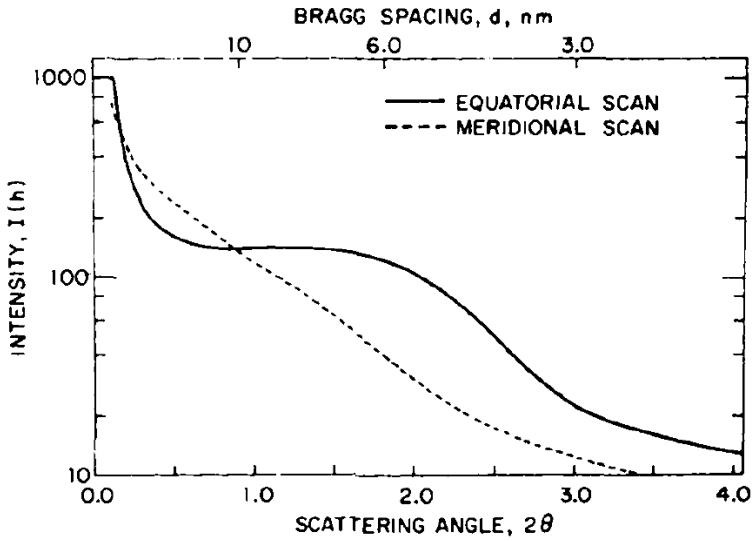

Figure 2. A general SAXS diffractograms of Nafion membranes (EW=1179, in sodium ion form, swollen with water) [13].

1. Three-region model.

Yeager *et al* proposed the existence of three regions in the membrane: (A) the Nafion backbone, (B) an interfacial zone, and (C) the ionic cluster (see Figure 3) [14]. It is necessary to note that the term "ionic clusters" is conventional used in Nafion literatures to describe nano-phase-separated ionic aggregates. The Nafion backbone is the polymer matrix and is not miscible with the sulfonic acid groups (the ionic clusters). Therefore they show phase-separated structures. Yeager *et al* further supposed that the ionic clusters are non-spherical and gives rise to the scattering maximum. In addition, they found the boundaries of the two phases are not sharp, and instead an interfacial zone is expected, where the sulfonic acid groups and polymer matrix mixed together. The evidence is the test of TEM of stained membranes, which shows there is a region surrounding the ionic clusters containing a lower concentration of sulfonic acid groups, and also containing parts of the polymer backbone [15].

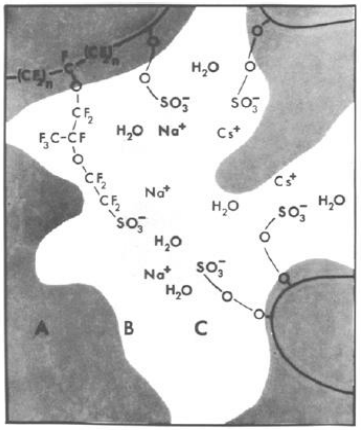

A: Nafion backbones (fluorocarbon)
B: Interfacial zone
C: Ionic clusters

Figure 3. An illustration of three-region model proposed by Yeager *et al* [14].

2. Cluster-Network model.

Apart from Yeager, Gierke *et al* proposed the cluster-network model in 1981 [13] and Hsu *et al* completed it in 1983 [16]. In this model, the water is contained in spherical domains of about 3-5 nm scale and these domains connect with each other to form a network. A unit of the domains is illustrated in Figure 4. Gierke *et al* ascribed the ground for this structure to the preferential energy state of the membrane. As the membrane initially takes up water, cations are dissociated from the hydrated sulfonic groups, and then departed from each other by coulombic repulsions, and hence they push the polymer matrix to deform. In this procedure, there should be a balance between the pushing electrostatic energy and the deformation elastic energy [16,17], resulting in the cluster-network structure. It is calculated that the clusters are connected by short pathways of around 1 nm [18]; and the connections are not permanent but transient stable on the order of ambient thermal fluctuations.

People began to accept this cluster-network model thanks to some following studies by X-ray. For example, Roche *et al* found in SAXS the intensity of the ionomer's peak increases and the maximum shifts to lower angles with the increase of water, indicating the water molecules in the hydrated ionomer are phase separated and the region size increases with the water contents. And the upturn of scattering intensity in low angles suggests the heterogeneous distribution of the clusters, which may due to the allowance of the cluster reorganization during the swelling of the cluster-network unit [19,20].

Though the X-ray studies are in agreement with the cluster-network model, all the agreements are mainly on the ascription of the lower-shifted maximum to the increased cluster size. However, it is not a significant criterion. Some other models could also verify themselves using this criterion. Moreover, since the swelling and de-swelling of Nafion is reversible, but the extent of morphological reorganization

required in the cluster-network model is argued to induce non-recoverable plastic flow [3]. Nevertheless, this cluster-network model is one of the most popular but still challenged by recent studies.

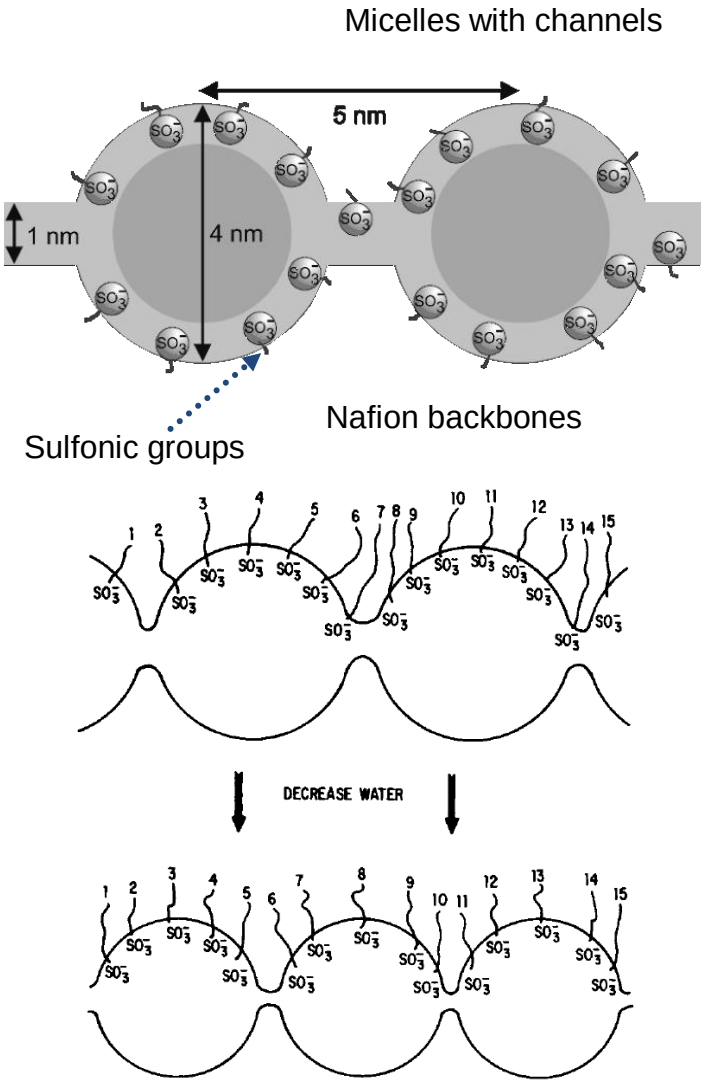

Figure 4. An illustration of cluster-network model proposed by Gierke and Hsu *et al* [13,16]. The size of ion cluster decreases with the decrease of water.

3. Interparticle hard sphere model and intraparticle core-shell model

These two models quite resemble each other. In interparticle hard sphere model, dual phase structures are presented, where the hard spheres of the ionic groups uniformly dispersed in the polymer matrix [21]. While in core-shell model, the hard sphere phase is replaced with the unit of an ion-rich core and an ion-poor shell. (see Figure 5) [22,23]. These hard spheres or the core-shell particles are dispersed in the matrix of the polymer backbone, and the short-range order of the particles gives rise to the scattering maximum.

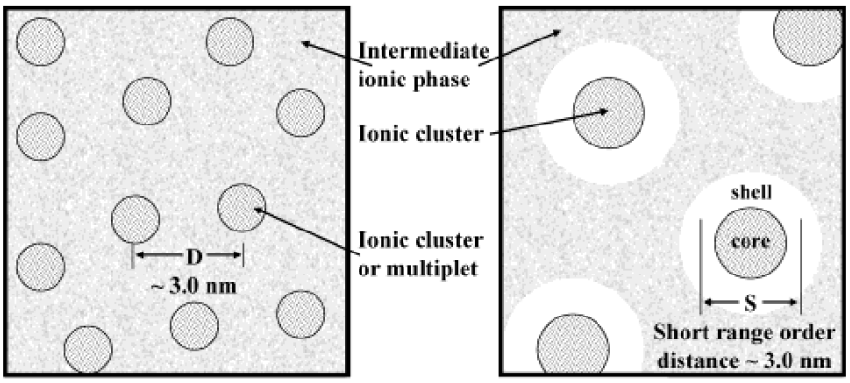

Figure 5. An illustration of interparticle hard sphere model proposed by Cooper *et al* (left), and intraparticle core-shell model proposed by MacKnight *et al* (right) [3].

Fujimura *et al* studied the X-ray of Nafion at dry state and found the existence of the ionic clusters even without being hydrated [24]. This is not in agreement with cluster-network model but supports these two models. Fujimura *et al* also found the swelling degree in microscopic scale is much greater than that of macroscopic scale. Thus they concluded the scattering behavior is better described by the core-shell model, where the "shell" region stores water molecules and swells the material mainly in microscopic scale [24,25].

But these models are argued over the years. The focus is the key assumptions that the distribution is uniform and no redistribution of the clusters can be occurred during swelling. This is not in agreement with the X-ray results by Roche *et al* that suggest the heterogeneous distribution of the clusters [20]. Some modifications are brought up by researchers, like Miura and Yoshida [26], who suggest some degree of ionic redistribution during swelling is possible due to the internal stress in the ionic clusters. Another argument is the variation of *d* spacing over the water absorption, which is discussed in detail in the following lamellar model.

4. Lamellar model and "sandwich-like" model

Since Gierke's cluster-network model is argued to explain the reversible swelling behavior of Nafion, a lamellar model is proposed up to explain Nafion's swelling and de-swelling process. In lamellar model, the ionic domains are defined as hydrophilic-micelle-layers separated by thin lamellar polymer crystallites. The distance between the polymer lamella gives rise to the scattering maximum [27]. And other aspects like crystalline and inter-lamellar interactions are all ignored in the modeling, which entitles the lamellar model as probably the simplest structural model of Nafion in the conventional literatures [3]. While Nafion is taking up water, water molecules gather between the polymer lamella and separate them to trigger the scattering maximum shift to lower angles.

The evidence of the lamellar model is the dependence of *d* spacing on the water volume fraction [27]. As water is being absorbed, the evolution of the *d* spacing is almost linear with water volume fraction, this is opposed to the sphere-based models that expect the 1/3 power dependence [27]. But, it is in accordance with the expectation of the lamellar model. Though it is agreed with the intra-lamellar spacing, the arguments come from the inter-lamellar spacing, which has a larger linear

expansion range and shifts with water content in a significant different manner from this lamellar model [28,32]. The reason is of course the over-simplification which ignores the long-term interactions.

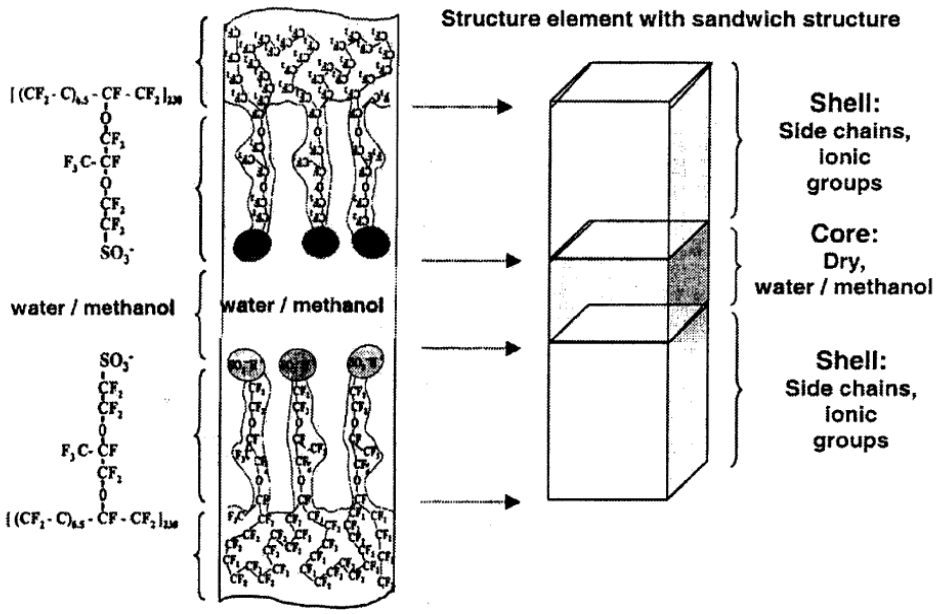

Figure 6. An illustration of sandwich-like model proposed by Haubold *et al* [29].

To overcome this problem, a variation of lamellar model was proposed up by Haubold *et al* in 2001 [29]. The basic structural unit of this model is a "sandwich", which is shown in Figure 6. Though this sandwich-like model present a layer-by-layer structure, it may resemble the concepts of the core-shell model, where the outer portion of this sandwich (the "shell") consists of the side chains, and the inner liquid portion (the "core") consists of the water (or methanol) molecules. To provide channels as conduction pathways through the membrane, these structural elements are

proposed to be juxtaposed in a linear fashion so that the liquid core regions are contiguous [29]. Haubold *et al* used this model to explain the behaviors of the dry Nafion membranes, and membranes equilibrated with a range of water/methanol solutions. Results show the usual ionomer peak at d = 4 nm, and the lateral dimensions of the sandwich a and b between 1.5 and 4.5 nm [29].

Although this model is in good harmony with the SAXS results, it does not offer a complete, unambiguous 3-D pattern of hydrophobic / hydrophilic organization, nor the existence of the crystalline regions which is known in Nafion membranes.

5. Parallel water cylinder model, structural-inversion network model and percolation network model

Based on modeling the SAXS patterns of hydrated Nafion membranes, Schmidt-Rohr *et al* proposed a more complicated structural model consisted of arrays of parallel ionic nano-cylinders which are embedded in a locally aligned polymer matrix [30]. A schematic illustration of this model is given in Figure 7.

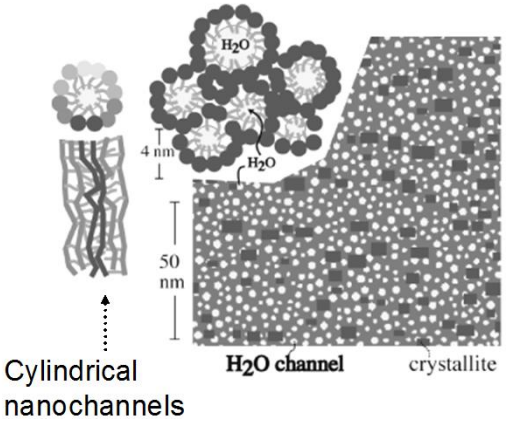

Figure 7. An illustration of parallel water cylinder model proposed by Schmidt-Rohr *et al* [30].

In detail, the hydrophilic sulfuric groups of Nafion stack inside the cylinders to yield an ionic channel. During the hydration, the channels are swollen by taking up water. Schimdt-Rohr *et al* attributed the diameter of the channels to the scattering maximum. While taking up water, the diameter increases with water uptakes, which give rise to the shift of scattering maximum.

This modeling-based structure fits well with the SAXS patterns at different hydration degree. But still some researchers argue that if large amount of water can be absorbed into the hydrophilic channels which are only within 3-5 nm and stacked inside the big hydrophobic Teflon-like matrix.

Based on this question, Gebel *et al* proposed that maybe the phase structures can be reversed by taking large amount of water, thus the hydrophilic groups align on the surface of hydrophobic Teflon-like rods [31]. It gives more space for water and also fits well with the SAXS patterns. Further, Gebel *et al* summarized the conventional structural models and their evidences; they proposed a structural phase-inversion network model [32]. As shown in Figure 8a, the hydration is accompanied by phase transitions from isolated cubic phase to a connected network of polymer rods. Figure 8 illustrates the schematic phase transitions.

Weber *et al* holds a similar opinion that the structure changes during the hydration of Nafion. Based on this, Weber *et al* proposed the percolation network model which is very similar to the structural-inversion network model [33]. As presented in Figure 8b, the evolution of phase rises from the isolated cubic domains at dry state, and stops at the percolated network upon water uptake reaches 22. Unlike the structural-inversion network model, the percolated network model does not go further to the “phase inversion” state.

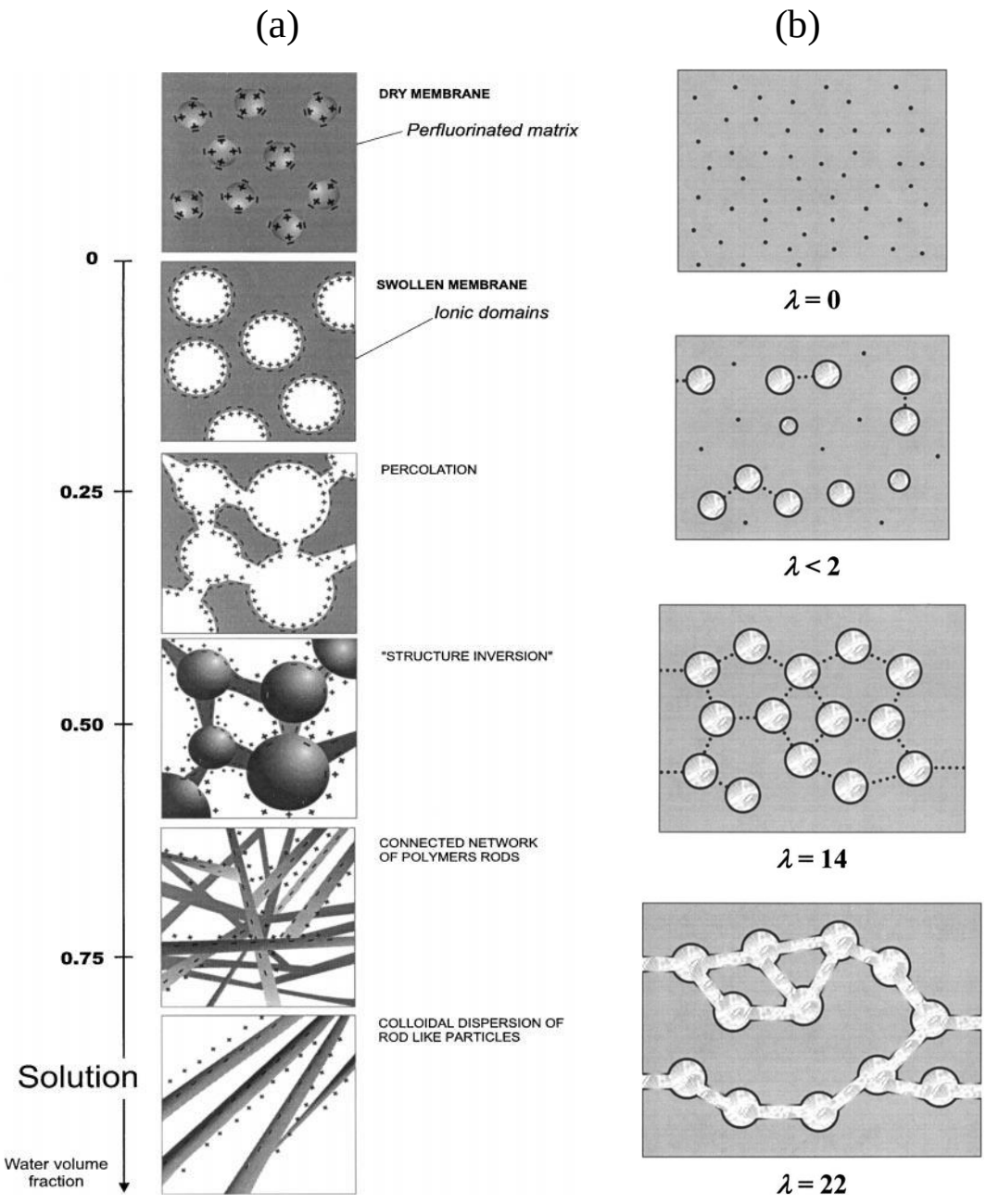

Figure 8. (a) An illustration of the structural-inversion network model proposed by Gebel *et al* [32]. (b) An illustration of the percolation network model proposed by Weber *et al* [33].

Many more models, such as bimodal network model [34], and etc. can be found in literature. All the models of Nafion proposed so far imply a microphase separation, and can provide explanation for certain experimental results. However, none of these models can deliver an accurate view of the Nafion's structure, since none of them can explain all the SAXS features and the unique ion conductive and selective properties of Nafion.

1.1.3 Ion conductivity of Nafion membranes

In the application of Nafion membranes, the ion conductivity plays a significant role since it determines to a large extent the performances of the membranes [35,36].

In conventional determinations of Nafion's ion conductivity, the approach of alternative circuit (AC) impendence spectroscopy is dominantly applied [37-43]; although sometimes the direct circuit (DC) method is also adopted [44,45]. The measurements are carried out by varying external conditions including water activity, water immersion, acid concentration, temperature, and etc. Such various factors result in a wide range of Nafion's ion conductivity in literature, some of which are summarized in Table 1.

Table 1. A summary of proton conductivity of Nafion of 1100EW series [35].

Nafion	Condition	Method Thickness (μm)	Ion conductivity (S/cm)	Ref.
117	RH 100%, 25 ℃	AC, 175	0.070	[37]
117	RH 100%, 30 ℃	AC, 175	0.060	[38-39]
112	RH 100%, 65 ℃	AC, 52	0.144	[41]
117	RH 100%, 65 ℃	AC, 210	0.140	[41]
117	Immerse in water, 30 ℃	AC, 175	0.100	[38-40]
117	Immerse in water, 90 ℃	AC, 175	0.190	[38-40]
117	Immersed in 1M H_2SO_4, 25 ℃	AC, 175	0.076	[42,43]
117	Immersed in 1 M H_2SO_4, 20 ℃	DC, 231	0.088	[44,45]
117	Immersed in 1 M H_2SO_4, 80 ℃	DC, 231	0.231	[44,45]

Furthermore, the thickness of the membrane affects the ion conductivity as well. Figure 9 presents the dependence of ion conductivity on membrane thickness of Nafion. It is found that such dependence originates from the different water uptake (the ratio of the count of water molecules over a single sulfonate group) for different thickness of the membrane [36].

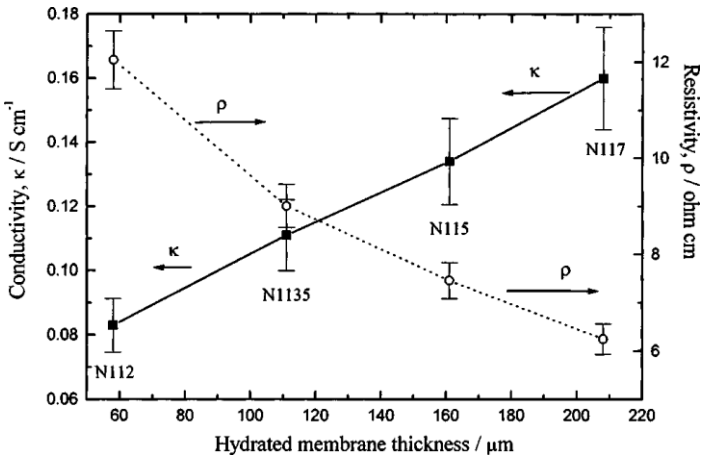

Nafion membrane (Extruded)	EW	λ (H_2O at 25°C)	λ (H_2SO_4 at 25°C)	λ (H_2O at 80°C; hot-pressed)
117	1075	23.2 ± 0.4	19.1 ± 0.6	16.3 ± 0.5
115	1010	21.9 ± 0.6	18.8 ± 0.3	15.8 ± 0.4
1135	1020	21.1 ± 0.6	18.3 ± 0.4	14.9 ± 0.4
112	1020	20.7 ± 0.5	15.5 ± 0.1	14.1 ± 0.5

Figure 9. The variation in the conductivity, resistivity and water uptake of the Nafion 1100 EW membranes in 1 M H_2SO_4 at 25 ℃ [5,36].

The comparison of ion conductive properties between Nafion and other sulfonated polymers that are believed to have no strong microphase-separated structure plays an important role in the study of their structural models [38,46,47]. Figure 10 presents an example of the conductivity comparison between Nafion and

sulfonated polyetheretherketone (SPEEK) [46]. It can be seen that Nafion exhibits a much higher ion conductivity especially at moderate water activity (a_w that equals the equilibrium relative humidity).

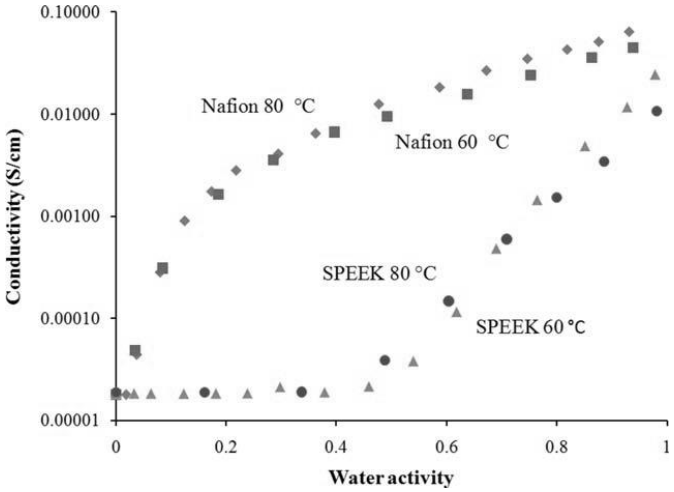

Figure 10. The comparison of Nafion and SPEEK on the dependence of ion conductivity on water activity [46].

From the analysis of Nafion membranes in both structure and ion conductivity, it becomes clear that the outstanding ion conductive properties of Nafion are closely related to its unique microphase-separated structure, i.e. the formation of ionic channels. The geometry of the channels is the focus of debate in the structural models. In this work, supramolecular self-organization is applied as the tool to construct ionic channels, and the influence of the channel structure on the conductive properties is the focus of this study.

1.2. Self-Assembly of Wedge-Shaped Amphiphilic Molecules

Supramolecular assembly of low molecular weight compounds is known to generate a large diversity of nanostructures [48]. The design of such molecules is abundant in the rapid development of material science as one of the most prospective fields for both fundamental and applied researches [49-54].

Of great interest recently are wedge-shaped amphiphilic molecules bearing a small polar group at the tip of the wedge and a large hydrophobic rim [55-61]. Depending on the hydrophilic/hydrophobic ratio of the molecules, they are able to form various supramolecular structures including spheres, cylinders and lamellae, which in turn are stacked to form cubic, columnar and lamellar mesophases, respectively. Figure 11 illustrates the geometry of the wedge-shaped amphiphilics and the schematic formations of the mesostructures.

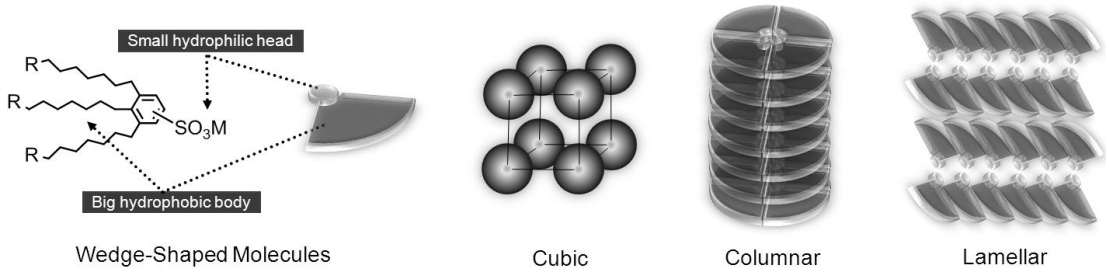

Figure 11. The geometry of the wedge-shaped amphiphilics and the schematic formations of the lamellar, cubic, and columnar mesostructures.

A well-defined ionic channel structure can be constructed by these wedge-shaped amphiphilic molecules. The general strategy is the introduction of an ionic or ion-acceptor group to the tip of the wedge. By self-assembly e.g. into a cylindrical

structure, the ionic or ion-acceptor groups are stacked along the axis of the cylinder, forming an ionic channel. These molecules are also modified with polymerizable groups on the periphery in order to embed the ionic channels in polymer membranes by polymerization.

Examples of the wedge-shaped supramolecular molecules include three-tailed acrylate and diene derivatives of gallic acid salts [62,63] with the chemical structure shown in Figure 12. D Gin *et al* demonstrates that the cross-linked films by photo-polymerization of such compounds present hexagonally packed, monodisperse channels that are typically ca. 1.5 nm in diameter with an interchannel spacing of ca. 4 nm [64,65]. As can be seen from Figure 12, the light circles in the TEM image are the cross sections of the cylindrical channels. [65].

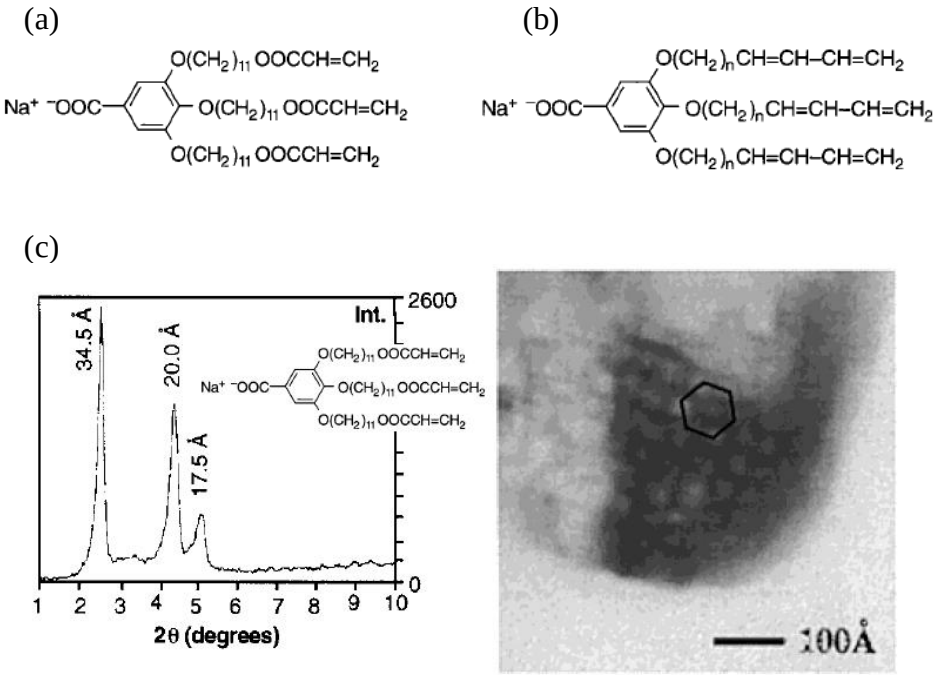

Figure 12. (a) (b) The chemical structures of polymerizable wedge-shaped amphiphilic compounds used by D. Gin *et al.* [62,63]. (c) The X-ray profile and TEM image of the cross-linked film of the compound A containing 5 wt % of H_2O [65].

Such cylindrical channels of well-defined geometry can be applied as effective pathways for an effective transportation of ions [66-69], electrons [68-70] and molecules [71]. Further, due to the flexibility of the long alkyl chains on the rim of wedge-shaped molecules, the cylindrical-channel domains in the mesostructures are able to be oriented in external fields. After the orientation of channels, much high conductivity along the orientation direction can be expected.

Recently, H Shimura *et al* introduces a 1D lithium ion-conductor prepared by complexation of a liquid-crystalline propylene carbonate derivative and a lithium salt (Figure 13) [72] to form a hexagonal columnar (Col_h) structure. These columnar assemblies are macroscopically aligned by applying AC electric fields to form homeotropic structures. Under an external electric field (2.5 V/μm, 1 KHz), the birefringence between polarizers fades away in 90 minutes and the ion conductivity increases up to ca. 4 times that before electric field is applied.

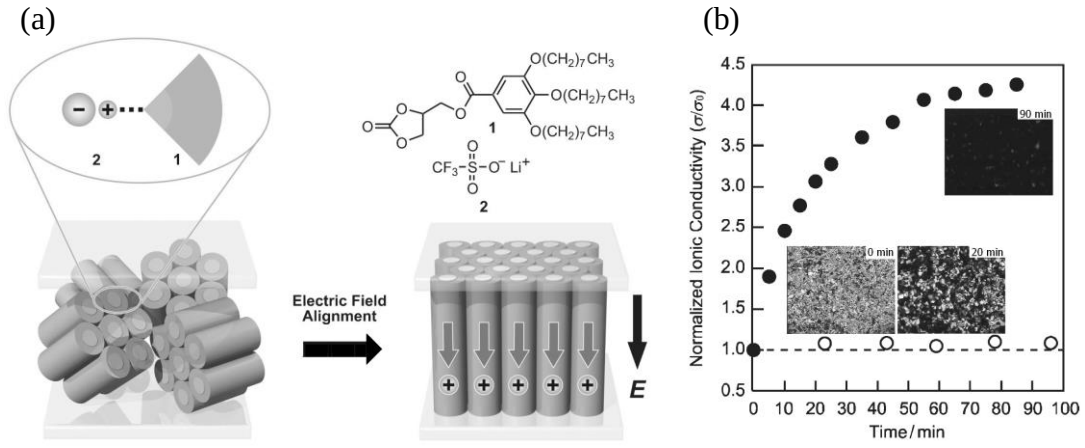

Figure 13. (a) Molecular structures of compound 1 and 2, and schematic illustration of the alignment of the columnar phase by electric fields [72]. (b) Time variation of normalized ionic conductivity for the complex of 1 and 2 (the molar ratio is 10: 1) at 22 ℃ (filled circles) with an electric field (2.5 V/mm 1.1 kHz) (open circles) without an electric field [72].

Other than the low-dimensional transportation applications, the nanostructured LC assemblies exhibiting bicontinuous cubic (Cub_{bi}) phases are emerging as a new generation because of their three-dimensional (3D) interconnected network structures. In particular, the Cub_{bi} phases can be formed either thermotropically [73-77] or lyotropically [62,78] and these assemblies have been used for lithium ion conductor [73], ion-diffusion systems [74], and toxicity-protection systems [78]. The biggest advantage of the 3D generation is that the channels in the interconnected network are able to construct the effective pathways for transportation without the orientation of liquid crystal domains.

T Ichikawa *et al* introduces a series of wedge-shaped amphiphilic molecules (Figure 14) that exhibit thermotropic Cub_{bi} mesophases [75-77]. An example is given in Figure 15 [77], the mesophase evolution from Cub_{bi} to Col_h and then to isotropic state is observed upon heating. Further, these structures can be successfully preserved by in-situ photo-polymerization through UV irradiation to form nanostructured free-standing films. It is found that 3D interconnected ionic channels derived from the Cub_{bi} phases (Film-B) function as efficient ion-conductive pathways and bring up the ion conductivity to ca. 4 times higher than that of the film in the Col_h (Film-C) phase and ca. 36 times higher than that of film in the isotropic state (Film-I) [77].

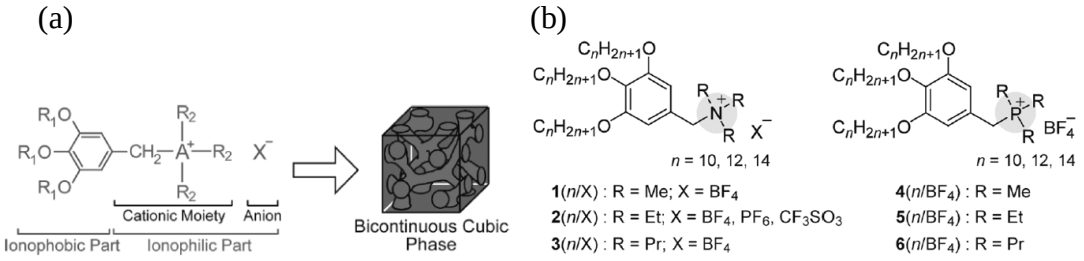

Figure 14. (a) Molecular design for the thermotropic LC materials forming bicontinuous cubic phases [76]. (b) Molecular structures of wedge-shaped ammonium salts 1-3(n/X) and phosphonium salts 4-6(n/BF4) [76].

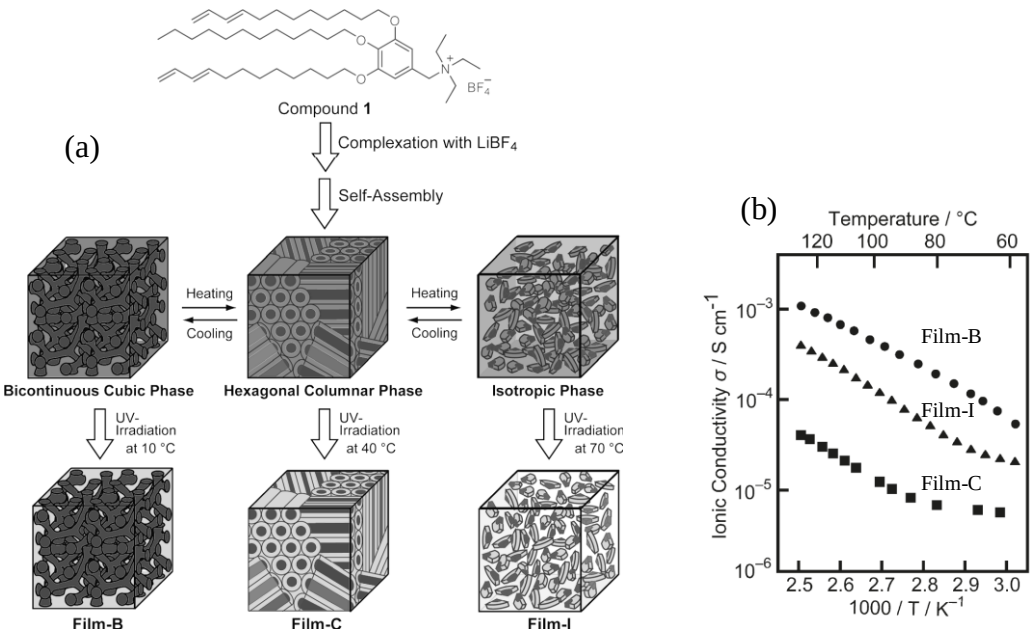

Figure 15. (a) Schematic illustration of the preparation of Film-B (*Cub*$_{bi}$), Film-C (*Col*$_h$) and Film-I (Isotropic) by the complexation of compound 1 and LiBF4 and subsequent polymerization [77]. (b) The dependences of ion conductivity on temperature of Film-B (circles), Film-I (triangles), and Film-C (squares) [77].

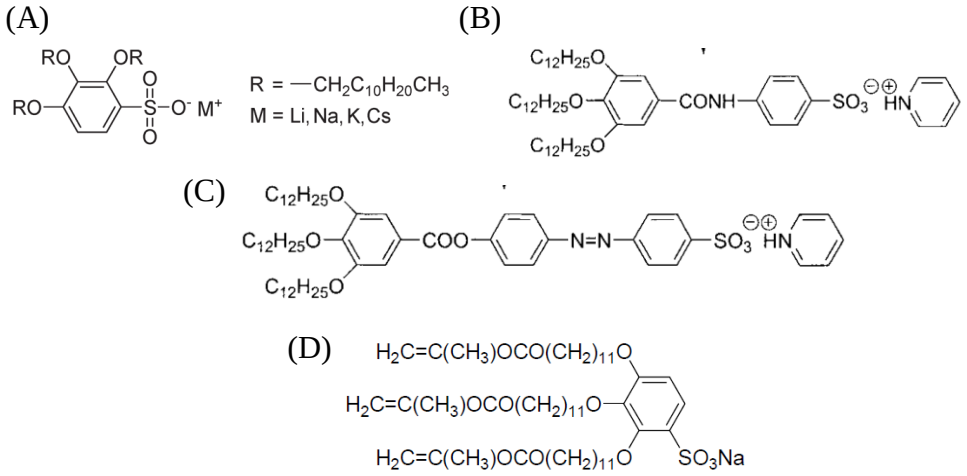

Figure 16. The wedge-shaped compounds developed in our group, which can form lamellar, cubic, and *Col*$_{hd}$ phases by self-assembly [79-87].

For years our group has carried out a systematical study on wedge-shaped amphiphilic sulfonate molecules [79-87]. The typical compounds are listed in Figure 16.

For the series of compound ***A*** in Figure 16 with different counter ions, it is found that with smaller counter ions like Li^+ and Na^+, the compounds form cubic phases. While with bigger counter ions like K^+ and Cs^+, they tend to form Col_{hd} phases. It is deduced that the phase occurrence is more ruled by the geometric shape than the ionic interactions between the cation and sulfonate anion. Table 2 summarizes the transition temperature of these compounds [85].

Table 2. Phase sequence of compound ***A*** (Figure 16) [85].

Compound ***A***, M=	Phase sequence
Li	*Cr*, -11 ℃ → *Cub*, 161 ℃ → *Iso*
Na	*Cr*, -3 ℃ → *Cub*, 103 ℃ → *Iso*
K	*Cr*, 18 ℃ → *M1* 47 ℃ → *M2*, 124 ℃ → Col_{hd}, 171 ℃ → *Iso*
Cs	*Cr*, 50 ℃ → Col_{hd}, 193 ℃ → *Iso*

Cr, crystalline phase. ***Cub***, cubic mesophase. $\boldsymbol{Col_{hd}}$, columnar hexagonal disordered mesophase. ***M***, mesophase type not determined. ***Iso***, isotropic liquid.

Wedge-shaped amphiphilic sulfonates with more complexed chemical structures (compounds ***B*** and ***C***) are synthesized as well [86]. They are also capable of forming columnar structures. It should be noted for compound ***C*** it is possible to manipulate the structure by photo-isomerization due to the presence of azo-fragment in the molecule. However, this has not been studied yet.

Further, in order to allow cross-linking of the supramolecular columns with polymer matrices, wedge-shaped sulfonate molecules containing olefinic groups on the periphery of the molecular wedges (compounds ***D***) are synthesized. Compound ***D*** forms the Col_{hd} mesophase at ambient temperature. Polymerization of thin films of this compound in the mesophase yields free-standing, solid but flexible membranes containing the defined sulfonate stacks in a permanently arrested state [87]. However, the detailed structure analysis and the ion conductivity measurements have not been performed.

1.3. The Objective of this Thesis

The objective of this thesis is to develop a novel type of ion-conductive membranes containing supramolecular self-organized ionic channels that may resemble the structure and properties of Nafion membranes. For this purpose, it is pursued that the supramolecular self-assembly of wedge-shaped amphiphilic sulfonate molecules is able to create ionic channels of different geometry. The introduction of polymerizable groups is intended to allow in the second step the covalent incorporation of these channels into a polymer matrix by means of polymerization reaction.

Two kinds of wedge-shaped amphiphilic sulfonates of different chemical structures, namely lithium / sodium / potassium / cesium 2,3,4-tris(11'-acryloyloxyundecyl-1'-oxy)benzenesulfonates (A-Li, A-Na, A-K and A-Cs), and sodium 4'-[3",4",5"-tris(11'"-methacryloyloxyundecyl-1'"-oxy)benzoyloxy]-azo-benzene-4-sulfonate (Azo-Na) (Figure 18) are synthesized in the framework of this thesis. We focus on the investigation on the influence of humidity on both the conducting properties and the mesostructures of the ionic liquid crystals. The polymerization is carried out under different humidity in order to arrest the mesostructures in the polymer membranes.

In addition, wedge-shaped sulfonates with deuterated alkly tails are synthesized with the aim to investigate the alkyl packing in different mesostructures formed by these molecules.

1.4. The Outline of this Thesis

This thesis contains 8 chapters.

Chapter 1 provides a literature review on the structure and properties of Nafion membranes and the self-assembly of wedge-shaped amphiphilic molecules. **Chapter 2** describes the synthesis and characterization of lithium / sodium / potassium / cesium 2,3,4-tris(11'-acryloylundecyl-1'-oxy)benzenesulfonates (A-Li, A-Na, A-K and A-Cs). In **Chapter 3,** the dependence of mesostructures and ion conductivity on the relative humidity of A-Na is studied. In **Chapter 4**, the homeotropic alignments of A-Na salt is successfully achieved by using porous anodized aluminum oxide templates as substrates, and the influence of the homeotropic structure on ion conductivity is addressed as well. In **Chapter 5**, the photo-polymerization of the A-Na is carried out and the phase structures and ion conductivity before and after the polymerization are investigated. Further, in **Chapter 6** the phase structures of A-Li, A-Na, A-K and A-Cs are investigated by means of small-angle X-ray scattering (SAXS), and the ion conductivity of the four salts in different relative humidity conditions and the relations between mesophases and ion conductivity is studied.

In **Chapter 7**, another example of wedge-shaped sulfonate molecule: sodium 4'- [3", 4", 5"- tris (11'"- methacryloylundecyl- 1'"- oxy) benzoyloxy] azobenzene- 4-sulfonate (Azo-Na) is prepared. The phase transitions upon temperature and humidity and the dependence of ion conductivity on relative humidity are studied.

In **Chapter 8**, the synthesis of two partially deuterated wedge-shaped amphiphilic sulfonate molecules: sodium and potassium 2,3,4-tris(n-butyl-d9-octyl-oxy)benzenesulfate is reported. These compounds will be studied in future by means of solid state ^{2}H NMR spectroscopy regarding the packing of alkyl chains in different meosphases.

1.5. References

[1] Alberts, B; Johnson, A; Walter, P; Lewis, J; Raff, M; Roberts, K. Molecular Biology of the Cell 5th Ed., Garland Science, New York, **2008**.

[2] Peinemann, KV; Nunes, SP. Membrane Technology in the Chemical Industry, Wiley-VCH, **2006**.

[3] Mauritz, KA; Moore, RB. State of understanding of Nafion, *Chem. Rev.*, **2004**, *104* (10), 4535-4585.

[4] Curtin, DE; Lousenberg, RD; Henry, TJ; Tangeman, PC; Tisack, ME. Advanced materials for improved PEMFC performance and life, *J. Power Sources*, **2004**, *131* (1-2), 41-48.

[5] Wang, HS; Li, TH; Jia, WL; Xu, HY. Highly selective and sensitive determination of dopamine using a Nafion/carbon nanotubes coated poly(3-methylthiophene) modified electrode, *Biosens. Bioelectron.*, **2006**, *22* (5), 664-669.

[6] Iwai, Y; Hiroki, A; Tamada, M; Yamanishi, T. Radiation deterioration in mechanical properties and ion exchange capacity of Nafion n117 swelling in water, *J. Membr. Sci.*, **2008**, *322* (1), 249-255.

[7] Majsztrik, PW; Bocarsly, AB; Benziger, JB. Viscoelastic response of Nafion. Effects of temperature and hydration on tensile creep, *Macromolecules*, **2008**, *41* (24), 9849-9862.

[8] Alentiev, A; Kostina, J; Bondarenko, G. *Chemical aging of Nafion: FTIR study*, Conference of the European Membrane Society, Giardini Naxos, ITALY, 2006.

[9] Casciola, M; Alberti, G; Sganappa, M; Narducci, R. *Factors affecting the stability of Nafion conductivity at high temperature and relative humidity*, Conference of the European Membrane Society, Giardini Naxos, ITALY, 2006.

[10] Lee, HJ; Nam, EJ; Woo, JJ; Moon, SH; Lee, J. Improved dimensional stability of Nafion membrane modified using a layer by layer self-assembly of biophilic polymers, *Curr. Appl Phys.*, **2012**, *12* (5), 1235-1238.

[11] Thompson, EL; Capehart, TW; Fuller, TJ; Jorne, J. Investigation of low-temperature proton transport in Nafion using direct current conductivity and differential scanning calorimetry, *J. Electrochem. Soc.*, **2006**, *153* (12), A2351-A2362.

[12] Hora, CJ; Maloney, DE. Chemically modified Nafion perfluorosulfonic acid membranes as separators in chlor-alkali cells, *J. Electrochem. Soc.***,** *124* (8), C319-C319.

[13] Gierke, TD; Munn, GE; Wilson, FC. The morphology in Nafion perfluorinated membrane products, as determined by wide-angle and small-angle X-ray studies, *J. Polym. Sci., Part B: Polym. Phys.*, **1981**, *19* (11), 1687-1704.

[14] Yeager, HL; Steck, A. Cation and water diffusion in Nafion ion-exchange membranes - Influence of polymer structure, *J. Electrochem. Soc.*, **1981**, *128* (9), 1880-1884.

[15] Xue, T; Trent, JS; Osseoasare, K. Characterization of Nafion membranes by transmission electron-microscopy, *J. Membr. Sci.*, **1989**, *45* (3), 261-271.

[16] Hsu, WY; Gierke, TD. Ion-transport and clustering in Nafion perfluorinated membranes, *J. Membr. Sci.*, **1983**, *13* (3), 307-326.

[17] Mauritz, KA; Rogers, CE. A water sorption isotherm model for ionomer membranes with cluster morphologies, *Macromolecules*, **1985**, *18* (3), 483-491.

[18] Xie, G; Okada, T. Characteristics of water transport in relation to microscopic structure in Nafion membranes, *J. Chem. Soc., Faraday Trans.*, **1996**, *92* (4), 663-669.

[19] Roche, EJ; Pineri, M; Duplessix, R; Levelut, AM. Small-angle scattering studies of Nafion membranes, *J. Polym. Sci., Part B: Polym. Phys.*, **1981**, *19* (1), 1-11.

[20] Roche, EJ; Pineri, M; Duplessix, R. Phase-separation in perfluorosulfonate ionomer membranes, *J. Polym. Sci., Part B: Polym. Phys.*, **1982**, *20* (1), 107-116.

[21] Marx, CL; Caulfield, DF; Cooper, SL. Morphology of ionomers, *Macromolecules*, **1973**, *6* (3), 344-353.

[22] Macknight, WJ; Taggart, WP; Stein, RS. Model for structure of ionomers, *J. Polym. Sci. Polym. Symp.***,** *45*, 113-128.

[23] Roche, EJ; Stein, RS; Russell, TP; Macknight, WJ. Small-angle X-ray-scattering study of ionomer deformation, *J. Polym. Sci., Part B: Polym. Phys.*, **1980**, *18* (7), 1497-1512.

[24] Fujimura, M; Hashimoto, T; Kawai, H. Small-angle X-ray-scattering study of perfluorinated ionomer membranes .1. Origin of 2 scattering maxima, *Macromolecules*, **1981**, *14* (5), 1309-1315.

[25] Fujimura, M; Hashimoto, T; Kawai, H. Small-angle X-ray-scattering study of perfluorinated ionomer membranes .2. Models for ionic scattering maximum, *Macromolecules*, **1982**, *15* (1), 136-144.

[26] Miura, Y; Yoshida, H. Effects of water and alcohols on molecular-motion of perfluorinated ionomer membranes, *Thermochim. Acta*, **1990**, *163*, 161-168.

[27] Litt, M. A reevaluation of Nafion morphology, *Polym. Prepr.*, **1997**, *213*, 33-33.

[28] Young, SK; Trevino, SF; Tan, NCB. Small-angle neutron scattering investigation of structural changes in Nafion membranes induced by swelling with various solvents, *J. Polym. Sci., Part B: Polym. Phys.*, **2002**, *40* (4), 387-400.

[29] Haubold, HG; Vad, T; Jungbluth, H; Hiller, P. Nano structure of Nafion: A SAXS study, *Electrochim. Acta*, **2001**, *46* (10-11), 1559-1563.

[30] Schmidt-Rohr, K; Chen, Q. Parallel cylindrical water nanochannels in Nafion fuel-cell membranes, *Nat. Mater.*, **2008**, *7* (1), 75-83.

[31] Aldebert, P; Dreyfus, B; Gebel, G; Nakamura, N; Pineri, M; Volino, F. Rod like micellar structures in perfluorinated ionomer solutions, *J. Phys.*, **1988**, *49* (12), 2101-2109.

[32] Gebel, G. Structural evolution of water swollen perfluorosulfonated ionomers from dry membrane to solution, *Polymer*, **2000**, *41* (15), 5829-5838.

[33] Weber, AZ; Newman, J. Transport in polymer-electrolyte membranes - I. Physical model, *J. Electrochem. Soc.*, **2003**, *150* (7), A1008-A1015.

[34] Hwang, GS; Kaviany, M; Gostick, JT; Kientiz, B; Weber, AZ; Kim, MH. Role of water states on water uptake and proton transport in Nafion using molecular simulations and bimodal network, *Polymer*, **2011**, *52* (12), 2584-2593.

[35] Ralph, TR; Hards, GA; Keating, JE; Campbell, SA; Wilkinson, DP; Davis, M; Stpierre, J; Johnson, MC. Low cost electrodes for proton exchange membrane fuel cells - Performance in single cells and ballard stacks, *J. Electrochem. Soc.*, **1997**, *144* (11), 3845-3857.

[36] Slade, S; Campbell, SA; Ralph, TR; Walsh, FC. Ionic conductivity of an extruded Nafion 1100 EW series of membranes, *J. Electrochem. Soc.*, **2002**, *149* (12), A1556-A1564.

[37] Rieke, PC; Vanderborgh, NE. Temperature-dependence of water-content and proton conductivity in polyperfluorosulfonic acid membranes, *J. Membr. Sci.*, **1987**, *32* (2-3), 313-328.

[38] Zawodzinski, TA; Springer, TE; Davey, J; Jestel, R; Lopez, C; Valerio, J; Gottesfeld, S. A comparative-study of water-uptake by and transport through ionomeric fuel-cell membranes, *J. Electrochem. Soc.*, **1993**, *140* (7), 1981-1985.

[39] Zawodzinski, TA; Derouin, C; Radzinski, S; Sherman, RJ; Smith, VT; Springer, TE; Gottesfeld, S. Water-uptake by and transport through Nafion(r) 117 membranes, *J. Electrochem. Soc.*, **1993**, *140* (4), 1041-1047.

[40] Zawodzinski, TA; Springer, TE; Uribe, F; Gottesfeld, S. Characterization of polymer electrolytes for fuel-cell applications, *Solid State Ionics*, **1993**, *60* (1-3), 199-211.

[41] Nouel, KM; Fedkiw, PS. Nafion (R)-based composite polymer electrolyte membranes, *Electrochim. Acta*, **1998**, *43* (16-17), 2381-2387.

[42] Yoshitake, M; Tamura, M; Yoshida, N; Ishisaki, T. Studies of perfluorinated ion exchange membranes for polymer electrolyte fuel cells, *Denki Kagaku***,** *64* (6), 727-736.

[43] Yoshida, N; Ishisaki, T; Watakabe, A; Yoshitake, M. Characterization of flemion (R) membranes for PEFC, *Electrochim. Acta*, **1998**, *43* (24), 3749-3754.

[44] Verbrugge, MW; Hill, RF. Analysis of promising perfluorosulfonic acid membranes for fuel-cell electrolytes, *J. Electrochem. Soc.*, **1990**, *137* (12), 3770-3777.

[45] Verbrugge, MW; Schneider, EW; Conell, RS; Hill, RF. The effect of temperature on the equilibrium and transport-properties of saturated poly(perfluorosulfonic acid) membranes, *J. Electrochem. Soc.*, **1992**, *139* (12), 3421-3428.

[46] Wu, XM; Wang, XW; He, GH; Benziger, J. Differences in water sorption and proton conductivity between Nafion and SPEEK, *J. Polym. Sci., Part B: Polym. Phys.*, **2011**, *49* (20), 1437-1445.

[47] Safronova, EY; Volkov, VI; Yaroslavtsev, AB. Ion mobility and conductivity of hybrid ion-exchange membranes incorporating inorganic nanoparticles, *Solid State Ionics*, **2011**, *188* (1 Special), 129-131.

[48] Demus, D; Goodby, JWG; Gray, W; Spiess, HW; Vill, L. Handbook of Liquid Crystals, Wiley-VCH, Weinheim, **1998**.

[49] Kato, T; Mizoshita, N; Kishimoto, K. Functional liquid-crystalline assemblies: Self-organized soft materials, *Angew. Chem. Int. Ed.*, **2006**, *45* (1), 38-68.

[50] Sergeyev, S; Pisula, W; Geerts, YH. Discotic liquid crystals: A new generation of organic semiconductors, *Chem. Soc. Rev.*, **2007**, *36* (12), 1902-1929.

[51] Ikeda, T; Mamiya, J; Yu, YL. Photomechanics of liquid-crystalline elastomers and other polymers, *Angew. Chem. Int. Ed.*, **2007**, *46* (4), 506-528.

[52] Hori, R; Furukawa, D; Yamamoto, K; Kutsumizu, S. Light-driven phase transition in a cubic-phase-forming binary system composed of 4 '-N-docosyloxy-3 '-nitrobiphenyl-4-carboxylic acid and an azobenzene derivative, *Chem. Eur. J.*, **2012**, *18* (24), 7346-7350.

[53] Yoshio, M; Mukai, T; Ohno, H; Kato, T. One-dimensional ion transport in self-organized columnar ionic liquids, *J. Am. Chem. Soc.*, **2004**, *126* (4), 994-995.

[54] Yoshizawa, A. Liquid crystal supermolecules stabilizing an optically isotropic phase with frustrated molecular organization, *Polym. J.*, **2012**, *44* (6 Special), 490-502.

[55] Wiesenauer, BR; Gin, DL. Nanoporous polymer materials based on self-organized, bicontinuous cubic lyotropic liquid crystal assemblies and their applications, *Polym. J.*, **2012**, *44* (6 Special), 461-468.

[56] Percec, V; Cho, WD; Moller, M; Prokhorova, SA; Ungar, G; Yeardley, DJP. Design and structural analysis of the first spherical monodendron self-organizable in a cubic lattice, *J. Am. Chem. Soc.*, **2000**, *122* (17), 4249-4250.

[57] Prokhorova, SA; Sheiko, SS; Mourran, A; Azumi, R; Beginn, U; Zipp, G; Ahn, CH; Holerca, MN; Percec, V; Moller, M. Epitaxial adsorption of monodendron-jacketed linear polymers on highly oriented pyrolytic graphite, *Langmuir*, **2000**, *16* (17), 6862-6867.

[58] Prokhorova, SA; Sheiko, SS; Ahn, CH; Percec, V; Moller, M. Molecular conformations of monodendron-jacketed polymers by scanning force microscopy, *Macromolecules*, **1999**, *32* (8), 2653-2660.

[59] Percec, V; Ahn, CH; Cho, WD; Jamieson, AM; Kim, J; Leman, T; Schmidt, M; Gerle, M; Moller, M; Prokhorova, SA; Sheiko, SS; Cheng, SZD; Zhang, A; Ungar, G; Yeardley, DJP. Visualizable cylindrical macromolecules with controlled stiffness from backbones containing libraries of self-assembling dendritic side groups, *J. Am. Chem. Soc.*, **1998**, *120* (34), 8619-8631.

[60] Prokhorova, SA; Sheiko, SS; Moller, M; Ahn, CH; Percec, V. Molecular imaging of monodendron jacketed linear polymers by scanning force microscopy, *Macromol. Rapid Commun.*, **1998**, *19* (7), 359-366.

[61] Percec, V; Ahn, CH; Ungar, G; Yeardley, DJP; Moller, M; Sheiko, SS. Controlling polymer shape through the self-assembly of dendritic side-groups, *Nature*, **1998**, *391* (6663), 161-164.

[62] Smith, RC; Fischer, WM; Gin, DL. Ordered poly(p-phenylenevinylene) matrix nanocomposites via lyotropic liquid-crystalline monomers, *J. Am. Chem. Soc.*, **1997**, *119* (17), 4092-4093.

[63] Hoag, BP; Gin, DL. Cross-linkable liquid crystal monomers containing hydrocarbon 1,3-diene tail systems, *Macromolecules*, **2000**, *33* (23), 8549-8558.

[64] Gin, DL; Gray, DH; Smith, RC. Polymerizable liquid crystals as building blocks for functional, nanostructured materials, *Synlett***,** *10*, 1509-1522.

[65] Pindzola, BA; Hoag, BP; Gin, DL. Polymerization of a phosphonium diene amphiphile in the regular hexagonal phase with retention of mesostructure, *J. Am. Chem. Soc.*, **2001**, *123* (19), 4617-4618.

[66] Yoshio, M; Ichikawa, T; Shimura, H; Kagata, T; Hamasaki, A; Mukai, T; Ohno, H; Kato, T. Columnar liquid-crystalline imidazolium salts. Effects of anions and cations on mesomorphic properties and ionic conductivity, *Bull. Chem. Soc. Jpn.*, **2007**, *80* (9), 1836-1841.

[67] Cho, BK; Jain, A; Gruner, SM; Wiesner, U. Mesophase structure-mechanical and ionic transport correlations in extended amphiphilic dendrons, *Science*, **2004**, *305* (5690), 1598-1601.

[68] Percec, V; Glodde, M; Bera, TK; Miura, Y; Shiyanovskaya, I; Singer, KD; Balagurusamy, VSK; Heiney, PA; Schnell, I; Rapp, A; Spiess, HW; Hudson, SD; Duan, H. Self-organization of supramolecular helical dendrimers into complex electronic materials, *Nature*, **2002**, *419* (6905), 384-387.

[69] Xiao, SX; Myers, M; Miao, Q; Sanaur, S; Pang, KL; Steigerwald, ML; Nuckolls, C. Molecular wires from contorted aromatic compounds, *Angew. Chem. Int. Ed.*, **2005**, *44* (45), 7390-7394.

[70] Hirai, Y; Monobe, H; Mizoshita, N; Moriyama, M; Hanabusa, K; Shimizu, Y; Kato, T. Enhanced hole-transporting behavior of discotic liquid-crystalline physical gels, *Adv. Funct. Mater.*, **2008**, *18* (11), 1668-1675.

[71] Zhou, MJ; Kidd, TJ; Noble, RD; Gin, DL. Supported lyotropic liquid-crystal polymer membranes: Promising materials for molecular-size-selective aqueous nanofiltration, *Adv. Mater.*, **2005**, *17* (15), 1850-1853.

[72] Shimura, H; Yoshio, M; Hamasaki, A; Mukai, T; Ohno, H; Kato, T. Electric-field-responsive lithium-ion conductors of propylenecarbonate-based columnar liquid crystals, *Adv. Mater.*, **2009**, *21* (16), 1591-1594.

[73] Kerr, RL; Miller, SA; Shoemaker, RK; Elliott, BJ; Gin, DL. New type of Li ion conductor with 3D interconnected nanopores via polymerization of a liquid organic electrolyte-filled lyotropic liquid-crystal assembly, *J. Am. Chem. Soc.*, **2009**, *131* (44), 15972-15973.

[74] Frise, AE; Ichikawa, T; Yoshio, M; Ohno, H; Dvinskikh, SV; Kato, T; Furo, I. Ion conductive behaviour in a confined nanostructure: NMR observation of self-diffusion in a liquid-crystalline bicontinuous cubic phase, *Chem. Commun.*, **2010**, *46* (5), 728-730.

[75] Ichikawa, T; Yoshio, M; Hamasaki, A; Kagimoto, J; Ohno, H; Kato, T. 3D interconnected ionic nano-channels formed in polymer films: Self-organization and polymerization of thermotropic bicontinuous cubic liquid crystals, *J. Am. Chem. Soc.*, **2011**, *133* (7), 2163-2169.

[76] Ichikawa, T; Yoshio, M; Hamasaki, A; Mukai, T; Ohno, H; Kato, T. Self-organization of room-temperature ionic liquids exhibiting liquid-crystalline bicontinuous cubic phases: Formation of nano-ion channel networks, *J. Am. Chem. Soc.*, **2007**, *129* (35), 10662-10663.

[77] Ichikawa, T; Yoshio, M; Hamasaki, A; Taguchi, S; Liu, F; Zeng, XB; Ungar, G; Ohno, H; Kato, T. Induction of thermotropic bicontinuous cubic phases in liquid-crystalline ammonium and phosphonium salts, *J. Am. Chem. Soc.*, **2012**, *134* (5), 2634-2643.

[78] Lu, XY; Nguyen, V; Zhou, MJ; Zeng, XH; Jin, JZ; Elliott, BJ; Gin, DL. Crosslinked bicontinuous cubic lyotropic liquid-crystal/butyl-rubber composites: Highly selective, breathable barrier materials for chemical agent protection, *Adv. Mater.*, **2006**, *18* (24), 3294-3298.

[79] Beginn, U; Zipp, G; Moller, M. Synthesis and characterization of tris-methacrylated 3,4,5-tris[(alkoxy)benzyloxy]benzoate derivatives, *Chem. Eur. J.*, **2000**, *6* (11), 2016-2023.

[80] Beginn, U; Zipp, G; Moller, M. Self-organization of liquid crystalline 3,4,5-tris[(11-methacryloyl-undecyl-1-oxy)-4-benzyloxy]benzoates in low-shrinkage methacrylate mixtures, *J. Polym. Sci., Part A: Polym. Chem.*, **2000**, *38* (3), 631-640.

[81] Beginn, U; Zipp, G; Moller, M. Functional membranes containing ion-selective matrix-fixed supramolecular channels, *Adv. Mater.*, **2000**, *12* (7), 510-513.

[82] Beginn, U; Zipp, G; Mourran, A; Walther, P; Moller, M. Membranes containing oriented supramolecular transport channels, *Adv. Mater.*, **2000**, *12* (7), 513-516.

[83] Zhu, XM; Beginn, U; Moller, M; Gearba, RI; Anokhin, DV; Ivanov, DA. Self-organization of polybases neutralized with mesogenic wedge-shaped sulfonic acid molecules: An approach toward supramolecular cylinders, *J. Am. Chem. Soc.*, **2006**, *128* (51), 16928-16937.

[84] Zhu, XM; Mourran, A; Beginn, U; Moller, M; Anokhin, DV; Ivanov, DA. Self-assembled structures formed by a wedge-shaped molecule in 2D and 3D: The role of flexible side chains and polar head groups, *Phys. Chem. Chem. Phys.*, **2010**, *12* (7), 1444-1452.

[85] Beginn, U; Yan, LL; Chvalun, SN; Shcherbina, MA; Bakirov, A; Moller, M. Thermotropic columnar mesophases of wedge-shaped benzenesulfonic acid mesogens, *Liq. Cryst.*, **2008**, *35* (9), 1073-1093.

[86] Zhu, XM; Tartsch, B; Beginn, U; Moller, M. Wedge-shaped molecules with a sulfonate group at the tip - A new class of self-assembling amphiphiles, *Chem. Eur. J.*, **2004**, *10* (16), 3871-3878.

[87] Zhu, XM; Scherbina, MA; Bakirov, AV; Gorzolnik, B; Chvalun, SN; Beginn, U; Moller, M. Methacrylated self-organizing 2,3,4-tris(alkoxy)benzenesulfonate: A new concept toward ion-selective membranes, *Chem. Mater.*, **2006**, *18* (19), 4667-4673.

Chapter 2

Wedge-Shaped Amphiphilic Sulfonate Molecules with Different Counterions: Synthesis

In this chapter, a series of wedge-shaped sulfonate amphiphiles, namely lithium / sodium / potassium / cesium 2,3,4-tris(11'-acryloyloxyundecyl-1'-oxy)benzene-sulfonate, are prepared. The whole synthetic procedure of each sulfonate consists of three steps. All intermediate and the final products are characterized by means of ^{1}H NMR, ^{13}C NMR and elemental analysis, which prove their high purity.

2.1. Introduction

Self-assembly of small molecules into supramolecular organizations provides a versatile approach towards complex aggregate architectures [1] and offers exciting perspectives for the development of nanostructured functional materials [2-5]. Layered, cylindrical and globular structures have been applied for the transport materials for ions [6-9], electrons [8-10] and molecules [11]. Wedge-shaped amphiphilic molecules bearing polar groups at the tip of the wedge generally tend to form cylindrical superstructures with the polar groups aligned along the cylinder axis [12-14]. This approach is previously employed to generate ion-selective membranes using stacks of crown-ether groups as ionic channels [15,16].

Recently, our group has developed a variety of wedge-shaped sulfonate amphiphiles which can self-assemble to supramolecular columns. The sulfonate groups are stacked along the columnar axis and thereby form an ionic channel with a well-defined geometry [17-19]. As shown in Scheme 1, the symmetry of the molecule can be controlled by reaction conditions since the possible substitution in either 4 or 5 position of the compound 1,2,3-trialkoxybenzene. By oxidation of pyrogallol with air in an alkaline solution of $NaSO_3$, 3,4,5-trihydroxybenzenesulfonic acid is obtained. Further alkylation yields symmetrically substituted wedge-shaped amphiphilic sulfonate: 3,4,5-trialkoxybenzenesulfonate (Scheme 1a). At the same time, by direct sulfonation with sulfuric acid of 1,2,3-trialkoxybenzene, the asymmetrically substituted wedge-shaped amphiphilic sulfonates: namely 2,3,4-trialkoxybenzene-sulfonates, are obtained (Scheme 1b). In this case, the phase transition temperature lies significantly lower than that of the corresponding symmetrical sulfonate [17]. Further, it is found that the counter ion plays a big role in the formation of mesostructures. Cubic, lamellar and columnar mesophases can be formed due to the different size of the counter ion [17].

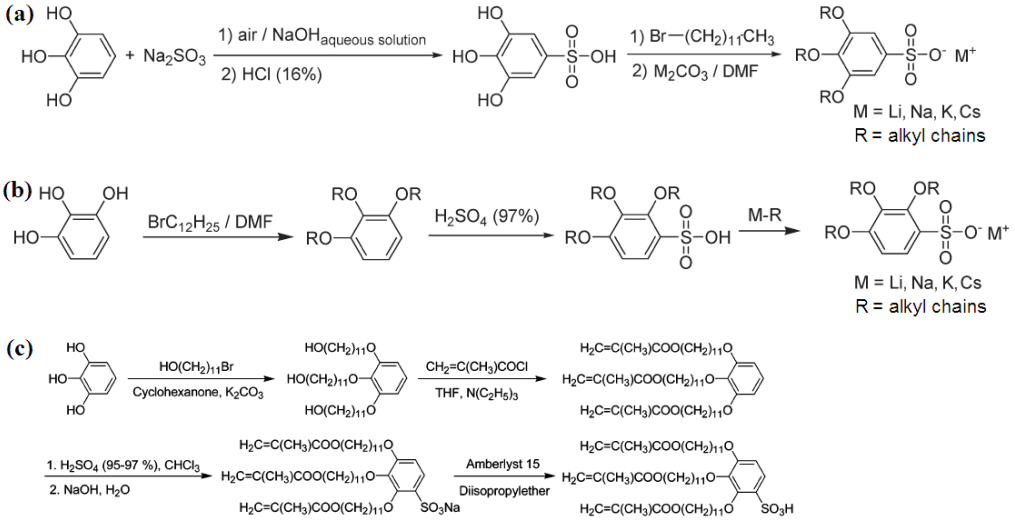

Scheme 1. (a) (b) Synthesis of symmetrically (a) and asymmetrically (b) substituted wedge-shaped amphiphilic sulfonates [17]. (c) The structure of the metacrylated wedge-shaped sulfonate [19].

To achieve the allowance of polymerization, a wedge-shaped sulfonate molecule with methacrylate groups at the end of the alkyl tails is also synthesized in our group (Scheme 1c) and the disordered hexagonal columnar mesophase is arrested under ambient conditions [19]. The polymerizable methacrylate groups will allow linking the supramolecular columns with a surrounding polymer matrix to form a membrane. In order to better resemble the Nafion strcutrual models, the equivalent weight of this compound is designed to be close to that of widely-used Nafion membranes with an equivalent weight of 1100 g/mol [20].

In this chapter, the synthesis of a series of acrylated wedge-shpaed amphiphilic sulfonate molecules with different counterions, namely lithium / sodium / potassium / cesium 2,3,4-tris(11'-acryloyloxyundecyl-1'-oxy)benzenesulfonates, is presented. The acrylic groups are used instead of methacylic groups in order to increase the flexibility of the resulting polymerized membranes.

2.2. Experimental

2.2.1 Materials

Pyrogallol (puriss 99%, Riedel-de Haen), 11-bromo-1-undecanol (98%, Sigma Aldrich), potassium carbonate (99%, Merck), N,N-dimethylformamide (anhydrous 99.8%, Sigma Al-drich), tetrahydrofuran (anhydrous >99.9%, Sigma Aldrich), 4-dimethylamine pyridine (>99%, Sigma Aldrich), 2,6-di-tert-butyl-4-methylphenol (>99%, Fluka), acryloyl chloride (97%, Fluka), triethylamine (puriss >99.5%, Fluka), sulfuric acid (98%, Merck), lithium/sodium/potassium hydroxide (for analysis, Merck), cesium hydroxide 50wt% solution in water (99%, Sigma Aldrich), ethyl acetate (99.9%, VWR), n-hexane (98.9%, VWR), ethanol (99.8%, VWR) are used as received.

2.2.2. Synthesis

1,2,3-Tris(11'-hydroxyundecyl-1'-oxy)benzene (*1*): In a flask equipped with a condenser, a magnet stirrer and a nitrogen inlet, 3 g (23.8 mmol) of pyrogallol and 20.6 g (82.1 mmol) of 11-bromo-1-undecanol are dissolved in 200 mL of anhydrous dimethylformamide. To this solution is added 32.88 g (237.9 mmol) of anhydrous potassium carbonate. The mixture is then stirred at 90 ℃ under nitrogen atmosphere for 24 hours. Subsequently, the whole mixture is hot-filtered and concentrated by a rotary evaporator, and then the residue is poured into 500 mL of ice water. The crude products were precipitated and are then separated by filtration. The precipitations are dissolved in ethyl acetate, washed with dilute hydrochloric acid and water, dried over anhydrous sodium sulfate, filtered and concentrated by a rotary evaporator. The product is purified by recrystallization three times from 50 mL of an n-hexane/ethyl acetate (1:1, v/v) solution, yielding a white powder of ***1*** of 10.2 g (16.0 mmol, yield: 67.3%). ^{1}H NMR ($CDCl_3$, chemical shift/ppm): 1.29 [m, 36H, -(C$\underline{H}_2$)$_6$-(CH$_2$)$_2$OH],

1.46 [m, 6H, -C$\underline{H_2}$(CH$_2$)$_2$OH], 1.56 [m, 6H, -C$\underline{H_2}$(CH$_2$)$_2$OH], 1.79 (m, 6H, -C$\underline{H}$2CH2OPh), 3.62 [t, 6H, -C$\underline{H_2}$OH], 3.96 [m, 6H, -CH$_2$C$\underline{H_2}$OPh], 6.55 [d, 2H, $\underline{H}_{aromatic}$, in 4 and 6 positions], 6.90 [t, 1H, $\underline{H}_{aromatic}$, in 5 position]. ^{13}C NMR (CDCl$_3$, chemical shift/ppm): 25.8 [-$\underline{C}$H$_2$CH$_2$CH$_2$OH], 26.2 [-$\underline{C}$H$_2$CH$_2$CH$_2$OPh], 29.6-30.3 [alkyl], 32.8 [-$\underline{C}$H$_2$CH$_2$OH], 63.1 [-$\underline{C}$H$_2$OH], 69.1 [-$\underline{C}$H$_2$OPh in 1 and 3 positions], 73.4 [-$\underline{C}$H$_2$OPh in 2 position], 106.8 [$C_{aromatic}$ in 4 and 6 positions], 123.1 [$C_{aromatic}$ in 5 position], 138.4 [$C_{aromatic}$ in 2 position], 153.4 [$C_{aromatic}$ in 1 and 3 positions]. Elemental analysis of ***1*** (C$_{39}$H$_{72}$O$_6$, 636.99 g mol^{-1}) is: C, 73.83; H, 12.05 wt %. Theoretical: C, 73.54; H, 11.39 wt %.

1,2,3-Tris(11'-acryloyloxy-undecyl-1'-oxy) benzene (*2*). In a flask equipped with a magnet stirrer and a nitrogen inlet, 6.0 g (9.42 mmol) of ***1***, 150 mg (12.3 mmol) of 4-dimethylamine pyridine, 30 mg (0.15 mmol) of 2,6-di-tert-butyl-4-methylphenol, 4.6 mL (33.0 mmol) of triethylamine are dissolved in 40 mL of anhydrous tetrahydrofuran. Under nitrogen atmosphere and stirring in an ice/water bath, a solution of 4.0 mL (33.0 mmol) of acryloyl chloride in 10 mL of anhydrous tetrahydrofuran is added dropwise. After complete addition, the solution is stirred at room temperature for 24 h. Subsequently, the solution was filtered, and the solvent is removed by a rotary evaporator. The residue is dissolved in ethyl acetate, ished with brine, dried over anhydrous sodium sulfate, filtered and concentrated again by a rotary evaporator. The crude product is purified using silica gel column chromatography with the mobile phase of hexane/ ethyl acetate (4:1, v/v), yielding a colourless liquid of ***2*** of 5.1 g (6.38 mmol, yield: 67.7%). ^{1}H NMR (CDCl$_3$, chemical shift/ppm): 1.28 [m, 30H, -(C$\underline{H_2}$)$_5$-(CH$_2$)$_3$OPh], 1.45 [m, 12H, -C$\underline{H_2}$(CH$_2$)$_2$OPh and -C$\underline{H_2}$(CH$_2$)$_2$OCOCH=CH$_2$], 1.66 (m, 6H, -C$\underline{H_2}$CH$_2$OCOCH=CH$_2$), 1.78 [s, 6H, -C$\underline{H_2}$CH$_2$OPh], 3.96 [m, 6H, -CH$_2$C$\underline{H_2}$OPh], 4.14 [m, 6H, -C$\underline{H_2}$OCOCH=CH$_2$], 5.82 [m, 3H, -COCH=C$\underline{H}$H], 6.12 [m, 3H, -COC$\underline{H}$=CH$_2$], 6.37 [m, 3H, -COCH=CH$\underline{H}$], 6.54 [d, 2H, $\underline{H}_{aromatic}$, in 4 and 6 positions], 6.90 [t, 1H, $\underline{H}_{aromatic}$, in 5 position]. ^{13}C

NMR ($CDCl_3$, chemical shift/ppm): 25.9 [-$\underline{C}H_2CH_2CH_2OCOCH=CH2$], 26.1 [-$\underline{C}H_2CH_2CH_2OPh$], 28.6-29.7 [alkyl], 64.7 [-$\underline{C}H_2OCOCH=CH_2$], 69.0 [-$\underline{C}H_2OPh$, in 1 and 3 positions], 73.3 [-$\underline{C}H_2OPh$, in 2 position], 106.8 [$C_{aromatic}$, in 4 and 6 positions], 123.1 [$C_{aromatic}$, in 5 position], 128.6 [-CO$\underline{C}H=CH_2$], 130.4 [-COCH=$\underline{C}H_2$], 138.4 [$C_{aromatic}$, in 2 position], 153.4 [$C_{aromatic}$, in 1 and 3 positions], 166.3 [-O$\underline{C}OCH=CH_2$]. Elemental analysis of ***2*** ($C_{48}H_{78}O_9$, 799.13 g mol^{-1}) is: C, 71.74; H, 10.02 wt %. Theoretical: C, 72.14; H, 9.84 wt%.

Lithium 2,3,4-tris(11'-acryloyloxyundecyl-1'-oxy) benzenesulfonate (*3*): Under a continuously intensive stirring, 1.5 mL of concentrated sulfuric acid (98%) is added into a solution of 1.080 g (1.351 mmol) of ***2*** in 10 mL of dichloromethane. The reaction suspension is stirred at 35 ℃ for 20 minutes and then slowly poured into 30 ml of ice water. The pH of the aqueous solution is adjusted to around 12 by adding a solution of lithium hydroxide. The resulting suspension is stirred for another half an hour and afterwards extracted by ethyl acetate three times. The organic phase is combined and then concentrated by a rotary evaporator at 35 ℃ with the addition of 2 mg of 2,6-di-tert-butyl-4-methylphenol (inhibitor). The crude product is purified by silica gel column chromatography. Ethyl acetate is firstly applied to wash away organic impurities. Ethanol is then used to wash out the product. After adding 2 mg of inhibitor, the solvent is evaporated again at 35 ℃ on a rotary evaporator. After drying in vacuum for 2 h, a light orange waxy solid of ***3*** (0.552 g, 0.624 mmol, yield: 46.2%) is obtained. ^{1}H NMR (DMSO-d6, chemical shift/ppm): 1.27 [m, 30H, -($C\underline{H}_2$)$_5$-$(CH_2)_3OPh$], 1.43 [m, 12H, -$C\underline{H}_2(CH_2)_2OPh$ and -$C\underline{H}_2(CH_2)_2OCOCH=CH_2$], 1.58 (m, 6H, -$C\underline{H}_2CH_2OCOCH=CH_2$), 1.69 [s, 6H, -$C\underline{H}_2CH_2OPh$], 3.84 [t, 2H, in 3 position], 3.96 [m, 4H, -$CH_2C\underline{H}_2OPh$ in 2 and 4 positions], 4.07 [m, 6H, -$C\underline{H}_2OCOCH=CH_2$], 5.92 [m, 3H, -COCH=C$\underline{H}$H], 6.14 [m, 3H, -COC$\underline{H}$=$CH_2$], 6.27 [m, 3H, -COCH=CH$\underline{H}$], 6.64 [d, 1H, $\underline{H}_{aromatic}$, in 5 position], 7.34 [d, 1H, $\underline{H}_{aromatic}$, in 6 position]. ^{13}C NMR (DMSO-d6, chemical shift/ppm): 25.4 (-$\underline{C}H_2CH_2CH_2OH$), 25.6

(-$\underline{C}H_2CH_2CH_2OPh$), 28.0-29.9 (alkyl), 63.9 (-$\underline{C}H_2OCOCH=CH_2$), 68.0 (-$\underline{C}H_2OPh$, in 2 and 4 positions), 72.5 (-$\underline{C}H_2OPh$, in 3 position), 106.6 ($C_{aromatic}$, in 4 position), 122.7 ($C_{aromatic}$, in 1 position), 128.3 (-CO$\underline{C}H=CH_2$), 131.1 (-COCH=$\underline{C}H_2$), 134.5 ($C_{aromatic}$, in 3 position), 141.7 ($C_{aromatic}$, in 2 position), 150.2 ($C_{aromatic}$, in 6 position), 153.5 ($C_{aromatic}$, in 5 position), 165.3 (-O$\underline{C}OCH=CH_2$). Elemental analysis of ***3*** ($C_{48}H_{77}O_{12}LiS$, 885.12 g mol^{-1}) is: C, 65.57; H, 8.70 wt %. Theoretical: C, 65.13; H, 8.77 wt %.

Sodium / Potassium / Cesium 2,3,4-tris(11'-acryloyloxyundecyl-1'-oxy) benzenesulfonate (*4,5,6*): Under intensive stirring, 1.5 mL of concentrated sulfuric acid (98%) is added into a solution of 0.700 g (0.876 mmol) of ***2*** in 10 mL of chloroform. The reaction suspension is stirred at 40 ℃ for 15 minutes and is subsequently slowly poured into 30 ml of ice water. The aqueous solution is adjusted to pH around 12 by adding a corresponding solution of sodium / potassium / cesium hydroxide. The resulting suspension is stirred for another half an hour and afterwards is extracted by ethyl acetate three times. The organic phase is then dried over corresponding sulfates or chlorides, filtered and concentrated by a rotary evaporator at 40 ℃. The crude product is purified using silica gel column chromatography. Firstly, ethyl acetate is applied to wash away organic impurities. Secondly ethanol is used to wash out the product. After evaporation of solvent and drying in vacuum, a yellow waxy solid of ***4*** (0.454 g, 0.504 mmol, yield: 57.5%), a yellow waxy solid of ***5*** of (0.332 g, 0.382 mmol, yield: 41.0%), a light yellow viscous solid of ***6*** (0.557 g, 0.578 mmol, yield: 62.0%) are obtained. ^{1}H NMR (DMSO-d6, chemical shift/ppm, the compounds of ***4***,***5*** and ***6*** present the same ^{1}H NMR spectra): 1.27 [m, 30H, -($C\underline{H}_2$)$_5$-$(CH_2)_3OPh$], 1.43 [m, 12H, -$C\underline{H}_2(CH_2)_2OPh$ and -$C\underline{H}_2(CH_2)_2OCOCH=CH_2$], 1.58 (m, 6H, -$C\underline{H}_2CH_2OCOCH=CH_2$), 1.69 [s, 6H, -$C\underline{H}_2CH_2OPh$], 3.84 [t, 2H, in 3 position], 3.96 [m, 4H, -$CH_2C\underline{H}_2OPh$ in 2 and 4 positions], 4.07 [m, 6H, -$C\underline{H}_2OCOCH=CH_2$], 5.92 [m, 3H, -COCH=C$\underline{H}$H], 6.14 [m, 3H, -COC$\underline{H}$=$CH_2$], 6.27

[m, 3H, -COCH=CH*H*], 6.64 [d, 1H, *H*$_{aromatic}$, in 5 position], 7.34 [d, 1H, *H*$_{aromatic}$, in 6 position]. ^{13}C NMR (DMSO-d6, chemical shift/ppm, the compounds of ***4***,***5*** and ***6*** have the same ^{13}C NMR spectra): 25.4 (-*C*H$_2$CH$_2$CH$_2$OH), 25.6 (-*C*H$_2$CH$_2$CH$_2$OPh), 28.0-29.9 (alkyl), 63.9 (-*C*H$_2$OCOCH=CH$_2$), 68.0 (-*C*H$_2$OPh, in 2 and 4 positions), 72.5 (-*C*H$_2$OPh, in 3 position), 106.6 (*C*$_{aromatic}$, in 4 position), 122.7 (*C*$_{aromatic}$, in 1 position), 128.3 (-CO*C*H=CH$_2$), 131.1 (-COCH=*C*H$_2$), 134.5 (*C*$_{aromatic}$, in 3 position), 141.7 (*C*$_{aromatic}$, in 2 position), 150.2 (*C*$_{aromatic}$, in 6 position), 153.5 (*C*$_{aromatic}$, in 5 position), 165.3 (-O*C*OCH=CH$_2$). The elemental analysis of ***4*** ($C_{48}H_{77}O_{12}NaS$, 901.17 g mol^{-1}) is: C, 61.45; H, 8.88 wt %. Theoretical: C, 63.97; H, 8.61 wt %. ***5*** ($C_{48}H_{77}O_{12}KS$, 917.28 g mol^{-1}) is: C, 60.07; H, 8.30 wt %. Theoretical: C, 62.85; H, 8.46 wt %. ***6*** ($C_{48}H_{77}O_{12}CsS$, 1011.09 g mol^{-1}) is: C, 57.69; H, 8.03 wt %. Theoretical: C, 58.21; H, 7.68 wt %.

2.2.3. Techniques

^{1}H NMR (400 MHz) and ^{13}C NMR (100 MHz) spectra are recorded by a Bruker DRX-400 NMR spectrometer calibrated by tetramethylsilane (TMS) as an internal standard. Deuterated chloroform ($CDCl_3$) or deuterated dimethyl sulfoxide (DMSO-d6) is used as the solvent. The concentration of each sample is around 20 mg/mL.

Elemental analysis is performed using a Carlo Erba MOD 1106 instrument.

2.3. Results and Discussion

2.3.1 Synthesis

The whole synthesis route is presented as Scheme 2. Each product is numbered sequentially from ***1*** to ***6***. Pyrogallol is reacted with 11-bromo-1-undecanol in anhydrous dimethylformamide in the presence of anhydrous potassium carbonate to yield 1,2,3-tris(11'-hydroxyundecyl-1'-oxy)benzene ***1***, which is subsequently reacted with acryl chloride to yield the tri-ester ***2***. The sulfonation of ***2*** is performed in a mild condition by adding concentrated sulfuric acid (98%) to the chloroform solution to avoid the damage of acrylic groups. After that, the product is neutralized to the sulfonate using an aqueous solution of corresponding hydroxides.

For the lithium salt, as described in the experimental part, the synthesis is carried out in the presence of an inhibitor in order to avoid the polymerization of the product, while the other salts do not polymerize under the reaction conditions. At room temperature, the sodium and potassium salts are wax-like solids while the lithium and cesium sulfonates are obtained as liquids. The NMR spectroscopy and elemental analysis are performed to identify the chemical structure and to prove the purity of all synthesized compounds.

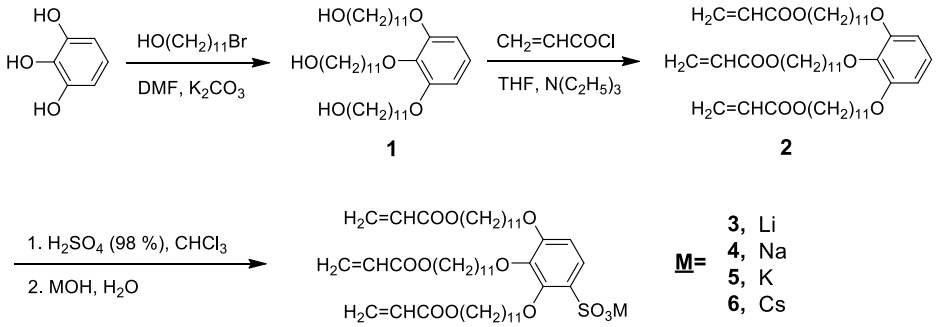

Scheme 2. Synthesis of lithium / sodium / potassium / cesium 2,3,4-tris(11'-acryloyloxyundecyl-1'-oxy) benzenesulfonates.

2.3.2 NMR spectroscopy results

Step 1 is a kind of Williamson ether synthesis, where three hydroxyalkyl chains are added to pyrogallol to yield compound ***1***. It is very important to employ excessive amount of 11-bromo-1-undecanol so that the full substitution would be achieved. The ^{1}H and ^{13}C NMR spectra are depicted in Figure 1. In both ^{1}H and ^{13}C NMR spectra, signals corresponding to all structural units of compound ***1*** are observed. Furthermore, in ^{1}H NMR spectrum the ratio of peak areas of H atoms of –C$\underline{H_2}$OH (δ = 3.62 ppm), –CH_2OPh and benzene ring (δ = 6.90 ppm and 6.55 ppm) is found to be 2:2:1, indicating that all three hydroxyl groups of pyrogallol are substituted with hydroxyalkyl groups.

Step 2 is an ester formation with the end hydroxyl groups using acryloyl chloride to yield compound ***2***. The presence of C=C double bonds in the compound is confirmed by both ^{1}H and ^{13}C NMR spectroscopy showing ^{1}H signals at chemical shifts of 5.82, 6.12 and 6.37 ppm and ^{13}C signals at 126.8, 130.4 and 166.3 ppm (Figure 2). Further, the ratio of the peak areas of aromatic protons at δ = 6.55 and 6.90 ppm and acrylic protons at δ = 5.82 and 6.37 ppm is found to be 1:3, indicating the full substitution of the end hydroxyl groups.

Step 3 is the sulfonation of the benzene ring of compound ***2*** and subsequent neutralization with corresponding metal hydroxides to yield compound ***3***,***4***,***5*** and ***6***. The four sulfonates have the similar NMR spectra, as an example is plotted in Figure 3. Since the wedge-shaped sulfonates show broad NMR signals in chloroform indicating a strong molecular association [21], the NMR spectra of these compounds are obtained in deuterated DMSO in order to reveal the hyperfine chemical structure. On the ^{1}H NMR spectrum, the doublets appeared at δ = 6.64 ppm and δ = 7.34 ppm can be ascribed to the H atoms in positions 5 and 6 of the pyrogallol ring, respectively. Thus, the NMR data indicate that the sulfonation takes place at position 4 of the

benzene ring, which is activated by two alkoxy groups at positions 1 and 3. The ratio of the peak areas of the acrylic and aromatic protons is found to be 9:2, indicating that the sulfonation is successful and the acrylic groups remain intact.

Table 1 summarizes the results of elemental analysis of all intermediates and final products. Accordingly, their high purity has been confirmed.

Table 1. The elemental analysis results of each compound.

No.	Chemical formula Molecular weight (g/mol)		Measured results (wt%)		Theoretical calculated results (wt%)	
			C	H	C	H
1	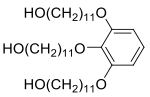	$C_{39}H_{72}O_6$ 636.99	73.83	12.05	73.54	11.39
2	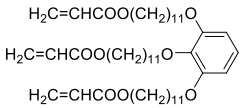	$C_{48}H_{78}O_9$ 799.13	71.74	10.02	72.14	9.84
3	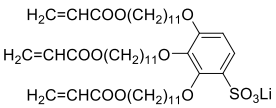	$C_{48}H_{77}O_{12}LiS$ 885.12	65.57	8.70	65.13	8.77
4	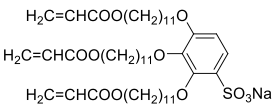	$C_{48}H_{77}O_{12}NaS$ 901.17	61.45	8.88	63.97	8.61
5	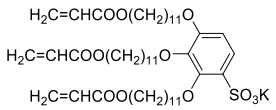	$C_{48}H_{77}O_{12}KS$ 917.28	60.07	8.30	62.85	8.46
6	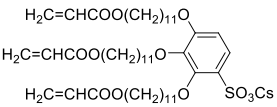	$C_{48}H_{77}O_{12}CsS$ 1011.09	57.69	8.03	58.21	7.68

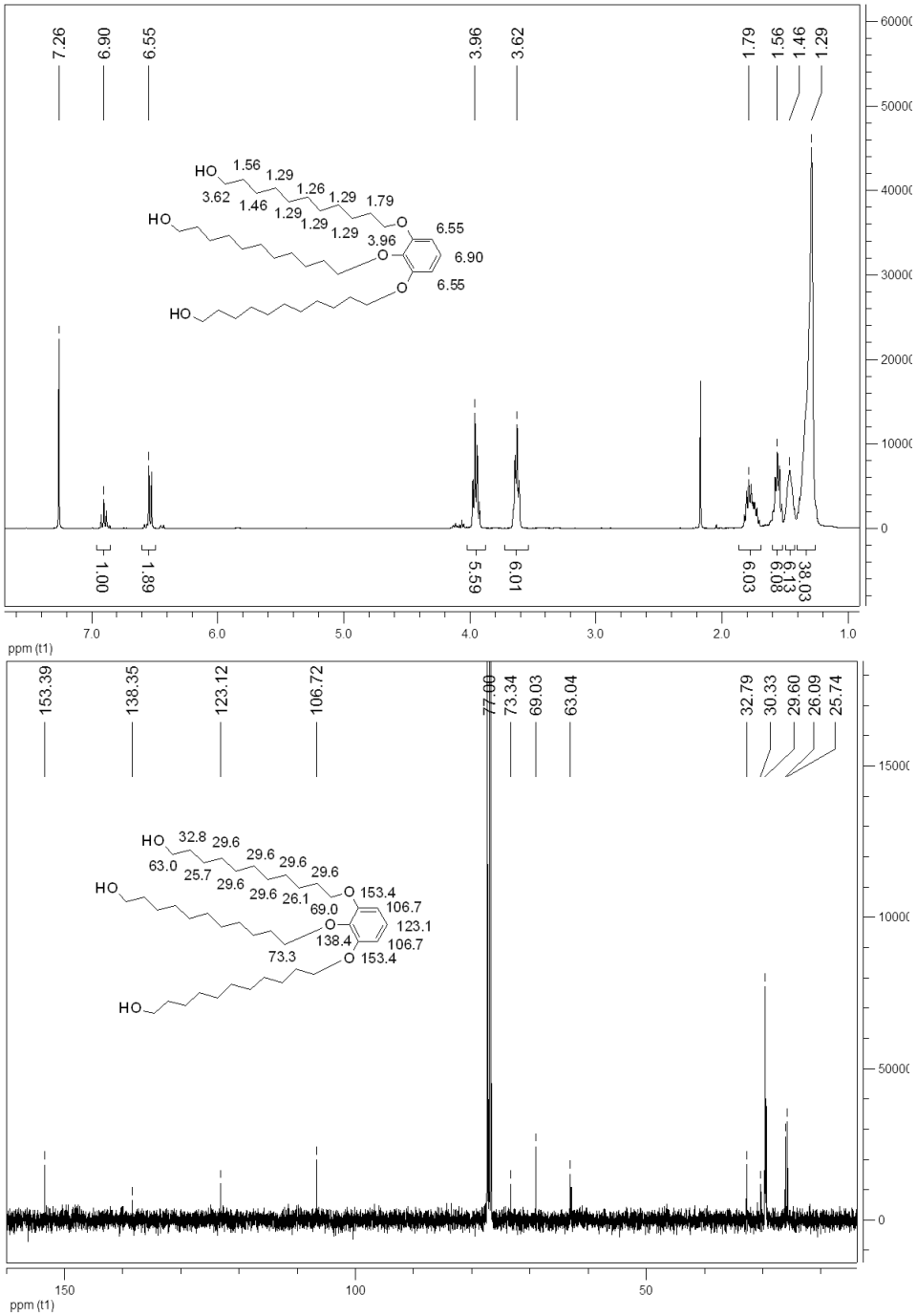

Figure 1. ^{1}H NMR and ^{13}C NMR spectra of 1,2,3-tris(11'-hydroxyundecyl-1'-oxy)benzene (***1***) in $CDCl_3$.

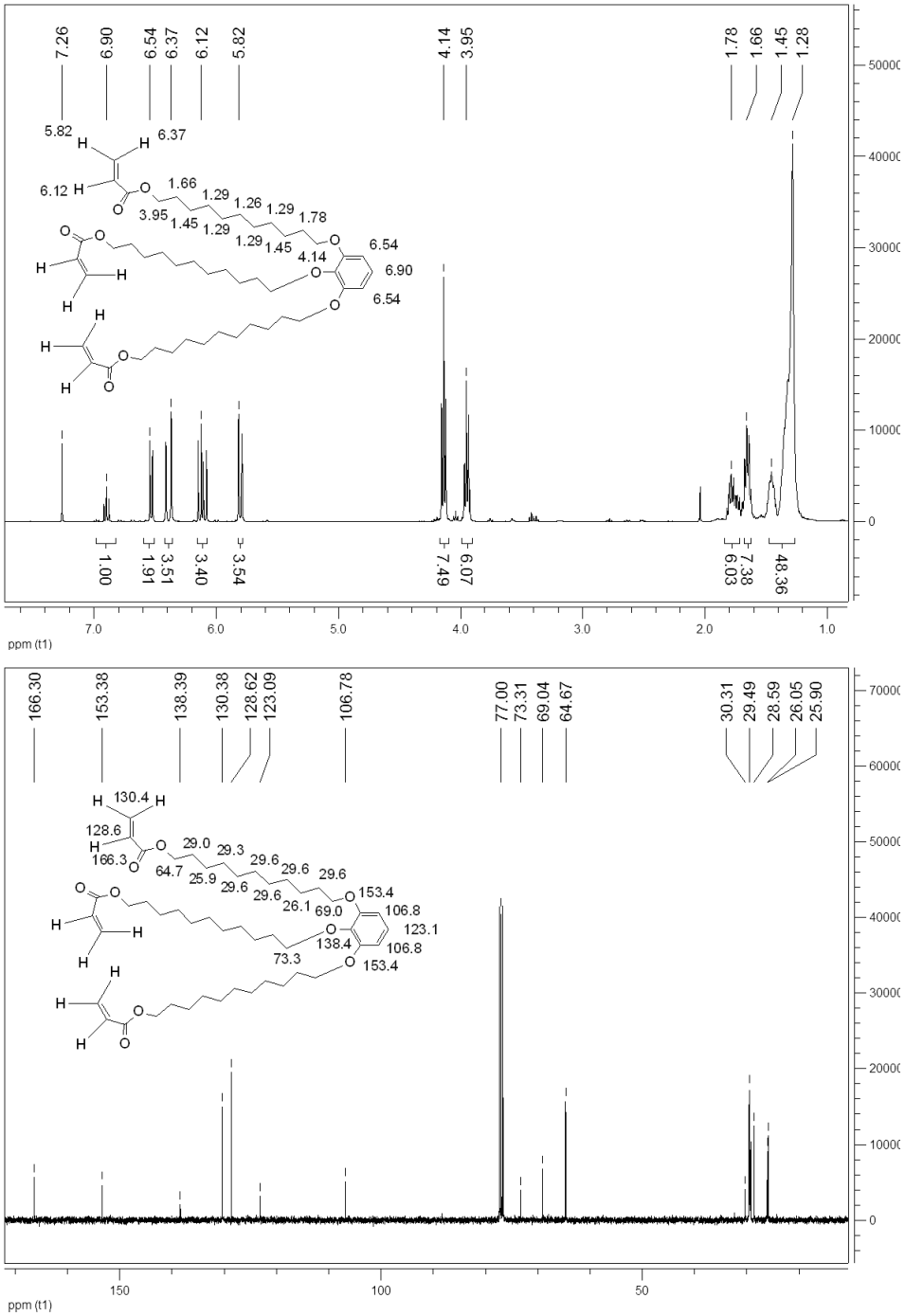

Figure 2. ^{1}H NMR and ^{13}C NMR spectra of 1,2,3-tris(11'-acryloyloxyundecyl-1'-oxy)benzene (***2***) in $CDCl_3$.

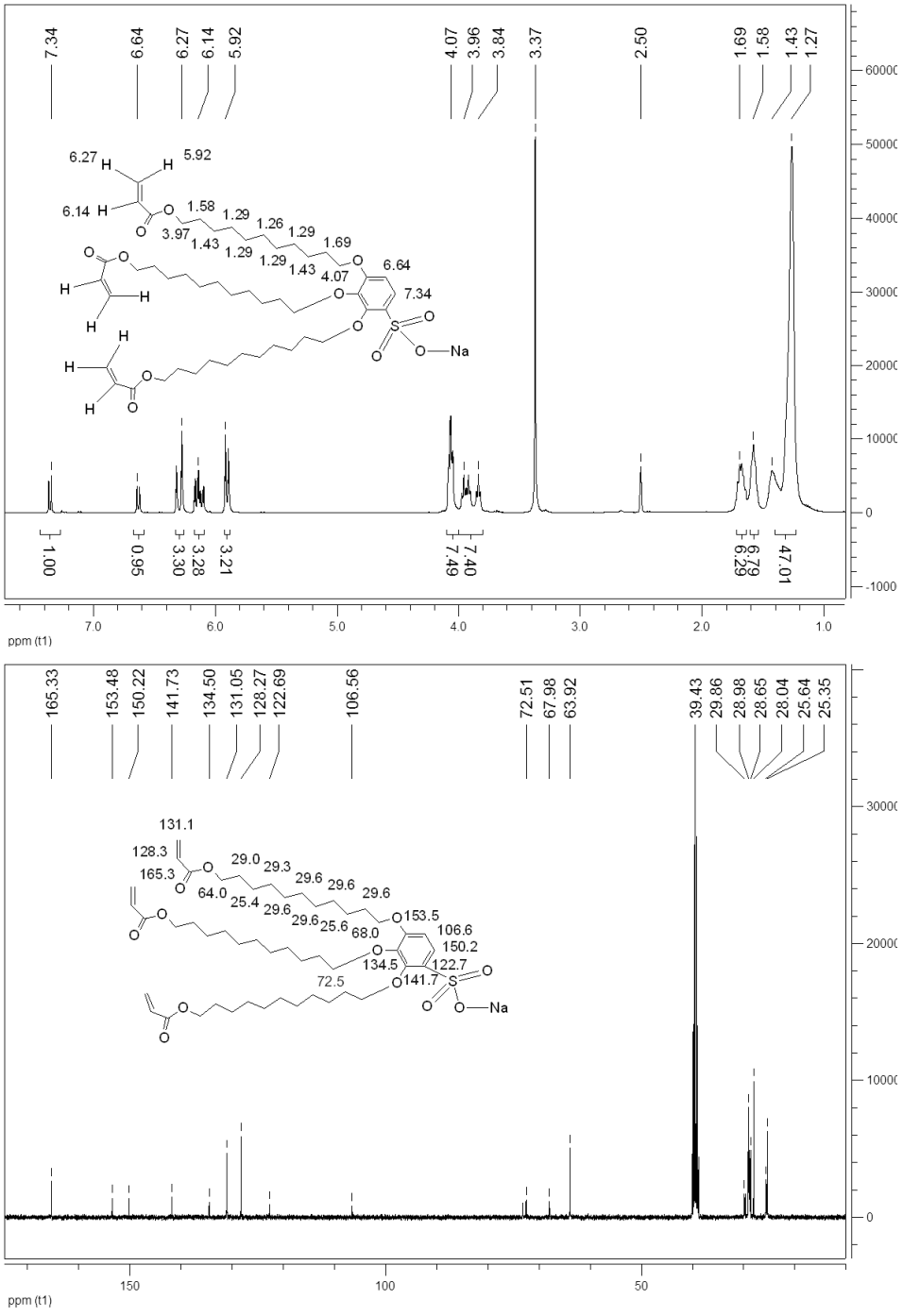

Figure 3. ^{1}H NMR and ^{13}C NMR spectra of sodium 2,3,4-tris(11'-acryloyloxyundecyl-1'-oxy)benzenesulfonate (***4***) in DMSO-d6.

2.4. Conclusion

Four wedge-shaped sulfonate amphiphiles, lithium / sodium / potassium / cesium 2,3,4-tris(11'-acryloyloxyundecyl-1'-oxy)benzenesulfonates are successfully synthesized. The purity of all intermediates and final products are confirmed by means of ^{1}H NMR, ^{13}C NMR spectroscopy and elemental analysis.

2.5. References

[1] Lehn, JM. Supramolecular Chemistry, Concepts and Perspectives, VCH, Weinheim, **1995**.

[2] Ariga, K; Kunitake, T. Supramolecular Chemistry - Fundamentals and Applications, Springer-Verlag, Berlin Heidelberg, **2006**.

[3] Vos, JG; Forster, RJ; Keyes, TE. Interfacial Supramolecular Assemblies, John Wiley & Sons Ltd, Chichester, **2003**.

[4] Fujita, M. Molecular Self-Assembly, Organic Versus Inorganic Approaches in Structure and Bonding, Springer, Berlin, **2000**.

[5] Shimizu, T. Self-Assembled Nanomaterials I - Nanofibers, Springer, Berlin, **2008**.

[6] Yoshio, M; Ichikawa, T; Shimura, H; Kagata, T; Hamasaki, A; Mukai, T; Ohno, H; Kato, T. Columnar liquid-crystalline imidazolium salts. Effects of anions and cations on mesomorphic properties and ionic conductivity, *Bull. Chem. Soc. Jpn.*, **2007**, *80* (9), 1836-1841.

[7] Cho, BK; Jain, A; Gruner, SM; Wiesner, U. Mesophase structure-mechanical and ionic transport correlations in extended amphiphilic dendrons, *Science*, **2004**, *305* (5690), 1598-1601.

[8] Percec, V; Glodde, M; Bera, TK; Miura, Y; Shiyanovskaya, I; Singer, KD; Balagurusamy, VSK; Heiney, PA; Schnell, I; Rapp, A; Spiess, HW; Hudson, SD; Duan, H. Self-organization of supramolecular helical dendrimers into complex electronic materials, *Nature*, **2002**, *419* (6905), 384-387.

[9] Xiao, SX; Myers, M; Miao, Q; Sanaur, S; Pang, KL; Steigerwald, ML; Nuckolls, C. Molecular wires from contorted aromatic compounds, *Angew. Chem. Int. Ed.*, **2005**, *44* (45), 7390-7394.

[10] Hirai, Y; Monobe, H; Mizoshita, N; Moriyama, M; Hanabusa, K; Shimizu, Y; Kato, T. Enhanced hole-transporting behavior of discotic liquid-crystalline physical gels, *Adv. Funct. Mater.*, **2008**, *18* (11), 1668-1675.

[11] Zhou, MJ; Kidd, TJ; Noble, RD; Gin, DL. Supported lyotropic liquid-crystal polymer membranes: Promising materials for molecular-size-selective aqueous nanofiltration, *Adv. Mater.*, **2005**, *17* (15), 1850-1853.

[12] Percec, V; Heck, J; Johansson, G; Tomazos, D; Kawasumi, M; Chu, P. Molecular recognition directed self-assembly of supramolecular liquid-crystals, *Mol. Cryst. Liq. Cryst. Sci. Technol., Sect. A*, **1994**, *254*, 137-196.

[13] Rosen, BM; Wilson, CJ; Wilson, DA; Peterca, M; Imam, MR; Percec, V. Dendron-mediated self-assembly, disassembly, and self-organization of complex systems, *Chem. Rev.*, **2009**, *109* (11), 6275-6540.

[14] Beginn, U. Thermotropic columnar mesophases from N-H center dot center dot center dot O, And N center dot center dot center dot H-O hydrogen bond supramolecular mesogenes, *Prog. Polym. Sci.*, **2003**, *28* (7), 1049-1105.

[15] Beginn, U; Zipp, G; Moller, M. Functional membranes containing ion-selective matrix-fixed supramolecular channels, *Adv. Mater.*, **2000**, *12* (7), 510-513.

[16] Beginn, U; Zipp, G; Mourran, A; Walther, P; Moller, M. Membranes containing oriented supramolecular transport channels, *Adv. Mater.*, **2000**, *12* (7), 513-516.

[17] Beginn, U; Yan, LL; Chvalun, SN; Shcherbina, MA; Bakirov, A; Moller, M. Thermotropic columnar mesophases of wedge-shaped benzenesulfonic acid mesogens, *Liq. Cryst.*, **2008**, *35* (9), 1073-1093.

[18] Zhu, XM; Mourran, A; Beginn, U; Moller, M; Anokhin, DV; Ivanov, DA. Self-assembled structures formed by a wedge-shaped molecule in 2D and 3D: The role of flexible side chains and polar head groups, *Phys. Chem. Chem. Phys.*, **2010**, *12* (7), 1444-1452.

[19] Zhu, XM; Scherbina, MA; Bakirov, AV; Gorzolnik, B; Chvalun, SN; Beginn, U; Moller, M. Methacrylated self-organizing 2,3,4-tris(alkoxy)benzenesulfonate: A new concept toward ion-selective membranes, *Chem. Mater.*, **2006**, *18* (19), 4667-4673.

[20] Mauritz, KA; Moore, RB. State of understanding of Nafion, *Chem. Rev.*, **2004**, *104* (10), 4535-4585.

[21] Zhu, XM; Tartsch, B; Beginn, U; Moller, M. Wedge-shaped molecules with a sulfonate group at the tip - A new class of self-assembling amphiphiles, *Chem. Eur. J.*, **2004**, *10* (16), 3871-3878.

Chapter 3

Humidity-Induced Phase Transition in a Wedge-Shaped Sulfonate Amphiphile (*)

In this chapter, the relation between the structure and conducting properties of a wedge-shaped sulfonate amphiphile, sodium 2,3,4-tris(11'-acryloyloxyundecyl-1'-oxy) benzenesulfonate (A-Na) is studied as a function of relative humidity (RH). This compound is able to self-assemble at ambient conditions into a disordered columnar (Col_{hd}) structure with an ionic channel along the axis of the cylinder. Upon increase of RH up to 55%, the columnar structure remains but a minor water uptake and a slight swelling of the cylinders are observed, which results, however, in a significant enhancement of the ion conductivity by 4 orders of magnitude. Further water uptake by increasing humidity leads to a dramatic change of the mesophase structure whereby bicontinuous cubic phases (Cub_{bi}) are formed. The $Col_{hd} \rightarrow Cub_{bi}$ transition is accompanied by an additional substantial increase of conductivity due to the formation of an interconnected network of ionic channels. The obtained results are discussed in the context of studies of Nafion membranes which are believed to present ionic channel structures.

(*) The results and descriptions of this Chapter have been published in the article: Zhang, H; Li, Lei; Möller, M; Zhu, X; Rueda, J; Rosenthal, M; Ivanov, D. From channel-forming ionic liquid crystals exhibiting humidity-induced phase transitions to nanostructured ion-conducting polymer membranes, *Adv. Mater.*, 2013, *25* (26), 3543-3548.

3.1. Introduction

Biological membranes establish the fundamental barrier within or around a cell in organs. They contain highly selective channels or pores consisting of reversibly self-organized aggregates of functional proteins to regulate the permeation of nutrients and osmolytes [1]. A supreme challenge in synthetic materials design lies in mimicking such behavior in order to prepare functional membranes with characteristics of native protein-assisted ion transport.

A well-known example of synthetic ion-selective membranes is the perfluorinated ionomer membranes, e.g. Nafion [2]. In addition to the robust mechanical properties and chemical stability, Nafion membranes provide an unusual degree of permeability selectivity in favor of cations over anions, which exceeds the limit of Donnan permselectivity [3]. This unique feature has been referred as "superselectivity" that is related to the formation of ionic clusters in Nafion membranes. A number of structural models have been proposed to address the unique properties of Nafion, the typical of which are presented in Figure 1. Yeager *et al* proposed a model with three different regions of Nafion backbone, interfacial zone and ionic cluster [4]. Gierke *et al* proposed an ionic cluster model which was based on the formation of micelles that are interconnected via narrow ionic channels [5]. Recently, by modeling the SAXS diffractograms of hydrated Nafion, Schmidt-Rohr *et al* proposed that Nafion membranes consist of arrays of oriented ionic nano-channels which are embedded in a locally aligned polymer matrix [6]. The channel structure was further evidenced by the study of anisotropy of water diffusion as probed by NMR spectroscopy [7,8]. Although these models do not provide an unambiguous explanation of the ion conduction in Nafion, the formation of ionic transport channels is now generally accepted. It is clear that controlling the properties of ion conducting membranes requires a profound knowledge of their chemical

structure and nanoscale morphology. Therefore, a study of a model system with a well-defined ionic channel structure, which holds promise for membrane applications, can be very instructive for a better understanding the structure and properties of Nafion.

Supramolecular assembly of low molecular weight compounds is known to generate a large diversity of cylindrical structures [9]. Of particular interest are wedge-shaped amphiphilic molecules bearing a large hydrophobic rim and a polar group at the tip of the wedge. Such systems generally tend to form well-defined cylindrical superstructures with polar groups aligned in the vicinity of the cylinder axis [10-13]. Recently, it is demonstrated in our group that wedge-shaped sulfonate amphiphiles self-assemble into supramolecular columns with sulfonate groups stacked along the columnar axis, thereby forming an ion channel with a well-defined geometry [14-16]. In this work, a wedge-shaped sulfonate molecule, namely sodium 2,3,4-tris(11'-acryloyloxyundecyl-1'-oxy)benzenesulfonate (A-Na), is studied.

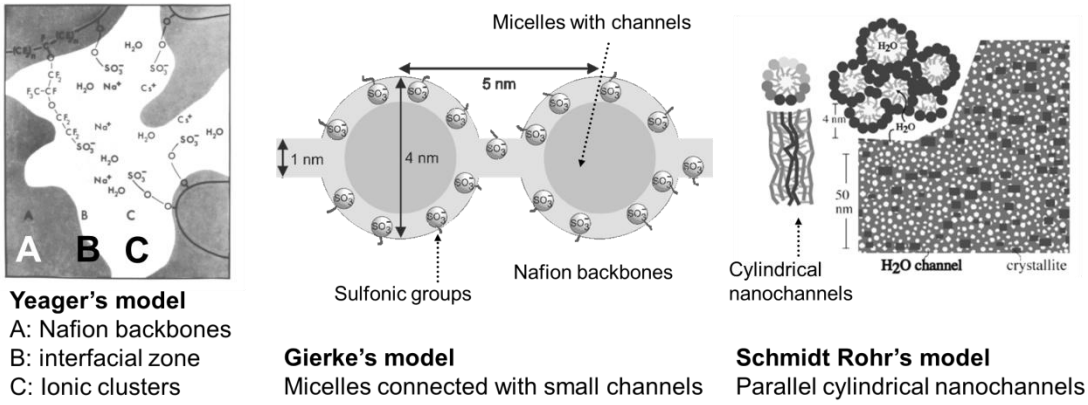

Figure 1. Schematic illustrations of structural models of Nafion proposed by Yeager *et al* [4], Gierke *et al* [5] and Schmidt-Rohr *et al* [6], respectively.

In addition, it is known that an "ionic peak" appears in SAXS in the hydrated state of Nafion and shifts to lower angles with the increase of water content [17], indicating that water plays a pivotal role in the structure of Nafion. Thus, the mesostructure of A-Na is studied as a function of RH, and is then correlated to the water uptake and ion conductivity. Henceforward, a relationship between the mesostructure, ion conductivity and water content of a well-defined channel-forming supramolecular system is established, and is then compared with the structural models of Nafion membranes.

3.2. Experimental

3.2.1. Synthesis

The synthesis and chemical characterization of sodium 2,3,4-tris(11'-acryloyloxyundecyl-1'-oxy)benzenesulfonate (A-Na) are described in Chapter 2.

3.2.2 Differential scanning calorimetry (DSC)

The DSC measurements are performed using a Netzsch DSC 204 unit. Samples (typical weight, 8 mg) are enclosed in standard Netzsch 25 μL aluminum crucibles. The measurement steps are (1) heating from 25 ℃ to 100 ℃ at 10 ℃/min, (2) isothermal process at 100 ℃ for 5 minutes, (3) cooling from 100 ℃ to -100 ℃ at 10 ℃/min, (4) isothermal process at -100 ℃ for 5 minutes, (5) heating from -100 ℃ to 100 ℃ at 10 ℃/min.

3.2.3. Polarized optical microscopy (POM)

POM is carried out by sandwiching A-Na film between two glass covers. Images are obtained by using a LEITZ Laborlux 12 POL S with crossed polarizers

equipped with a digital camera DCM 310 with C-mount. Samples are placed in a Mettler stage (FP82HT) together with a container with over-saturated salt solutions of $MgCl_2$, $Mg(NO_3)_2$, KCl and deionized water (33, 55, 86 and 100% RH, respectively) in order to obtain an equilibrated RH atmosphere.

3.2.4. Small-angle X-ray scattering (SAXS)

For SAXS measurements, oriented samples (fibers) of A-Na are prepared with a home-made micro-extruder having the aperture size of 300 μm. The SAXS experiments are performed in transmission geometry at the BM26 beamline of the European Synchrotron Radiation Facility (ESRF) in Grenoble (France). The wavelength is 1.03 Å. The X-ray patterns are recorded with a Pilatus 1M detector. The norm of the reciprocal space vector *s* is calibrated by silver behenate (AgBe). The patterns are corrected for the air scattering.

3.2.5. Grazing-incidence small-angle X-ray scattering (GISAXS)

The GISAXS measurements are performed at the X6B beamline of the National Synchrotron Light Source (NSLS) at Brookhaven National Laboratory (BNL) in New York. The energy used is 11 KeV (the corresponding wavelength is 1.12 Å). X-ray patterns are recorded with a 2D CCD detector (PI-SCX-4300, Princeton Instruments). The norm of the reciprocal space vector *s* is calibrated by silver behenate (AgBe). In the experiments, an incidence angle of 0.4° is used. On the one hand, this value ensures that the structural information is collected over the whole film thickness. On the other hand, it allows simplifying the appearance of GISAXS patterns since the intensity of reflections generated by the reflected beam becomes negligible.

The A-Na thin films (ca. 100 nm thick) are prepared by spin-coating the solutions in chloroform (20 g/L) on Si substrates (100) (ITME, Institute of Electronic Materials Technology Warszawa; Poland). The silicon wafers are preliminary cleaned

by immersion in piranha solution (H_2SO_4:H_2O_2, 3:1) for 20 minutes and subsequent rinsing with deionized water. For spin-coating, a rotation speed of 2500 rpm is applied during 45 seconds. The surface morphology of spin-coated films of A-Na is investigated with Atomic Force Microscopy (AFM) using a multimode instrument coupled to a NanoScope IV controller from Veeco Metrology Group.

A humidity chamber containing an open vessel filled with deionized water (Figure 2) is used to create saturated H_2O vapor atmosphere. This allows monitoring in real time the swelling of the mesophase.

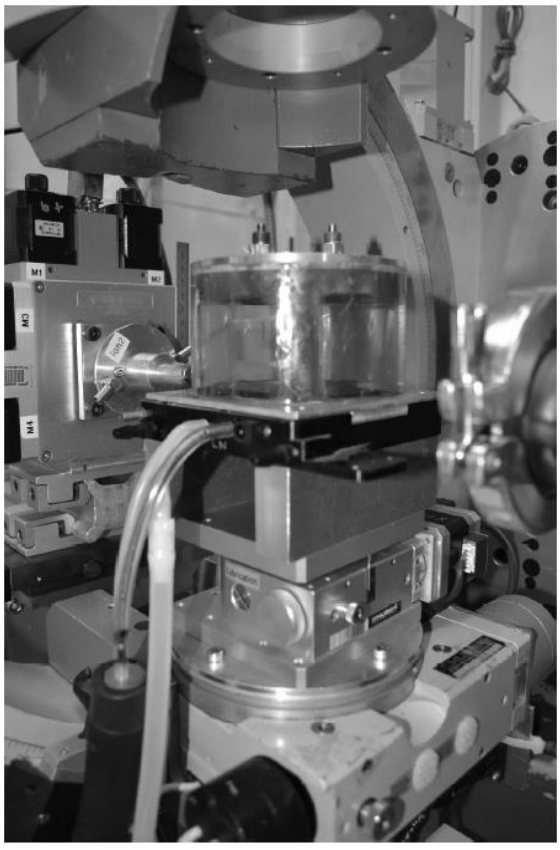

Figure 2. Humidity chamber used for in-situ GISAXS measurements at the X6B beamline of NSLS.

3.2.6 Through-plane ion conductivity

Through-plane ion conductivity is measured by impedance spectroscopy using an Electrochemical Workstation IM6 (Zahner-Elektrik GmbH&Co. KG, Germany). The spectra are recorded with amplitude of 1V in 10^0 to 10^6 Hz frequency range. The resistances of each sample are obtained by fitting the impedance spectra using a model containing a serial connection of a parallel and a serial RC-circuit with the details presented in Figure 3. An example is also given in Figure 3 as to show the fitting impedance spectrum of A-Na under RH=100%. Conductivity of each sample is then calculated according to the equation given in Figure 3.

Samples are prepared similarly as used in POM. The glass sheets are all coated with indium tin oxide (ITO) in a 1*1cm square with two wires connecting the electrodes from a Zahner electrochemical system. The thickness of the samples is around 40 μm.

3.2.7 Relative humidity and water uptake

For SAXS and conductivity measurements, samples are kept at 20 ℃ inside sealed containers under four different RH conditions. The over-saturated solutions of magnesium chloride ($MgCl_2$), magnesium nitrite ($Mg(NO_3)_2$), potassium chloride (KCl) and deionized water are applied to keep the RH at 33%, 55%, 86% and 100%, respectively. Water uptake (λ), expressed in terms of the number of water molecules per sulfonate group, is calculated according to the following equation:

$$\lambda = \frac{m(wet) - m(dry)}{m(dry)} \times \frac{M(Sample)}{M(H_2O)} \qquad \text{(Eq. 3.1)}$$

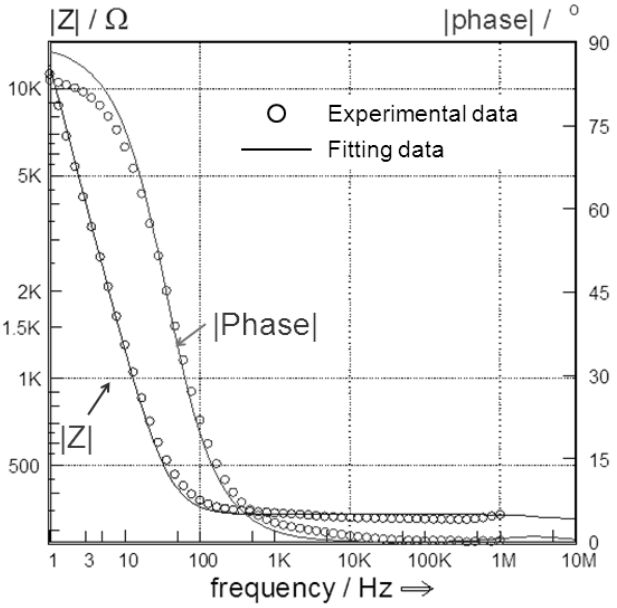

$$\text{Conductivity} = R_{\text{sample}} \frac{\text{Area}}{\text{Thickness}}$$

Figure 3. An example of the data fitting of A-Na sample at RH=100%. The resistance of the sample is obtained by the data fitting, and then the conductivity is obtained by the given equation.

3.3. Results and Discussion

3.3.1 Phase behavior in the dry state

The thermal behavior of A-Na is studied by means of DSC. The DSC thermogram of A-Na (Figure 4a) shows an isotropization temperature of 51 ℃ and a melting enthalpy of 2.86 J/g.

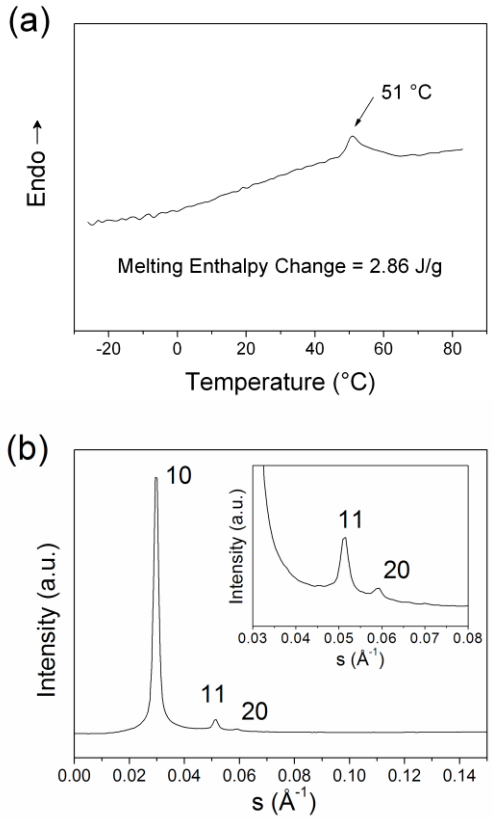

Figure 4. (a) DSC thermograms of A-Na. (b) X-ray diffractogram of dry A-Na.

According to SAXS data, at 25 ℃ the dry extruded fiber sample of A-Na shows three reflections located at s=0.0294 $Å^{-1}$, 0.0515 $Å^{-1}$ and 0.0593 $Å^{-1}$ along the equatorial direction (Figure 4b). Their ratio is found to be 1:√3:2 and they can be attributed to the 100, 110, and 200 reflections of a Col_{hd} lattice with a column diameter of a = 39.0 Å. Based on the lattice parameter and the density that is 1.06±0.04 g/cm^3, the number of molecules presented in the hexagonal elementary cell per average height is estimated to be 4 using the following equation [16], i.e. four molecules arranged into a planar "end-to-end" aggregate with a hydrophilic center

and a hydrophobic rim, which stacks one upon each other to build up a cylinder (Figure 5).

$$N_{EC} = N_A \frac{V \times \rho}{M} \qquad \text{(Eq. 3.2)}$$

where N_{EC} is the number of molecules per 2D unit cell,

N_A is the Avogadro ś number,

M is the molecular weight,

V is the average volume of the 2D unit cell (aliphatic chain distances measured by X-ray),

ρ is the density of each molecules.

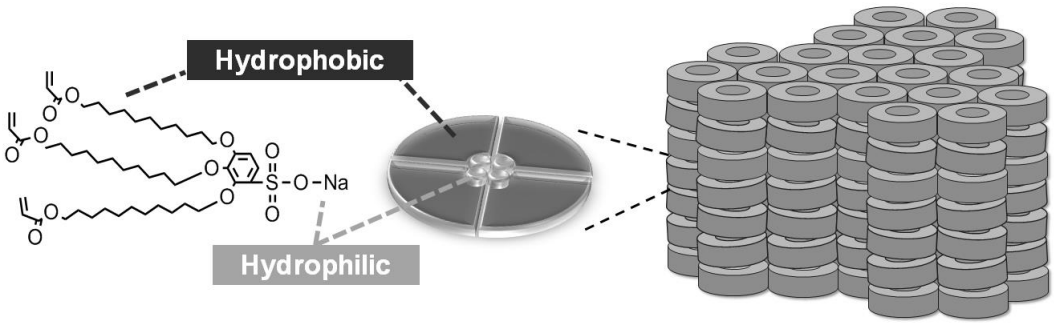

Figure 5. Schematic illustration of four molecules arranged into a planar "end-to-end" aggregate with a hydrophilic center and a hydrophobic rim.

3.3.2 Mesostructures under different relative humidity

To analyze the mesostructures of A-Na under different RH, grazing incidence small angle X-ray (GISAXS) and polarizing optical microscopy are applied, and the results are summarized in Figure 6 and Table 1.

While increasing RH till 55%, the birefringent texture is still visible, and the scattering maximums of 100 and 110 reflections on 2D X-ray patterns indicate that the Col_{hd} phase still remains (Figure 6 and Table 1). The lattice parameter of the Col_{hd} phase increases from 39.2 Å at RH=33% to 40.3 Å at RH=55%. This is resulted from the increase of water content.

However, at higher RH of 86% and 100%, no birefringent textures are observed and meanwhile the 2D X-ray patterns reveal that the mesostructures turn into bicontinuous cubic phases (Cub_{bi}). In detail, the *d* spacings from the scattering maximums are √6: √8: √10: √14: √16: √24: √26 and √2: √3: √4: √6: √8: √9:√10:√11, where the first sequence corresponds to a Gyroid (*G*) phase and the second to a Diamond (*D*) phase. The indexing of the *G* and *D* phases is indicated in Figure 6 and the details are listed in Table 1.

G and *D* phases are two of the three stable bicontinuous phases found in literature [17]. The transformation between them is related to the Bonnet transformation, which allows geometrical changes but coincidentally maintains a constant curvature of the structure [18]. In our system, the interplanar distance of the 321_G-211_D reflections remains almost the same, featuring the $G \rightarrow D$ Bonnet transformation. But according to literatures, the ratio between *G* and *D* lattice parameters should be theoretically around 1.57 [18,19], and in our case the ratio is 1.49. Such difference may originate in the lattice distortions by the stretching force during the $G \rightarrow D$ transition, as some researchers held the same opinion [20-23].

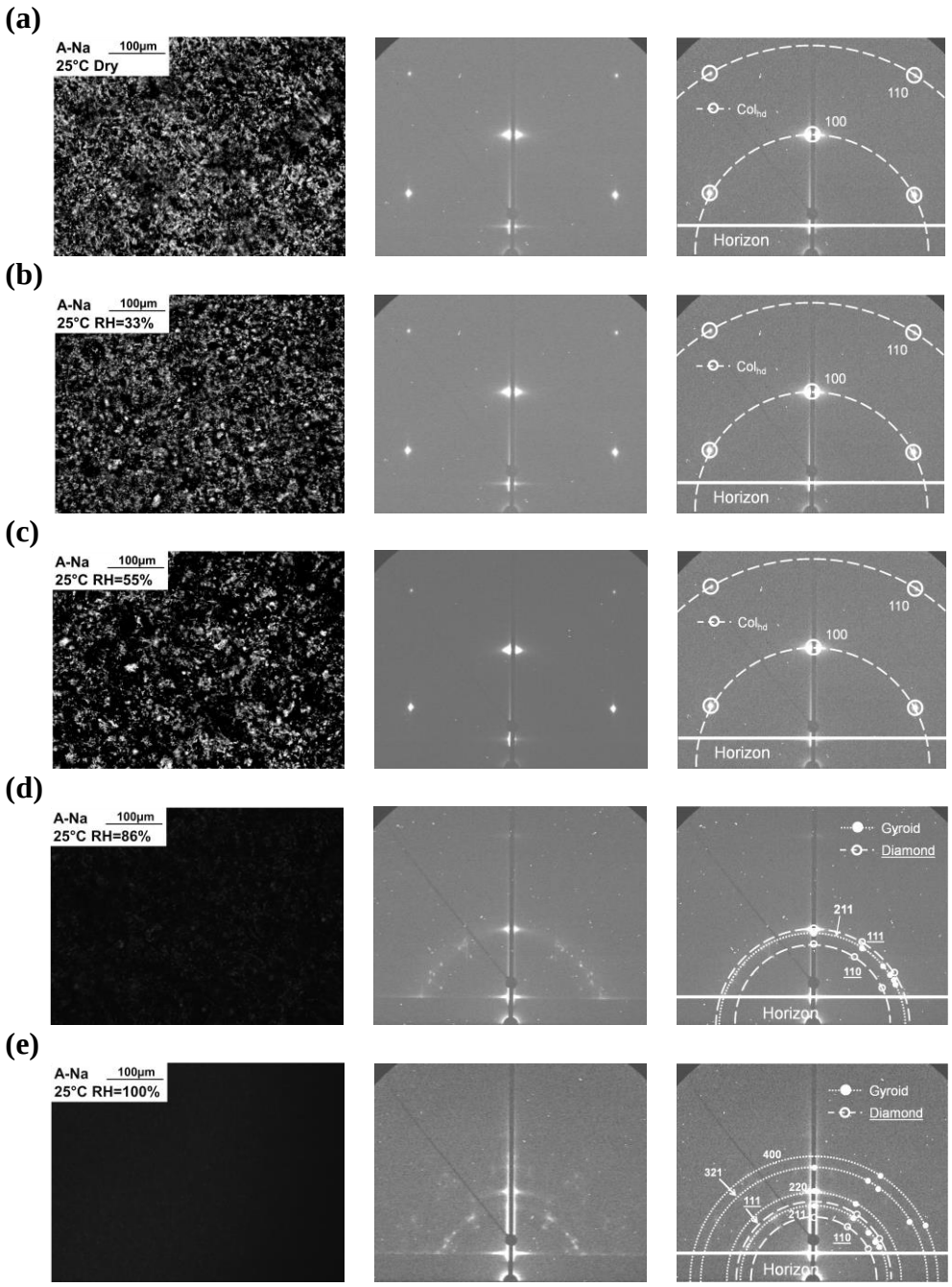

Figure 6. The POM images and 2D X-ray patterns of A-Na under conditions of 25 ℃ and RH of (a) 0% (dry sample), (b) 33%, (c) 55%, (d) 86% and (e) 100%.

Table 1. The indexing the each phase according Figure 6.

RH	Phase	*hkl*	d_{obs} (Å)	d_{calc} (Å)	Lattice Parameter (Å)
0%	Col_{hd}	100	34.0	33.8	39.0
		110	19.4	19.5	
33%	Col_{hd}	100	34.0	34.0	39.2
		110	19.7	19.6	
55%	Col_{hd}	100	34.9	34.9	40.3
		110	20.3	20.2	
86%	*Gyroid*	211	44.9	44.9	110.1
	Diamond	110	52.2	52.5	74.3
		111	43.2	42.9	
100%	*Gyroid*	211	55.4	55.3	135.4
		220	46.2	47.8	
		321	35.8	36.2	
		400	33.1	33.8	
	Diamond	110	64.4	64.7	91.6
		111	53.2	52.9	

3.3.3 The evolution of mesostructures at relative humidity of 100%

The evolution of the mesophase structure is studied with *in-situ* GISAXS on a spin-coated film during the exposure to an atmosphere of RH=100%. Figure 7a shows a Tapping Mode height AFM image of the just prepared film exhibiting "island" morphology typical of a layered structure. The layer thickness extracted from the height cross-section profile (Figure 7b) is approximately 3.7 nm, which is close to *d*-spacing of the peak 100 of the Col_{hd} phase (Figure 7c).

The kinetics of swelling process is monitored with in-situ grazing-incidence small-angle X-ray scattering (GISAXS). It is found that, for the employed sample thickness, the sample structure reaches the equilibrated state within ca. 1.5 hours. Four different states of the sample can be identified during swelling (Figure 7d-e). At the beginning, a highly oriented texture is observed, with the characteristic reflections of a Col_{hd} phase (*cf.* pattern I in Figure 7d). The angular positions of the peaks correspond to the planar alignment of the Col_{hd} phase as depicted in Figure 7c. As swelling proceeds, the *d*-spacing corresponding to the 100 reflection increases from 3.41 to 4.47 nm indicating an increase of the lattice parameter by more than 30 %, i.e. from 3.94 to 5.16 nm (*cf.* regions II in Figure 7e). At this stage, another phase forms, as can be inferred from appearance of a series of diffraction peaks (*cf.* pattern II in Figure 7d). A detailed study of the appearing phase shows that it consists of a mixture of two Cub_{bi} phases. The ratios of the *d*-spacings corresponding to the newly forming phases are given by $\sqrt{6}$: $\sqrt{8}$: $\sqrt{14}$: $\sqrt{16}$: $\sqrt{24}$ and $\sqrt{2}$: $\sqrt{3}$: $\sqrt{4}$, respectively. Taken into account the extinction rules, these peaks can be assigned to cubic lattices with space groups Ia3d and Pn3m, respectively. For the sake of brevity, these phases are commonly termed as gyroid (*G*) and diamond (*D*), although double gyroid and double diamond are more appropriate terms to define their structure according to the IUPAC recommendations [24].

The Miller indices of the main reflections of the Cub_{bi} phases are indicated in Figure 7d (*cf.* patterns III and IV). The azimuthal angles of the main reflections are in good agreement with those calculated and observed for similar structures [25,26]. The phase sequence observed in our experiment follows the behavior expected for hydration of the type II, or inverse, mesophases [27,28].

It is noteworthy that the *G* and *D* phases are two of the three stable Cub_{bi} phases identified so far [17,28,29]. During the swelling process, the lattice parameter of the *G*-mesophase continuously increases by about 30% from 10.73 to 13.91 nm. The

lattice parameter of the *D*-mesophase shows a comparable relative increase from 7.15 to 9.53 nm (*cf*. patterns III and IV in Figure 7d and region IV in Figure 7e). Both structures are topologically equivalent, showing degenerated curvature energies, and theoretically can be interconverted [17]. They are related by the so-called Bonnet transformations which allow geometrical changes while maintaining a constant interfacial curvature of the amphiphilic bilayer [17,21]. According to this model, the ratio between the lattice parameters of the two phases should be 1.57 [21,30,31]. In our case, the ratio is found to slightly increase during swelling from 1.41 to 1.55. The initial difference with the theoretical value may due to lattice distortions caused by swelling or due to stretching during the $G \rightarrow D$ transition, as is suggested by some authors [31].

Previously, several studies have addressed the epitaxial relationships in phase transitions involving bicontinous cubic phases [27,32-35]. According to these studies, the columnar axis of the Col_{hd} phase coincides with the **111** direction of the Cub_{bi} phase in Col_{hd} to *G* transition. In this case, reciprocal space vectors **100** of Col_{hd} phase and **211** of Cub_{bi} phase are expected to coincide. This relation can be indeed observed in pattern III of Figure 7d. The ratio between the lattice parameters of the Col_{hd} and *G* phases measured in region III (Figure 7e) is found to be close to 2.2, which is in good agreement with the values reported previously for type II mesophases [34]. It is worth mentioning that although the same orientation of *G* phases, i.e. with the **211** planes oriented parallel to the film surface, has been observed in different systems [36,37], the epitaxial relations pertinent to such phase transitions of ionic liquid crystals induced by humidity have not been reported in the literature to date, to our knowledge.

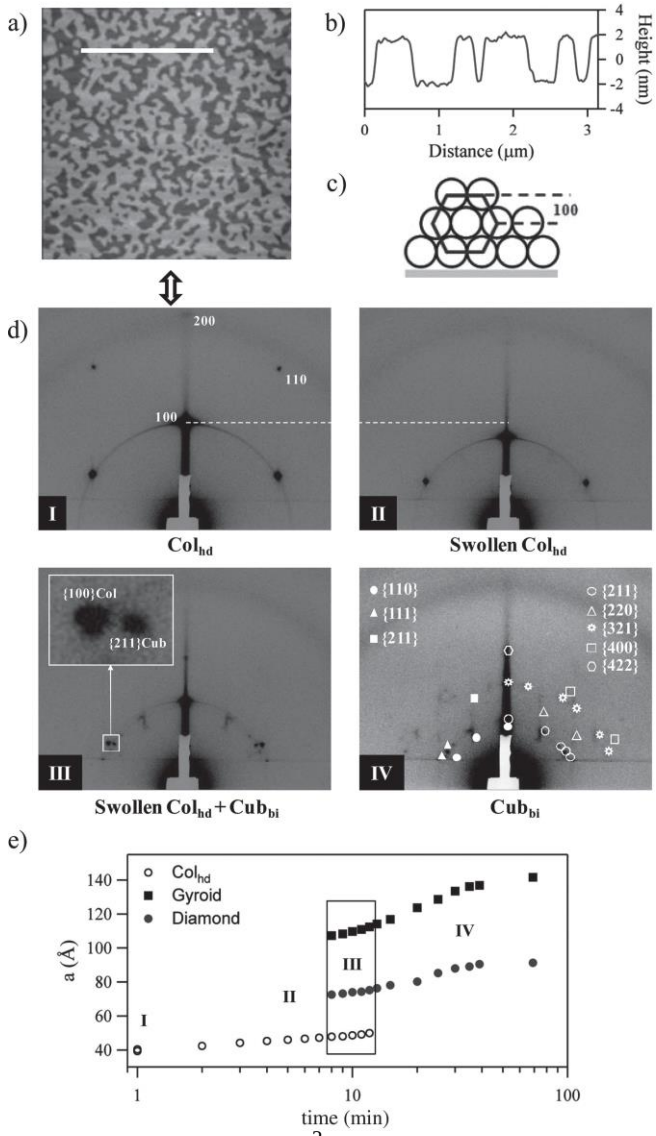

Figure 7. a) AFM height image (6*6 μm^2) of a spin-cast A-Na film. b) Height cross-section profile traced along the line indicated in (a). c) Schematic view of the planar orientation of the columnar mesophase. d) 2D GISAXS patterns recorded at different swelling times at RH of 100%. The Miller indices of the main reflections pertinent to each of the phases are indicated in (d-I) and (d-IV). *Cub$_{bi}$* phases are indicated as follows: Gyroid (empty symbols-right side of (3d-IV)) and Diamond phase (filled symbols-left side of (3d-IV)). The white dotted line highlights the shift of the *Col$_{hd}$* 100 peak position due to swelling. e) Evolution of the lattice parameter of *Col$_{hd}$* and *Cub$_{bi}$* phases during swelling. The region of coexistence of the two phases is highlighted with a box.

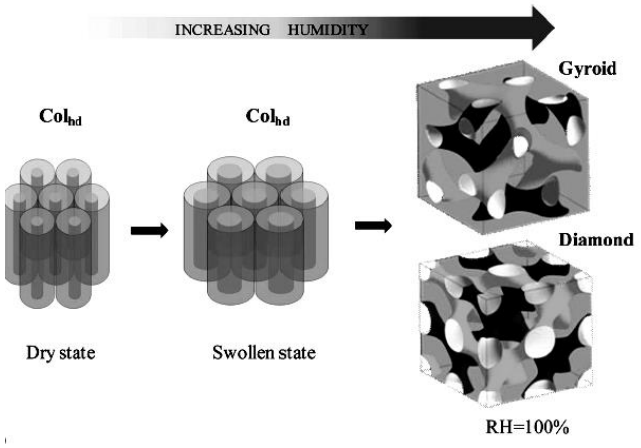

Figure 8. Evolution of the channel structure of A-Na with increase in water content. The channels are given in the Col_{hd} phase and the Cub_{bi} phase, respectively.

Figure 8 summarizes the phase evolution of the channel structure formed by the A-Na with increase of the water content. In the Col_{hd} structure, the columnar diameter continuously increases indicating that the mesophase structure and, in particular the packing of flexible alkyl chains, can efficiently adapt to a significant increase of the ionic channel radius [28].

3.3.4. Ion Conductivity Study

The ion conductivity is measured using AC impedance spectroscopy. As shown in Figure 9, the dry A-Na exhibits very low ion conductivity. By water uptake upon increasing humidity, the ion conductivity increases up to 4 orders of magnitude at RH=55%, and further 4 times at RH=100%. According to gravimetry analysis, the water uptake λ expressed in the number of water molecules per sulfonate group

depends strongly on the RH. Figure 9 shows a comparable small increase of λ to around 2 from dry state to RH=55%. After that, the water update is considerably enhanced by increasing λ *to* 8 at RH=100%. Interestingly, although the conductivity and water uptake of A-Na are systematically lower than that of the protonated Nafion [38], their humidity dependences of both systems look quite similar [39,40].

Figure 9 presents the impedance and phase spectra as a function of frequency. It can be seen that at dry state, A-Na exhibits a strong dependence of impedance on frequency, and meanwhile the absolute phases are very high (close to 80 degrees) at frequencies from 10^2 to 10^6 Hz. It implies that the mobility of the ions is very low. At wet state from RH=33% to 100%, A-Na shows a gradually weakened dependence of the impedance on frequency and reduced phase (Figure 7), indicating the improved ion conductivity.

Table 1. The ion conductivities of A-Na. The standard deviations are in the brackets with the same order of magnitude.

Sample	Ion Conductivity (S/m)				
	Dry state	RH=33%	RH=55%	RH=86%	RH=100%
A-Na	6.22×10^{-9} (2.44)	2.56×10^{-6} (0.83)	8.66×10^{-5} (0.70)	1.45×10^{-4} (0.26)	2.95×10^{-4} (1.45)

Table 2. The water uptakes of A-Na. The standard deviations are in the brackets.

Sample	Water Uptake (H_2O/SO_3^-)			
	RH=33%	RH=55%	RH=86%	RH=100%
A-Na	1.03 (0.03)	1.80 (0.26)	4.28 (0.47)	8.58 (0.35)

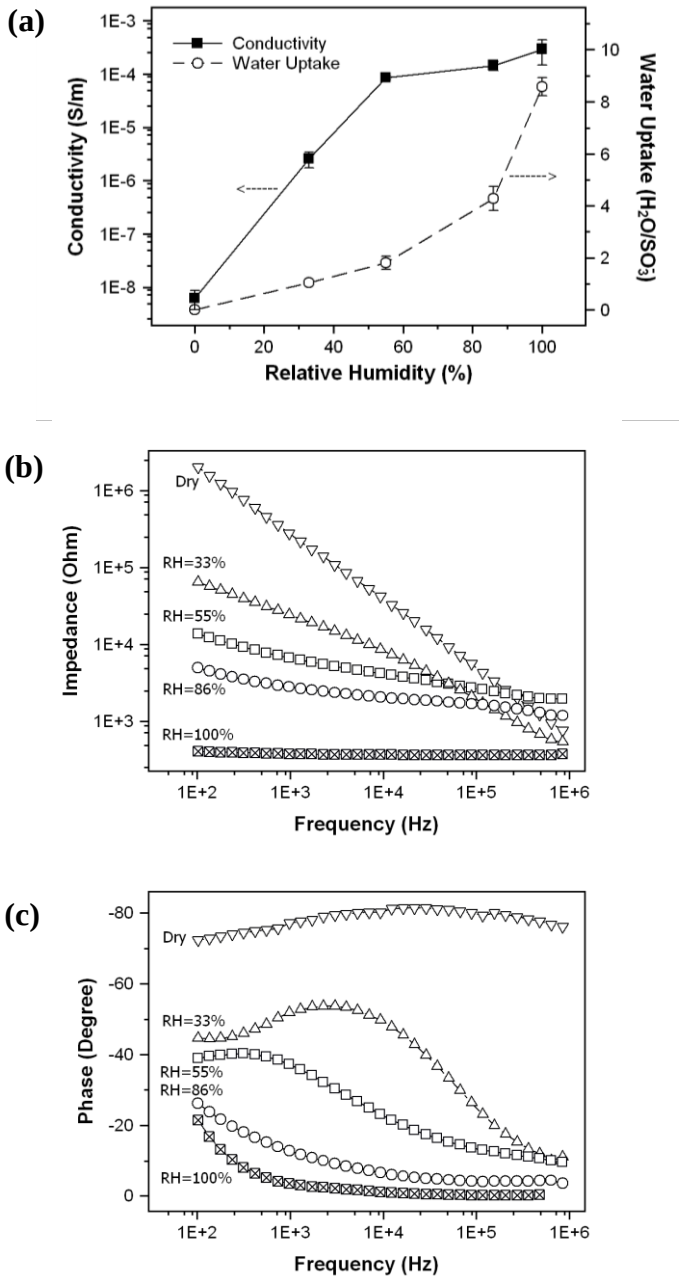

Figure 9. (a) The dependence of conductivity and water uptake (λ – number of water molecules per sulfonate group) with relative humidity. At dry state RH is set to be 0% and λ is 0. (b) The dependence of impedance on frequency under different RH. (c) The dependence of phase on frequency under different RH.

Similarly to the Nafion's behavior, the presence of water is necessary to reach high ion conductivity. As shown in Figure 2, the slight increase of water uptake in the Col_{hd} phase (λ from 0 to 2) is accompanied by a significant enhancement of the ion conductivity by approximately 4 orders of magnitude. It implies that, during swelling, water molecules penetrate into the ion channel, enlarge it and act as vehicles for the ion transport. At higher RH conditions, the formation of a 3D bicontinuous water channel structure has been observed. The newly formed gyroid structure generates more inter-connected conducting pathways, thus it improves the conductivity further by 4 times as compared with the swollen columnar structure. These results seem to be in favor of the water-channel model [6], the structural-inversion network model [41] and the percolation network model [42] of the Nafion structure. It has been shown that in a system with ion channels, a small amount of water can already efficiently create conductive channels for ions. Furthermore, the swelling of these channels can give rise to a percolated network of ion conductive paths, and improve further the conductivity.

In addition, the formation of Cub_{bi} phases can also be of paramount interest for separation applications. Unlike the columnar phases, the bicontinuous cubic phases would not require macroscopic channel alignment to facilitate ion transportation because of their 3D interconnected channel networks.

3.4. Conclusion

In conclusion, it is shown that in a supramolecular system with self-assembled ion channels a small amount of water can already efficiently create highly conductive pathways for ions. Furthermore, swelling of the hexagonal columnar structure can

give rise to the formation of a percolating network of ion conductive paths improving further the conductivity. The formation of a bicontinuous cubic phase on swelling can be of paramount interest for separation applications. Unlike columnar phases, the cubic phases would not require macroscopic channel alignment to facilitate ion transportation because of their 3D interconnected channel networks. These results provide a more detailed image of the processes occurring in a channel-forming system upon swelling and support the water-channel model over the cluster model for the structure of Nafion. In future, it is aimed to arrest different supramolecular morphologies by polymerization of acrylic end-groups to fabricate mechanically stable nanoporous membranes with a tailored channel structure for the applications in separation as well as catalysis.

3.5. References

[1] Alberts, B; Johnson, A; Walter, P; Lewis, J; Raff, M; Roberts, K. Molecular Biology of the Cell 5th Ed., Garland Science, New York, **2008**.

[2] Mauritz, KA; Moore, RB. State of understanding of Nafion, *Chem. Rev.*, **2004**, *104* (10), 4535-4585.

[3] Hefferich, F. Ion Exchange, McGraw-Hill, New York, **1962**.

[4] Yeager, HL; Steck, A. Cation and water diffusion in Nafion ion-exchange membranes - Influence of polymer structure, *J. Electrochem. Soc.*, **1981**, *128* (9), 1880-1884.

[5] Gierke, TD; Munn, GE; Wilson, FC. The morphology in Nafion perfluorinated membrane products, as determined by wide-angle and small-angle X-ray studies, *J. Polym. Sci., Part B: Polym. Phys.*, **1981**, *19* (11), 1687-1704.

[6] Schmidt-Rohr, K; Chen, Q. Parallel cylindrical water nanochannels in Nafion fuel-cell membranes, *Nat. Mater.*, **2008**, *7* (1), 75-83.

[7] Li, J; Park, JK; Moore, RB; Madsen, LA. Linear coupling of alignment with transport in a polymer electrolyte membrane, *Nat. Mater.*, **2011**, *10* (7), 507-511.

[8] Li, J; Wilmsmeyer, KG; Madsen, LA. Anisotropic diffusion and morphology in perfluorosulfonate ionomers investigated by NMR, *Macromolecules*, **2009**, *42* (1), 255-262.

[9] Shimizu, T. Self-Assembled Nanomaterials I - Nanofibers, Springer, Berlin, **2008**.

[10] Beginn, U. Thermotropic columnar mesophases from N-H center dot center dot center dot O, And N center dot center dot center dot H-O hydrogen bond supramolecular mesogenes, *Prog. Polym. Sci.*, **2003**, *28* (7), 1049-1105.

[11] Percec, V; Heck, J; Johansson, G; Tomazos, D; Kawasumi, M; Chu, P. Molecular recognition directed self-assembly of supramolecular liquid-crystals, *Mol. Cryst. Liq. Cryst. Sci. Technol., Sect. A*, **1994**, *254*, 137-196.

[12] Percec, V; Heck, J; Johansson, G; Tomazos, D; Ungar, G. Towards tobacco mosaic virus-like self-assembled supramolecular architectures, *Macromol. Symp.*, **1994**, *77*, 237-265.

[13] Rosen, BM; Wilson, CJ; Wilson, DA; Peterca, M; Imam, MR; Percec, V. Dendron-mediated self-assembly, disassembly, and self-organization of complex systems, *Chem. Rev.*, **2009**, *109* (11), 6275-6540.

[14] Beginn, U; Yan, LL; Chvalun, SN; Shcherbina, MA; Bakirov, A; Moller, M. Thermotropic columnar mesophases of wedge-shaped benzenesulfonic acid mesogens, *Liq. Cryst.*, **2008**, *35* (9), 1073-1093.

[15] Zhu, XM; Scherbina, MA; Bakirov, AV; Gorzolnik, B; Chvalun, SN; Beginn, U; Moller, M. Methacrylated self-organizing 2,3,4-tris(alkoxy)benzenesulfonate: A new concept toward ion-selective membranes, *Chem. Mater.*, **2006**, *18* (19), 4667-4673.

[16] Zhu, XM; Tartsch, B; Beginn, U; Moller, M. Wedge-shaped molecules with a sulfonate group at the tip - A new class of self-assembling amphiphiles, *Chem. Eur. J.*, **2004**, *10* (16), 3871-3878.

[17] Schwarz, US; Gompper, G. Stability of inverse bicontinuous cubic phases in lipid-water mixtures, *Phys. Rev. Lett.*, **2000**, *85* (7), 1472-1475.

[18] Luzzati, V. Polymorphism of lipid-water systems - Epitaxial relationships, area-per-volume ratios, polar apolar partition, *J. Phys. II*, *5* (11), 1649-1669.

[19] Barauskas, J; Landh, T. Phase behavior of the phytantriol/water system, *Langmuir*, **2003**, *19* (23), 9562-9565.

[20] Sadoc, JF; Charvolin, J. Infinite periodic minimal-surfaces and their crystallography in the hyperbolic plane, *Acta Crystallogr., Sect. A: Found. Crystallogr.***,** *45*, 10-20.

[21] Fogden, A; Hyde, ST. Continuous transformations of cubic minimal surfaces, *Eur. Phys. J. B*, **1999**, *7* (1), 91-104.

[22] Feng, Y; Yu, ZW; Quinn, PJ. Stable cubic phases in codispersions of glucocerebroside and palmitoyloleoylphosphatidylethanolamine, *Chem. Phys. Lipids*, **2003**, *126* (2), 141-148.

[23] Giacomelli, FC; Da Silveira, NP; Nallet, F; Cernoch, P; Steinhart, M; Stepanek, P. Cubic to hexagonal phase transition induced by electric field, *Macromolecules*, **2010**, *43* (9), 4261-4267.

[24] McNaught, AD; Wilkinson, A. IUPAC Compedium of Chemical Terminology, 2nd Ed., Blackwell Scientific Publicaions, **1997**.

[25] Lee, B; Park, I; Yoon, J; Park, S; Kim, J; Kim, KW; Chang, T; Ree, M. Structural analysis of block copolymer thin films with grazing incidence small-angle X-ray scattering, *Macromolecules*, **2005**, *38* (10), 4311-4323.

[26] Hayward, RC; Alberius, PCA; Kramer, EJ; Chmelka, BF. Thin films of bicontinuous cubic mesostructured silica templated by a nonionic surfactant, *Langmuir*, **2004**, *20* (14), 5998-6004.

[27] Seddon, JM; Templer, RH. Cubic phases of self-assembled amphiphilic aggregates, *Philos. Trans. R. Soc. London, Ser. A*, **1993**, *344* (1672), 377-401.

[28] Kaasgaard, T; Drummond, CJ. Ordered 2-D and 3-D nanostructured amphiphile self-assembly materials stable in excess solvent, *Phys. Chem. Chem. Phys.*, **2006**, *8* (43), 4957-4975.

[29] Hyde, ST; Holmberg, K. Handbook of Applied Surface and Colloid Chemistry, John Wiley & Sons, Weinheim, **2001**.

[30] Hyde, ST. Bicontinuous structures in lyotropic liquid crystals and crystalline hyperbolic surfaces, *Curr. Opin. Solid State Mater. Sci.*, **1996**, *1* (5), 653-662.

[31] Squires, AM; Templer, RH; Seddon, JM; Woenkhaus, J; Winter, R; Narayanan, T; Finet, S. Kinetics and mechanism of the interconversion of inverse bicontinuous

cubic mesophases, *Phys. Rev. E: Stat. Nonlinear Soft Matter Phys.*, **2005**, *72* (1), 011502.

[32] Chvalun, SN; Shcherbina, MA; Bykova, IV; Blackwell, J; Percec, V. Two- And three-dimensional mesophases formed by monodendrons based on gallic acid with partially fluorinated alkyl tails, *Polym. Sci. Ser. A Polym. Phys.***,** *44* (12), 1281-1289.

[33] Clerc, M; Levelut, AM; Sadoc, JF. Transitions between mesophases involving cubic phases in the surfactant-water systems - Epitaxial relations and their consequences in a geometrical framework, *J. Phys. II***,** *1* (10), 1263-1276.

[34] Luzzati, V. Polymorphism of lipid-water systems - Epitaxial relationships, area-per-volume ratios, polar apolar partition, *J. Phys. II*, **1995**, *5* (11), 1649-1669.

[35] Rancon, Y; Charvolin, J. Epitaxial relationships during phase-transformations in a lyotropic liquid-crystal, *J. Phys. Chem.*, **1988**, *92* (9), 2646-2651.

[36] Crossland, EJW; Kamperman, M; Nedelcu, M; Ducati, C; Wiesner, U; Smilgies, DM; Toombes, GES; Hillmyer, MA; Ludwigs, S; Steiner, U; Snaith, HJ. A bicontinuous double gyroid hybrid solar cell, *Nano Lett.*, **2009**, *9* (8), 2807-2812.

[37] Urade, VN; Wei, TC; Tate, MP; Kowalski, JD; Hillhouse, HW. Nanofabrication of double-gyroid thin films, *Chem. Mater.*, **2007**, *19* (4), 768-777.

[38] Zawodzinski, TA; Derouin, C; Radzinski, S; Sherman, RJ; Smith, VT; Springer, TE; Gottesfeld, S. Water-uptake by and transport through Nafion(r) 117 membranes, *J. Electrochem. Soc.*, **1993**, *140* (4), 1041-1047.

[39] Choi, P; Jalani, NH; Datta, R. Thermodynamics and proton transport in Nafion, *J. Electrochem. Soc.*, **2005**, *152* (3), E123-130.

[40] Hwang, GS; Kaviany, M; Gostick, JT; Kientiz, B; Weber, AZ; Kim, MH. Role of water states on water uptake and proton transport in Nafion using molecular simulations and bimodal network, *Polymer*, **2011**, *52* (12), 2584-2593.

[41] Gebel, G. Structural evolution of water swollen perfluorosulfonated ionomers from dry membrane to solution, *Polymer*, **2000**, *41* (15), 5829-5838.

[42] Weber, AZ; Newman, J. Transport in polymer-electrolyte membranes - I. Physical model, *J. Electrochem. Soc.*, **2003**, *150* (7), A1008-A1015.

Chapter 4

Alignment of Columnar Structures of Sodium 2,3,4-Tris(11'-acryloyloxyundecyl-1'-oxy)benzenesulfonate

In this chapter, the orientation of the disordered hexagonal columnar phase formed by a wedge-shaped amphiphilic sulfonate molecule: sodium 2,3,4-tris(11'-acryloyloxyundecyl-1'-oxy) benzenesulfonate (A-Na) is studied. The columns of A-Na are oriented preferentially in plane (homogeneous or planar orientation) on both hydrophilic and hydrophobic substrates. Anodized aluminium oxide (AAO) porous substrate with an average pore diameter of 25 nm is used to achieve a homeotropic orientation of the columnar phase. It is shown by X-ray scattering measurements that the supramolecular columns in the pores of AAO substrate are oriented perpendicular to the substrate plane and this orientation even spreads to the whole sample out of the pores. It is further demonstrated that the oriented sample has a higher conductivity than that of a non-oriented one.

4.1. Introduction

Perfluorinated sulfonic acid ionomer membranes, e.g. Nafion, are a well-known example of industrially applied ion-exchange membranes. According to the structural analysis using scattering techniques, several models have proposed to reveal the mesostructure of Nafion and the mechanism of high ion conducting properties [1-8]. Quite recently, Schmidt-Rohr *et al* proposes that the Nafion membranes consist of oriented ionic nano-channels which are embedded in the locally aligned polymer matrix [8]. This nano-channel formation is addressed by further studies, in which the alignment of nano-channels in different Nafion membranes is quantitatively measured using ^2H NMR on residually aligned absorbed D_2O. It is found that the channels are biaxially oriented in the membrane plane for extruded membranes, whereas they are uniaxially oriented perpendicular to the plane for dispersion-cast membranes [9]. Further, a linear coupling of alignment with water transport is detected [10]. However, so far the influence of the ionic channel orientation on the ion-conductivity of the Nafion membranes has not been reported.

Supramolecular assembly of low-molecular-weight compounds is a convenient tool to generate a large diversity of structures [11-17], some of which can be applicable for creating ion-conductive membranes. Of particular interest are wedge-shaped amphiphilic molecules bearing a large hydrophobic rim and a polar group at the tip of the wedge. These materials generally tend to form well-defined cylindrical superstructures with polar groups arranged along the cylinder axis, which in turn form columnar mesophases in bulk [15-17]. A major advantage of liquid crystalline materials is their ability to align over macroscopic lengths in external fields. In previous chapters we described the synthesis and characterization of wedge-shaped sulfonates, i.e. 2,3,4-tris(11'-acryloyloxyundecyl-1'-oxy)benzenesulfonates. It was shown that the sodium and potassium salts exhibited the formation of a disordered

hexagonal columnar (Col_{hd}) structure under ambient conditions, in which the sufonate groups are stacked in the center of the columns, forming a potential ionic channel. Such a columnar structure shows ionic conductivity especially in the humid atmosphere.

In terms of practical applications, the alignment of the columnar structures is crucial and it is desirable to obtain highly ordered columnar superstructures at a macroscopic level [18,19]. As depicted in Figure 1, there can be two typical column alignments. Planar alignment is when the columns lie parallel to the substrate, and homeotropic alignment is when the columns stand perpendicular. The planar alignment is appropriate for field effect transistors (FETs), while the homeotropic alignment is desired for photovoltaic cells, light emitting diodes (LEDs) or ion conducting membranes [20-23]. Especially for ion conducting membranes, much higher through-plane ion conductivity can be expected when the ionic channels are homeotropically aligned towards the membrane plane.

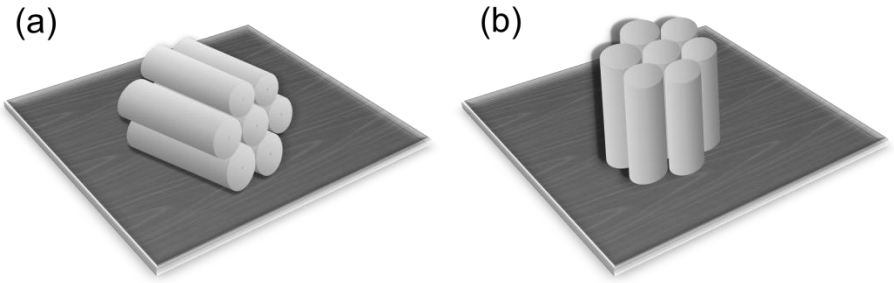

Figure 1. The schematic illustration of two typical column alignments: (a) planar and (b) homeotropic.

However, homeotropic alignment of the columnar structures is still a great challenge. Approaches reported in literature include the control of annealing process [21], the use of porous, nano-patterned or energy-tuned surfaces [24-28], the drive of alternative electric fields [29-31], and etc. In this chapter, an optimal condition for the

homeotropic alignment of the Col_{hd} phase formed by sodium 2,3,4-tris(11'-acryloyloxyundecyl-1'-oxy)benzenesulfonate (A-Na) is addressed and the influence of surface energy of substrates on the orientation of supramolecular columns is studied. Most importantly, it is described how nanoporous anodic aluminum oxide templates (AAO) can be used in a simple manner to obtain the homeotropic alignment of the Col_{hd} phase formed by A-Na. The oriented films are characterized by means of polarizing optical microscopy (POM), X-ray scattering technique and conductivity measurements.

4.2. Experimental

4.2.1 Synthesis

The materials and the synthesis of sodium 2,3,4-tris(11'-acryloyloxyundecyl-1'-oxy)benzenesulfonate (A-Na) are listed in Chapter 2.

4.2.2 Preparation of silicon wafer and AAO substrates

Silicon wafer substrates (ITME, Institute of Electronic Materials Technology Warszawa, Poland) are cleaned using piranha solution (H_2SO_4:H_2O_2, 3:1) prior to use. PTFE rubbed surface is obtained by sliding a PTFE rod at 330 ℃ at a speed of 0.6 mm s^{-1}. Both hydrophilic and hydrophobic surfaces are prepared using hexadecyltrichlorosilane and n-(6-aminohexylamino-propyl-trimethoxysilane) to functionalize the silicon wafer substrates with hexadecyl and amine groups, respectively. AAO substrates (Whatman. Nominal pore size: 25 nm diameter, 60 μm

thick) are cleaned in methanol under ultrasonication for 30 minutes. Thin films of A-Na on silica wafer substrates are prepared by spin coating from A-Na solutions in $CHCl_3$ (20 mg ml^{-1}) with a rotation speed of 2500 rpm during 45 s.

4.2.3 Scanning electron microscopy (SEM)

One side of the AAO substrate is coated with gold under argon in a coating equipment at 30 mBar for 30 seconds; while the other side is not coated. And then both sides are investigated by a scanning electron microscope (SEM, HITACHI, S-4800).

4.2.4 Preparation of films of A-Na on AAO and glass substrates

The A-Na thick films on the AAO substrate (AAO-samples) are prepared by drop-casting of a solution in $CHCl_3$ (20 mg/ml) on the AAO uncoated side. After the evaporation of the solvent, the AAO-sample is annealed for 3 hours at 50 ℃. The A-Na films on the glass substrate (glass-samples) are prepared as reference in the same way.

4.2.5 Polarized optical microscopy (POM)

POM images are obtained by using a LEITZ Laborlux 12 POL S with crossed polarizers equipped with a digital camera DCM 310 with C-mount.

4.2.6 X-ray diffraction measurements

X-ray diffraction experiments in transmission geometry were carried out at the ID13 beamline at the European Synchrotron Radiation Facility (ESRF) (Grenoble, France). The wavelength used was of $\lambda = 0.81$ Å. X-ray patterns were recorded by a two-dimensional CCD camera (FReLoN Kodak CCD). The sample detector distance was calibrated by using a silver behenate standard.

4.2.7 Through-plain ion conductivity

Through-plane ion conductivity measurements are carried out according to Part 3.2.2 Experimental in Chapter 3. The AAO-samples and glass-samples are prepared according to Part 4.2.4 and then sandwiched between two glass sheets coated with ITO. The measurements are carried out at three different relative humidity conditions (RH=0, 33 and 55%). The samples are enclosed at 20 ℃ inside a sealed container for 2 days to reach the equilibrium. Since AAO templates are not conductive, the side connected with the electrode wires is coated with gold in order to achieve a good contact.

4.3. Results and Discussion

4.3.1. Orientation of the Col_{hd} phase of A-Na on different silicon wafer substrates

Figure 2a illustrates the silicon wafer substrates substituted with hydroxyl (–OH), amine ($–NH_2$), alkyl ($–CH_3$), and Teflon ($–CF_2$) groups, and these surfaces are characterized by water contact angles of 16.8 °, 70.9 °, 104.3 °, and 110.7 °, respectively, i.e. ranging from hydrophilic to hydrophobic.

The 2D GIXS patterns obtained from thin film samples of A-Na on different substrates are shown in Figure 2b. All of these patterns reveal in-plane oriented Col_{hd} structures, indicating the columnar structure of A-Na exhibits preferentially a planar alignment on either hydrophilic or hydrophobic substrates. The column diameter of a=39.2Å remains constant for all samples. Miller indices of the reflections are presented in Figure 2b.

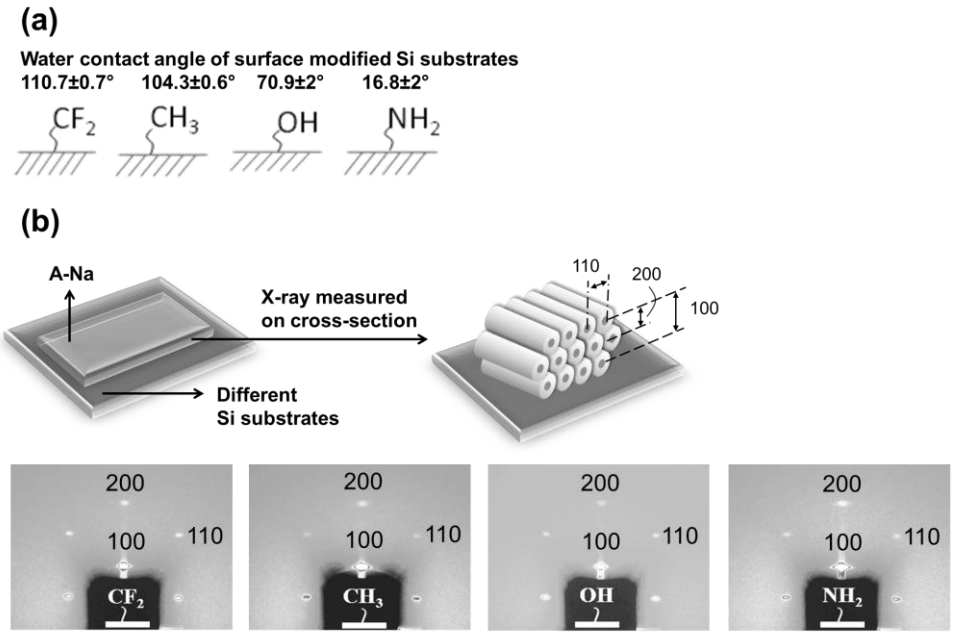

Figure 2. (a) Different silicon wafer substrates. (b) 2D GIXS patterns of thin film samples of A-Na on different silicon wafer substrates.

4.3.2. Orientation of the Col_{hd} phase of A-Na on AAO substrates

Since the homeotropic orientation cannot be achieved for A-Na by tuning the surface energy, nanoporous substrates with perpendicular oriented pores – AAO are used to orient the columnar structure formed by A-Na. Nanoporous materials, like AAO membranes, have shown to be effective substrates to impose orientation of liquid crystalline mesogenes due to confinement effects [32,33].

Prior to the orientation experiments, the AAO substrates were studied by SEM. Figure 4 shows the SEM images of the AAO substrates. On the uncoated side, the pores are quite irregular and the pore diameter is around 25 nm. On the gold-coated side, it seems that gold forms a porous coating with a pore diameter of ca. 250 nm on top of it.

A thick film of A-Na is drop-coated on the non-coated side of the AAO-substrate, and it is denoted as an AAO-sample. The gold-coated side is connected with ITO-coated glass sheets to ensure a good contact in the ion conductivity measurements. In detail, A-Na is firstly solvent-cast on the AAO substrate, and then it is annealed for 3 hours at 50 ℃ after the evaporation of the solvent. A reference sample on a glass substrate (glass sample) is prepared in the same way.

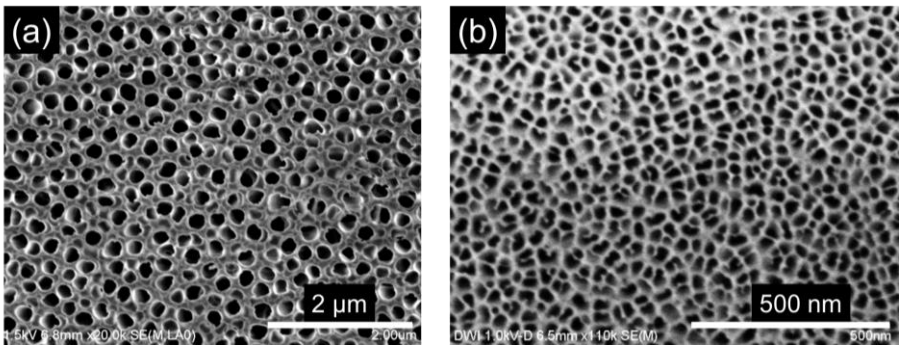

Figure 4. SEM images of AAO substrates: (a) gold-coated side, (b) uncoated side.

Figure 5 shows the polarizing optical microscopy (POM) images of the glass- and AAO- samples before and after thermal treatment, and the X-ray diffractograms of the AAO sample after the thermal treatment are presented in Figure 6.

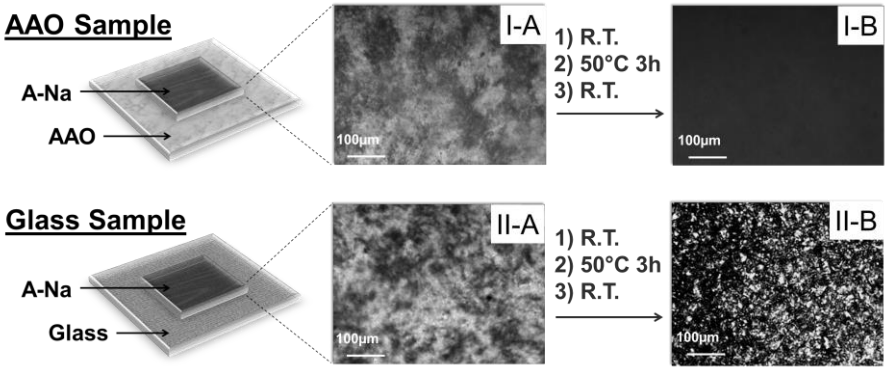

Figure 5. The polarizing optical microscopy images of the AAO- and glass- samples.

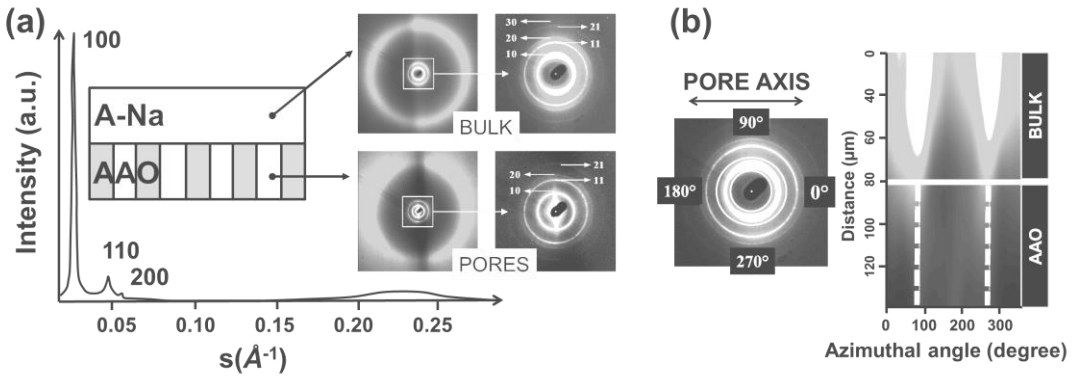

Figure 6. (a) X-ray diffractograms of the AAO sample. The 2D X-ray patterns show the reflections both inside and above the AAO substrate. (b) Azimuthal distribution of scattered intensity of the 100 reflection of the Col_{hd} phase. Two dash lines at 90 ºand 270 ºindicate where the scattering concentrates.

For the AAO-sample, the POM image changes from a birefringent texture into an isotropic one after the thermal treatment, while the texture of the glass sample remains always birefringent.

X-ray microdiffraction is used for the characterization of the films of A-Na on AAO after thermal annealing. A 200 nm diameter beam was used to scan along the cross section of the sample, with the beam parallel to the film surface. Diffraction patterns are collected at intervals of 1 µm allowing comparison of the structure of the mesophase in different regions of the sample, located on the remnant film and inside the AAO template. Figure 3a shows the corresponding 2D X-ray diffraction patterns and a 1D curve, where the scattered intensity is represented as a function of the norm of the scattering vector *s*, obtained by radial integration of the whole angular region. The X-ray diffractogramm displays reflections, which are characteristic of the Col_{hd} phase. The structural parameters both inside and outside the pores are the same. It is important to note that the scattered intensity corresponding to the diffraction peaks is

not homogeneously distributed along the azimuthal angle. This implies the existence of a preferred orientation of the Col_{hd} mesophase.

In order to evaluate the orientation of the columnar phase, a detailed study of the azimuthal distribution of scattered intensity is accomplished. The azimuthal intensity of the 10 reflection is represented as a function of the beam position during the scan. As shown in Figure 6b, the existence of a clear anisotropy can be inferred from the azimuthal intensity distribution, as the dash lines at 90 ºand 270 ºindicate the positions where the scattering concentrates and is coincident with the meridional direction.

To the bulk A-Na sample above the AAO interface, Herman's orientation function (f_ϕ) is applied to evaluate the columnar orientation of the Col_{hd} mesophase and is plotted in Figure 7. Herman's orientation function is calculated by

$$f_\phi = \frac{1}{2}\left(3\langle\cos^2\phi\rangle - 1\right) \qquad \text{(Eq. 4.1)}$$

where

$$\langle\cos^2\phi\rangle = \frac{\int_0^{2\pi} I(\phi)\cdot\cos^2\phi\cdot d\phi}{\int_0^{2\pi} I(\phi)\cdot d\phi} \qquad \text{(Eq. 4.2)}$$

and $I(\phi)$ is the intensity of the angle ϕ.

Referencing to the normal direction of the substrate, the f_ϕ takes the value of 1.0 or -0.5 when the scattered intensity concentrates in the normal or in the parallel direction, respectively. From Figure 7, the value of f_ϕ exhibits an exponential decay with the increase of distance from the A-Na/AAO interface. As where the value of f_ϕ is ca. 0.8 near the interface, it is expected that the columns inside the AAO template are oriented almost normal to the substrate, i.e. parallel to the pore walls. Meanwhile,

the value reduces to ca. 0.5 at the distance of 60 μm, where the orientation direction is somehow showing an angle of ca. 37 ° to the normal direction of the substrate. In summary, it can be concluded that that AAO substrate can lead to a homeotropic alignment of the Col_{hd} phase. The mechanism can be described as follows. Inside the pores of AAO, the supramolecular columns of A-Na are oriented parallel to the pore walls, this orientation is then transferred to the A-Na film on the AAO substrate due to the large size of liquid crystalline domains. Although there exists an exponential decay of the orientation of the columns from the AAO surface with a characteristic distance of 11.2 μm, the value of f_ϕ remains higher than 0.4 at the A-Na film/air interface.

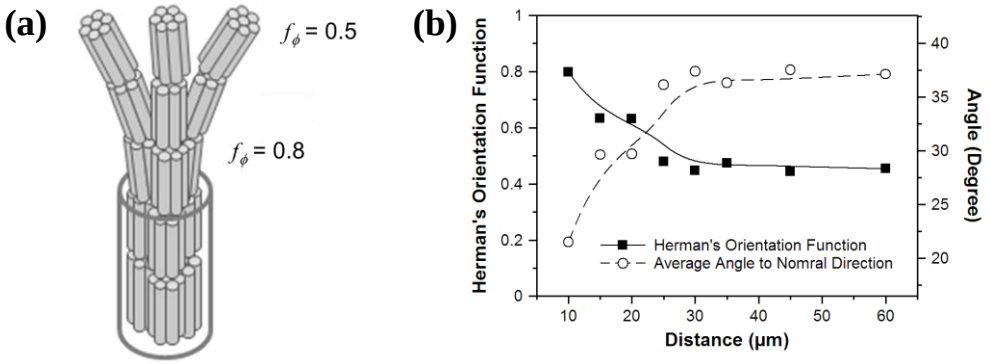

Figure 7. (a) The schematic view of the orientation of the columnar mesophase inside and outside the porous structure. (b) The dependences of Herman's orientation function (f_ϕ) and the average angle to the normal direction on the distance from the A-Na/AAO interface.

4.3.3 The ion conductivity study of the homeotropic aligned A-Na films

The ion conductivity of the glass- and AAO- samples after the thermal treatment is measured using the scheme as illustrated in Figure 8a. The impedance and phase spectra of the two samples are presented in Figure 9. The measurements

are carried out at different humidity conditions (RH=0%, 33% and 55%), where A-Na still forms the Col_{hd} phase. The conductivity results are shown in Figure 8b and summarized in Table 1. Water uptakes are summarized in Table 2.

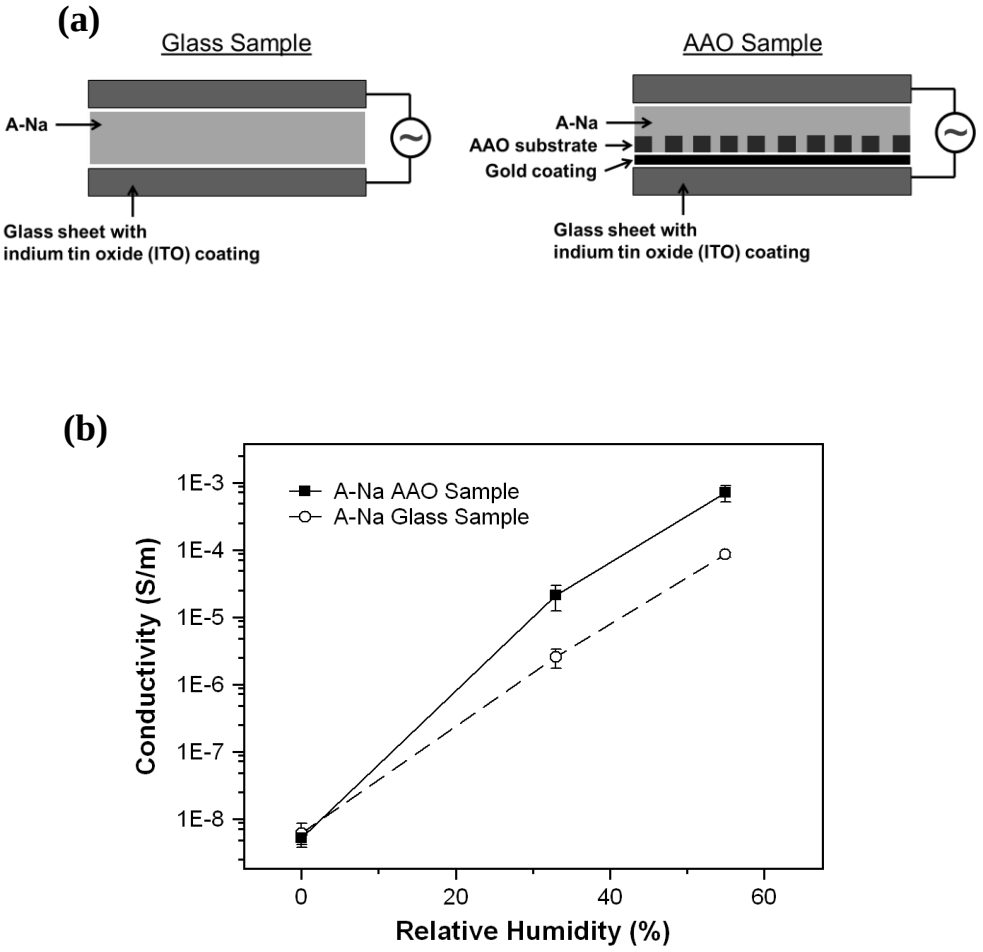

Figure 8. (a) The schematic illustration of how the glass- and AAO- samples are prepared for ion conductivity measurements. (b) Ion conductivity of glass- and AAO-samples at different relative humidity conditions.

Table 1. Ion conductivity of glass- and AAO-samples at different relative humidity (RH). The standard deviations are in the brackets with the same order of magnitude.

Sample	Ion Conductivity (S/m)		
	Dry	RH=33%	RH=55%
Glass-sample	6.22×10^{-9} (2.44)	2.56×10^{-6} (0.83)	8.66×10^{-5} (0.70)
AAO-sample	5.23×10^{-9} (0.97)	2.12×10^{-5} (0.86)	7.09×10^{-4} (1.90)

Table 2. Water uptakes of glass- and AAO-samples at different relative humidity conditions. The standard deviations are in the brackets.

Sample	Water Uptake (H_2O/SO_3^-)		
	Dry	RH=33%	RH=55%
Glass-sample	0 [a]	1.03 (0.03)	1.80 (0.26)
AAO-sample	0 [a]	1.55 (0.12)	2.07 (0.46)

[a] The water uptake of dry samples is set to be 0.

In the dry state, both AAO- and glass-samples show similar ion conductivity in the magnitude of 10^{-9} S/m. It is a rather low value, which may result from the lack of water molecules as ion carriers.

By increasing humidity, however, the AAO-sample exhibits much higher ion conductivity. The conductivity of the glass-sample jumps to an ion conductivity of 2.56×10^{-6} S/m at RH=33% and of 8.66×10^{-5} S/m at RH=55%. In contrast, the AAO-sample shows a conductivity of 2.12×10^{-5} S/m at RH=33% and 7.09×10^{-4} S/m at RH=55%. The conductivity of the homeotropically oriented sample (AAO-sample) is

almost 8 times higher than that of the non-oriented sample (glass sample). From Table 2 it can be seen that the water uptake of the oriented sample is also slightly increased. These results suggest that the homeotropic orientation of the ionic channels facilitates not only the ion transportation across the membrane, but also the water absorption.

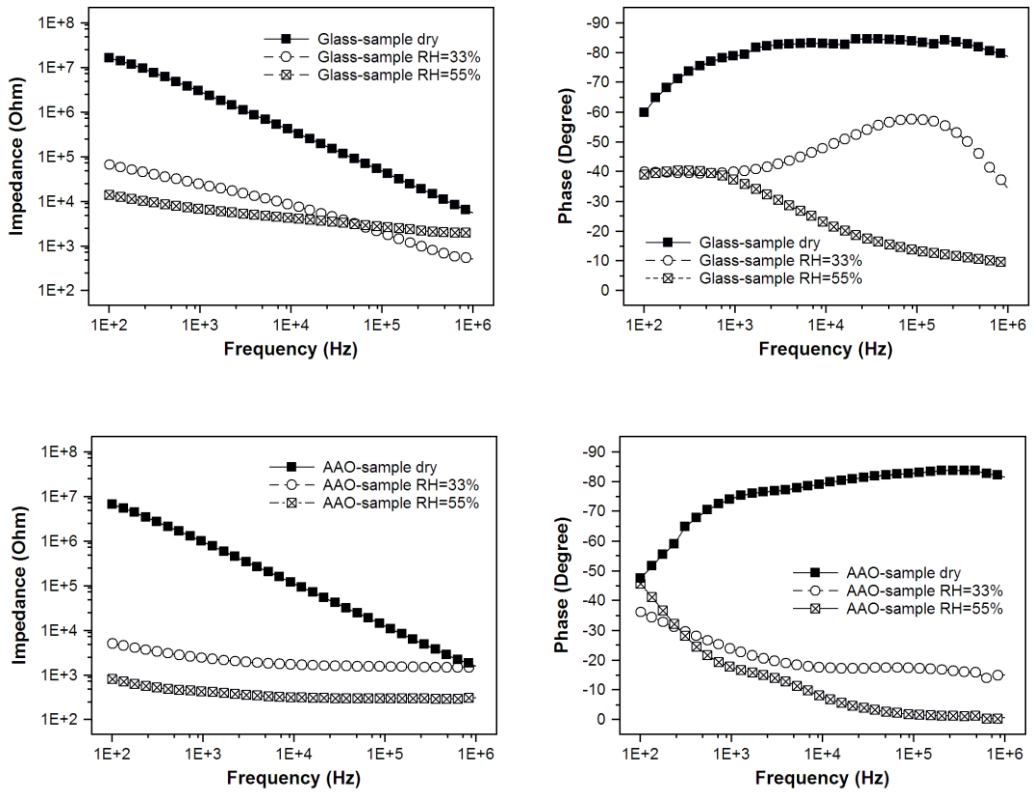

Figure 9. The impedance and phase spectra of the glass- and AAO- samples at different relative humidity conditions.

4.4. Conclusion

The effect of different substrates on the orientation of the Col_{hd} phase formed by a wedge-shaped amphiphilic sodium sulfonate (A-Na) molecule has been studied in this work, and a new approach for the homeotropic orientation of the Col_{hd} phase has been proposed. It is shown that the planar orientation of the Col_{hd} phase of A-Na is preferred on either hydrophilic or hydrophobic substrates. The homeotropic orientation has been achieved by using AAO porous substrates with an average pore diameter of 25 nm. According to X-ray results, the homeotropic alignment is observed not only in AAO pores but also in the A-Na film sample on the AAO surface. At the AAO/A-Na interface, the columns are oriented almost normal to the substrate, the orientation decays exponentially from the AAO surface with a characteristic distance of 11.2 μm, the value of Hermann orientation function f_ϕ remains still higher than 0.4 at the A-Na film/air interface. Furthermore, the homeotropically oriented sample presents an ion conductivity ca. 8 times higher than that of the non-oriented sample at RH=33% and 55%, meanwhile, its water uptake is also slightly higher.

4.5. References

[1] Gierke, TD; Munn, GE; Wilson, FC. The morphology in Nafion perfluorinated membrane products, as determined by wide-angle and small-angle X-ray studies, *J. Polym. Sci., Part B: Polym. Phys.*, **1981**, *19*, (11), 1687-1704.

[2] Yeager, HL; Steck, A. Cation and water diffusion in Nafion ion-exchange membranes - Influence of polymer structure, *J. Electrochem. Soc.*, **1981**, *128*, (9), 1880-1884.

[3] Fujimura, M; Hashimoto, T; Kawai, H. Small-angle X-ray-scattering study of perfluorinated ionomer membranes .2. Models for ionic scattering maximum, *Macromolecules*, **1982**, *15*, (1), 136-144.

[4] Aldebert, P; Dreyfus, B; Gebel, G; Nakamura, N; Pineri, M; Volino, F. Rod like micellar structures in perfluorinated ionomer solutions, *J. Phys.*, **1988**, *49*, (12), 2101-2109.

[5] Gebel, G. Structural evolution of water swollen perfluorosulfonated ionomers from dry membrane to solution, *Polymer*, **2000**, *41*, (15), 5829-5838.

[6] Haubold, HG; Vad, T; Jungbluth, H; Hiller, P. Nano structure of Nafion: A SAXS study, *Electrochim. Acta*, **2001**, *46*, (10-11), 1559-1563.

[7] Weber, AZ; Newman, J. Transport in polymer-electrolyte membranes - I. Physical model, *J. Electrochem. Soc.*, **2003**, *150*, (7), A1008-A1015.

[8] Schmidt-Rohr, K; Chen, Q. Parallel cyLindrical water nanochannels in Nafion fuel-cell membranes, *Nat. Mater.*, **2008**, *7*, (1), 75-83.

[9] Li, J; Wilmsmeyer, KG; Madsen, LA. Anisotropic diffusion and morphology in perfluorosulfonate ionomers investigated by NMR, *Macromolecules*, **2009**, *42*, (1), 255-262.

[10] Li, J; Park, JK; Moore, RB; Madsen, LA. Linear coupLing of aLignment with transport in a polymer electrolyte membrane, *Nat. Mater.*, **2011**, *10*, (7), 507-511.

[11] Shimizu, T. *Self-Assembled Nanomaterials I - Nanofibers*, Springer, BerLin, 2008.

[12] Percec, V; Heck, J; Johansson, G; Tomazos, D; Kawasumi, M; Chu, P. Molecular recognition directed self-assembly of supramolecular liquid-crystals, *Mol. Cryst. Liq. Cryst. Sci. Technol., Sect. A*, **1994**, *254*, 137-196.

[13] Percec, V; Heck, J; Johansson, G; Tomazos, D; Ungar, G. Towards tobacco mosaic virus-like self-assembled supramolecular architectures, *Macromol. Symp.*, **1994**, *77*, 237-265.

[14] Rosen, BM; Wilson, CJ; Wilson, DA; Peterca, M; Imam, MR; Percec, V. Dendron-mediated self-assembly, disassembly, and self-organization of complex systems, *Chem. Rev.*, **2009**, *109*, (11), 6275-6540.

[15] Beginn, U; Yan, LL; Chvalun, SN; Shcherbina, MA; Bakirov, A; Moller, M. Thermotropic columnar mesophases of wedge-shaped benzenesulfonic acid mesogens, *Liq. Cryst.*, **2008**, *35*, (9), 1073-1093.

[16] Zhu, XM; Scherbina, MA; Bakirov, AV; Gorzolnik, B; Chvalun, SN; Beginn, U; Moller, M. Methacrylated self-organizing 2,3,4-tris(alkoxy)benzenesulfonate: A new concept toward ion-selective membranes, *Chem. Mater.*, **2006**, *18*, (19), 4667-4673.

[17] Zhu, XM; Tartsch, B; Beginn, U; Moller, M. Wedge-shaped molecules with a sulfonate group at the tip - A new class of self-assembLing amphiphiles, *Chem. Eur. J.*, **2004**, *10*, (16), 3871-3878.

[18] Shimura, H; Yoshio, M; Hoshino, K; Mukai, T; Ohno, H; Kato, T. Noncovalent approach to one-dimensional ion conductors: Enhancement of ionic conductivities in nanostructured columnar liquid crystals, *J. Am. Chem. Soc.*, **2008**, *130*, (5), 1759-1765.

[19] Yoshio, M; Mukai, T; Ohno, H; Kato, T. One-dimensional ion transport in self-organized columnar ionic liquids, *J. Am. Chem. Soc.*, **2004**, *126*, (4), 994-995.

[20] Shimura, H; Yoshio, M; Hamasaki, A; Mukai, T; Ohno, H; Kato, T. Electric-field-responsive lithium-ion conductors of propylenecarbonate-based columnar liquid crystals, *Adv. Mater.*, **2009**, *21*, (16), 1591-+.

[21] Yoshio, M; Kagata, T; Hoshino, K; Mukai, T; Ohno, H; Kato, T. One-dimensional ion-conductive polymer films: Alignment and fixation of ionic channels formed by self-organization of polymerizable columnar liquid crystals, *J. Am. Chem. Soc.*, **2006**, *128*, (16), 5570-5577.

[22] Charlet, E; Grelet, E; Brettes, P; Bock, H; Saadaoui, H; Cisse, L; Destruel, P; Gherardi, N; Seguy, I. Ultrathin films of homeotropically aligned columnar liquid crystals on indium tin oxide electrodes, *Appl. Phys. Lett.*, **2008**, *92*, (2), 024107-0241-3.

[23] Kim, HS; Choi, SM; Lee, JH; Busch, P; Koza, SJ; Verploegen, EA; Pate, BD. Uniaxially oriented, highly ordered, large area columnar superstructures of discotic supramolecules using magnetic field and surface interactions, *Adv. Mater.*, **2008**, *20*, (6), 1105-1109.

[24] Mansky, P; Liu, Y; Huang, E; Russell, TP; Hawker, CJ. Controlling polymer-surface interactions with random copolymer brushes, *Science*, **1997**, *275*, (5305), 1458-1460.

[25] Huang, E; Rockford, L; Russell, TP; Hawker, CJ. Nanodomain control in copolymer thin films, *Nature*, **1998**, *395*, (6704), 757-758.

[26] Choudhury, TD; Rao, NVS; Tenent, R; Blackburn, J; Gregg, B; Smalyukh, II. Homeotropic alignment and director structures in thin films of triphenylamine-based discotic liquid crystals controlled by supporting nanostructured substrates and surface confinement, *J. Phys. Chem. B*, **2011**, *115*, (4), 609-617.

[27] Park, HG; Lee, JJ; Dong, KY; Oh, BY; Kim, YH; Jeong, HY; Ju, BK; Seo, DS. Homeotropic alignment of liquid crystals on a nano-patterned polyimide surface using nanoimprint lithography, *Soft Matter*, **2011**, *7*, (12), 5610-5614.

[28] Gearba, RI; Anokhin, DV; Bondar, AI; Bras, W; Jahr, M; Lehmann, M; Ivanov, DA. Homeotropic alignment of columnar liquid crystals in open films by means of surface nanopatterning, *Adv. Mater.*, **2007**, *19*, (6), 815-+.

[29] Amundson, K; Helfand, E; Quan, XN; Smith, SD. Alignment of lamellar block-copolymer microstructure in an electric-field .1. Alignment kinetics, *Macromolecules*, **1993**, *26*, (11), 2698-2703.

[30] Amundson, K; Helfand, E; Quan, XN; Hudson, SD; Smith, SD. Alignment of lamellar block-copolymer microstructure in an electric-field .2. Mechanisms of alignment, *Macromolecules*, **1994**, *27*, (22), 6559-6570.

[31] Morkved, TL; Lu, M; Urbas, AM; Ehrichs, EE; Jaeger, HM; Mansky, P; Russell, TP. Local control of microdomain orientation in diblock copolymer thin films with electric fields, *Science*, **1996**, *273*, (5277), 931-933.

[32] Hong, C; Tang, T; Hung, C; Pan, R; Fang, W. Liquid crystal alignment in nanoporous anodic aluminum oxide layer for LCD panel applications, *Nanotechnology*, **2010**, *21* (28), 285201 (10 pp.).

[33] Steinhart, M; Zimmermann, S; Goring, P; Schaper, AK; Gosele, U; Weder, C; Wendorff, JH. Liquid crystalline nanowires in porous alumina: Geometric confinement versus influence of pore walls, *Nano Lett.*, **2005**, *5* (3), 429-434.

Chapter 5

Membranes Prepared from Sodium 2,3,4-Tris(11'-acryloyloxyundecyl-1'-oxy)benzenesulfonate by Photopolymerization

In this chapter, membranes are prepared via photopolymerization of films of sodium 2,3,4-tris(11'-acryloyloxyundecyl-1'-oxy)benzenesulfonate under different relative humidity. The phase structure, water uptake, ion conductivity before and after polymerization are studied. It is found that the polymerization does not alter significantly the phase structure of the material at different humidity conditions. Interestingly, in comparison with the monomer sample, the membranes prepared by polymerization at RH=100% exhibits a higher ion conductivity, but those polymerized at RH≤55% are much less conductive. The conductivity results are in good agreement with the results of the water uptake measurements.

5.1. Introduction

Ion-exchange membranes belong to a very important class of synthetic separation membranes, and they are widely used in various industrial fields including dialysis, electrolysis, sensing, separator in batteries, and etc [1]. Perfluorinated sulfonic acid ionomer membranes, e.g. Nafion, are a well-known example [2,3] and can be applied in many fields ranging from electrolysis to fuel cells due to their unique properties such as high ion conductivity and selectivity [4], good mechanical strength [5,6], outstanding chemical and temperature resistance [7-10], and etc. Despite the fact that the existence of ionic channels in Nafion membranes is generally accepted, none of the structural models deliver a clear explanation of the ion conductive property. Most of the models assume 2D ion transportations in Nafion, such as the parallel water-channel model [11] where arrays of parallel ionic nano-cylinders are embedded in a locally aligned polymer matrix. In some other models, such as structural-inversion network model [12] and percolation network model [13], the structure of Nafion is however assumed to transform into a 3D network upon uptake of a large amount of water.

Self-assembly of low and high molecular weight compounds has attracted increasing attentions as a tool to develop conductive membranes due to the ability to form a variety of nanostructures [14]. Membranes presenting lamellar, columnar and cubic structures have triggered a thrust in the transport applications for charges [15-17], ions [16-19] and molecules [20]. Recently, ceratin ionic liquid crystals were shown to form bicontinuous cubic phases (Cub_{bi}) with 3D channel structures. In particular, these nanochannels can be successfully applied for the transport of ions [21-23] and gases [24]. The most important advantage of these systems is that the 3D channels in the interconnected network are able to construct effective pathways for transportation without the orientation of liquid crystal domains. In case of ion

transportation, Ichkawa *et al* found that the ion conductivity of membranes in Cub_{bi} phases is almost one order of magnitude higher than that in the hexagonal columnar (Col_h) phase [21].

In Chapter 3 of this thesis, the relation between the structure and conducting properties of a wedge-shaped amphiphilic sulfonate molecule, sodium 2,3,4-tris(11'-acryloyloxyundecyl-1'-oxy) benzenesulfonate (A-Na), as a function of relative humidity (RH) is studied. A-Na is able to self-assemble at ambient conditions into a disordered columnar (Col_{hd}) structure with ionic channels along the axis of the cylinder. Upon increase of RH to 55%, the Col_{hd} structure remains but with a slight swelling of the cylinders by a minor water uptake, which result however in a significant enhancement of the ion conductivity by 4 orders of magnitude. Further water uptake by increasing humidity induces a dramatic change of the mesophase structure where bicontinuous cubic phases (Cub_{bi}) are formed. The $Col_{hd} \rightarrow Cub_{bi}$ transition is accompanied by an additional substantial increase of conductivity due to the formation of an interconnected network of ionic channels. The challenge arises here that whether the different mesostructures formed under different RH conditions can be arrested by means of polymerization. In this Chapter, it is attempted to optimize the polymerization conditions in order to obtain membranes with preserved mesostructures. Further, the structure, water uptake and ion conductivity of the polymerized membranes are studied and compared with the monomer samples.

5.2. Experimental

5.2.1. Synthesis

The synthesis of sodium 2,3,4-tris(11'-acryloyloxyundecyl-1'-oxy)benzene-sulfonate (A-Na) is described in Chapter 2.

5.2.2. Polymerization

To do the polymerization, 0.5 wt% (for RH=100% sample, 3.0 wt%) of 2,2-dimethoxy-2-phenylacetophenone (photo initiator) is dissolved in the solution of A-Na in chloroform. The mixture is drop-cast onto a glass sheet coated with ITO. After the complete evaporation of the solvent, the whole set is equilibrated under different relative humidity conditions of 0 %, 33 %, 55 % and 100% for 2 days. The whole process is carried out in a sealed quartz chamber wrapped with Al-foil to prevent the polymerization during the equilibration. Afterwards the Al-foil is removed, the sealed quartz chamber is exposed to irradiation of 366 nm for 12 hours.

5.2.3. Fourier transform infrared spectroscopy (FTIR)

FTIR spectra are recorded on a Nicolet 710 FTIR spectrometer by means of photo-acoustic techniques.

5.2.4. Ultraviolet-Visible spectroscopy (UV-Vis)

UV-Vis spectra are recorded on a JASCO V-630 spectrophotometer from 200 nm to 600 nm and calibrated with the measurements of the corresponding clean glass sheets. The band width is 1.5 nm, and the scan speed is 1000 nm/min.

5.2.5 Other techniques

Small-angle X-ray scattering (SAXS) measurements, polarizing optical microscopy measurements (POM), through-plain ion conductivity measurements are all performed according to Part 3.2 in Chapter 3.

5.3. Results and Discussion

5.3.1 Polymerization of A-Na

FTIR and UV/Vis spectroscopy is employed to monitor the polymerization of A-Na. Figure 1 shows the FTIR spectra of A-Na before and after photo-polymerization. Before polymerization, the spectrum shows two absorption bands at 1640 cm^{-1} and 1625 cm^{-1}, which can be ascribed to the C=C stretching motion. In addition, a band corresponding to the C=C bending motion at 1412 cm^{-1} and two bands at 987 cm^{-1} and 971 cm^{-1} that are ascribed to the C=C twisting and wagging motion are observed as well. These bands prove the existence of the C=C double bond in A-Na before polymerization. After polymerization, however, all these bands disappear, indicating the success polymerization. The polymerization process has also been confirmed by means of UV/Vis spectroscopy. As shown in Figure 2, before polymerization the UV/Vis spectrum shows peaks at 218 nm, 232 nm and 274 nm that can be ascribed to the *E1* band ($\pi \rightarrow \pi^*$) of the benzene ring,the *K* band ($\pi \rightarrow \pi^*$) of the C=C-C=O group and the *R* band ($n \rightarrow \pi^*$) of the C=O group, respectiviely. After polymerization, the peak at 232 nm vanishes, indicating the polymerization of the C=C groups.

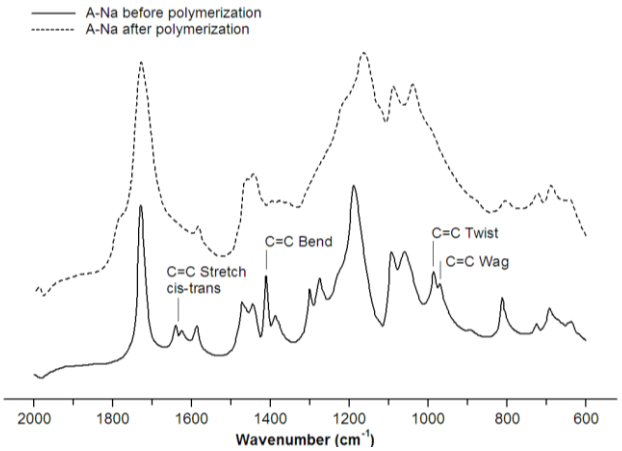

Figure 1. FTIR spectra of dry A-Na before and after polymerization.

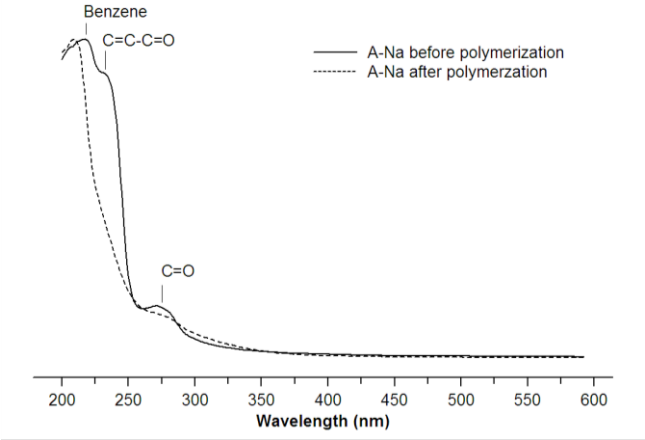

Figure 2. The UV/Vis spectra of the dry A-Na before and after the polymerization.

5.3.2 Phase structures after polymerization at different RH conditions

Polymerization of the films of A-Na is performed under different RH, i.e. in different mesophases. It is worth mentioning that at low RH (≤ 55%), 0.5 wt% of photoinitiator is already enough to obtain mechanically strong polymer membranes, however at RH=100%, a higher photoinitiator content of 3 wt% is required. POM and SAXS techniques are employed to analyze the structure of the resulting membranes. Figure 3 shows the X-ray diffractograms and POM images before and after polymerization at 25 ℃ at different RH conditions. The X-ray results are summarized in Table 1.

At dry and RH=55% conditions, A-Na forms a Col_{hd} phase before polymerization as demonstrated in Chapter 3. After polymerization at dry condition, as can be seen in Figure 3, the obtained membrane (Poly-A-Na-Dry) shows two peaks, which can be indexed as 10 and 11 reflections of a Col_{hd} lattice. At the same time, the membrane prepared by polymerization at RH=55% (Poly-A-Na-55) exhibits also a Col_{hd} phase. Both membranes show a birefringent texture. As show by the SAXS

data, the columns shrink after the polymerization, and the diameter of the columns in the polymer membranes is larger when the polymerization is carried out at higher RH. It seems that the columnar structure remains after the polymerization. In comparison with the monomer samples, the polymer membranes show much broader peaks, indicating the formation of a highly disordered columnar structure.

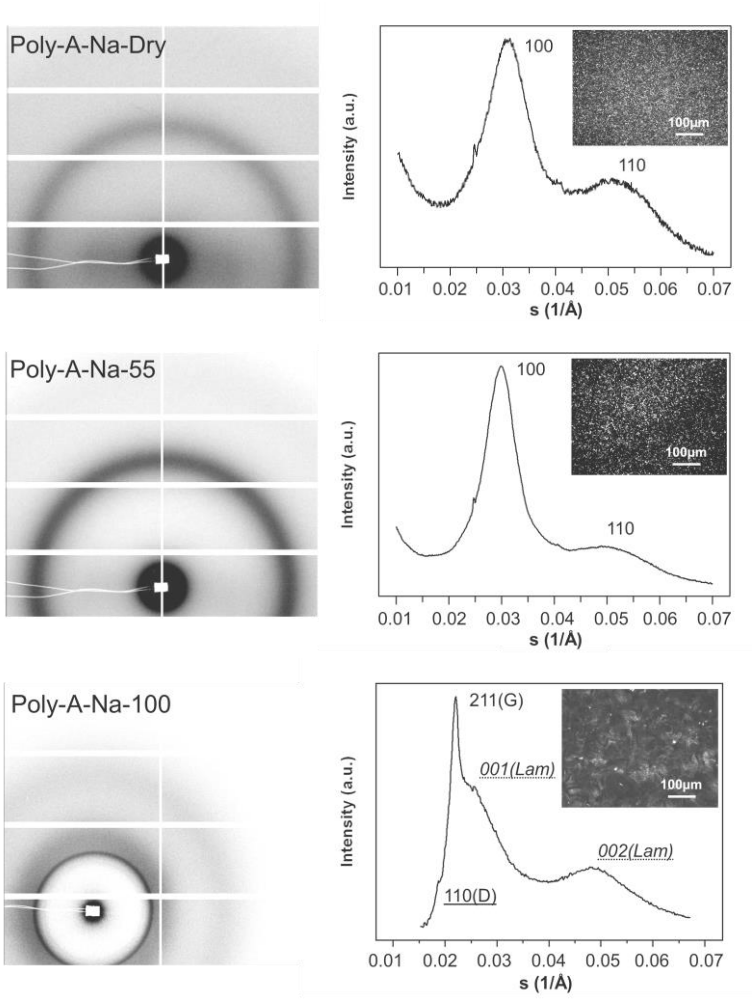

Figure 3. X-ray diffractograms and POM images of polymerized A-Na films at dry (Poly-A-Na-Dry), RH=55% (Poly-A-Na-55) and RH=100% (Poly-A-Na-100) conditions.

Table 1. SAXS results at 25 ℃ of polymerized A-Na films at dry (Poly-A-Na-Dry), RH=55% (Poly-A-Na-55) and RH=100% (Poly-A-Na-100) conditions.

Sample	Mesophase	*d* spacing (Å)	Lattice constant (Å)
Poly-A-Na-Dry	Col_{hd}	d_{100} = 32.4 d_{110} = 19 ~ 20	ca. 37
Poly-A-Na-55	Col_{hd}	d_{100} = 33.2 d_{110} = 19 ~ 20	ca. 38
Poly-A-Na-100	*Gyroid (G)*	d_{211} = 45.5	111.5
	Diamond (D)	d_{110} = 53.4	75.2
	Lamellar (Lam)	d_{001} = 39.3 d_{002} = 20.9	40.0

There can be two reasons for the disordering of the columnar structures during the polymerization. On one hand, the temperature can rise during the polymerization since it is an exothermic reaction, so the increase of temperature may lead to the worsening of the mesostructure. On the other hand, as illustrated in Figure 4, the polymerization takes place in both intercolumnar and intracolumnar manner. The random shrinkage in different directions should result in a more disordered structure.

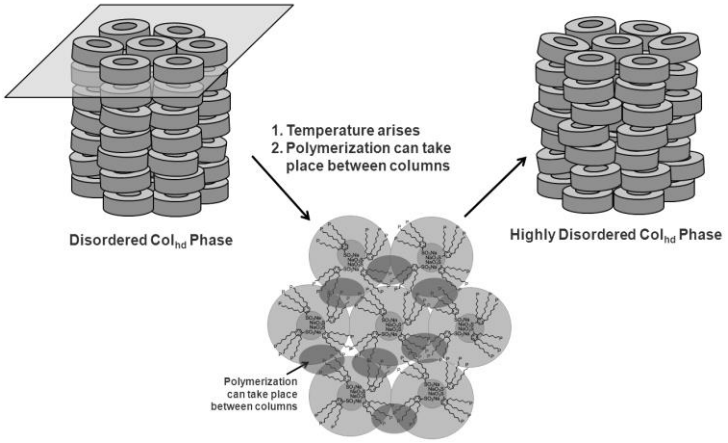

Figure 4. A schematic illustration of the highly disordered columnar hexagonal phase formed by polymerization.

At RH=100% condition, A-Na forms bicontinuous cubic phase (Cub_{bi} gyroid+diamond) before polymerization. After polymerization, as shown by the SAXS data in Figure 3, the resulting Poly-A-Na-100 sample shows the formation of a mixture of gyroid (*G*), diamond (*D*) and lamellar (*Lam*) phases. For a detail comparison, Figure 5 presents the enlarged 2D X-ray patterns and only 2 peaks of the bicontinuous cubic phase remains after polymerization, indication the disordering during the polymerization. In addition, the lattice parameter is reduced for around 30% after the poylemrization, apparently due to the contraction effect of the polymerization.

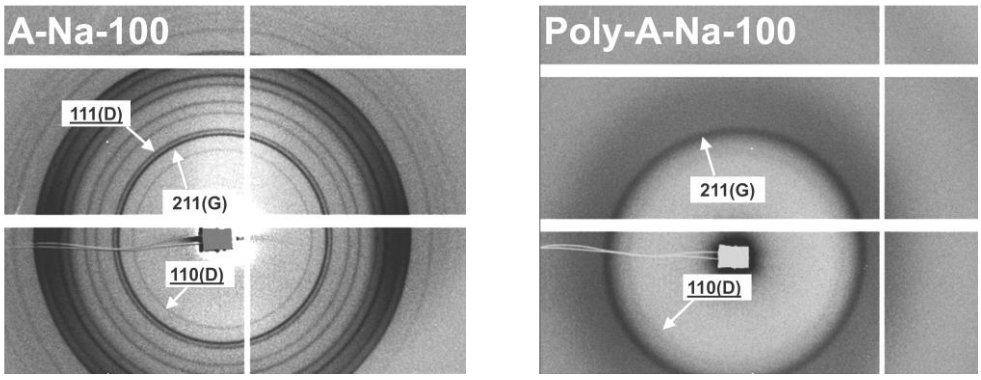

Figure 5. SAXS patterns of A-Na at RH=100% condition before (A-Na-100) and after (Poly-A-Na-100) polymerization.

5.3.3 Phase structures of polymer membranes at different temperatures and humidity

Figure 6 displays 1D SAXS diffractograms measured on the free-standing A-Na membrane (Poly-A-Na-55). It can be seen that after the polymerization, the columnar structure is stable at a temperature (80 ℃) well above the isotropization temperature

of A-Na. Moreover, the columnar structure is also preserved at RH=100%. These pieces of information clearly show that the phase behavior of the system is both temperature and humidity stable after polymerization. The humidity-induced phase evolution from hexagonal columnar structure to bicontinuous cubic phases does not occur in Poly-A-Na-55 membrane due to the cross-linking reaction.

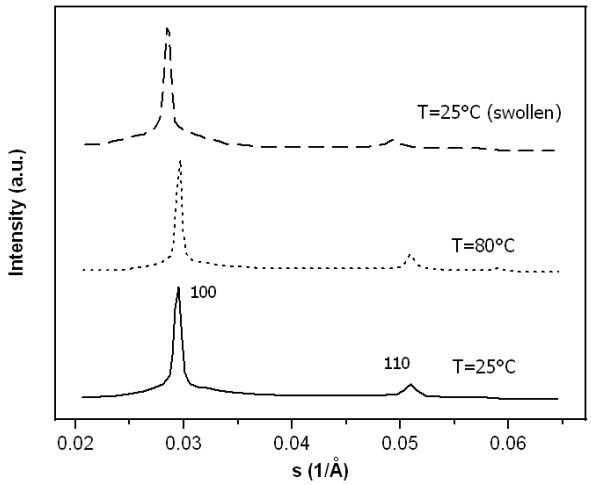

Figure 6. 1D SAXS diffractograms recorded on a free-standing membrane of **A-Na** at different temperatures (25 and 80 ℃) and also upon room-temperature swelling of the membrane at RH=100% (swollen).

5.3.4 Ion conductivity before and after the polymerization

The ion conductivity is measured using AC impedance spectroscopy during the polymerization. As shown in Figure 7, each sample is polymerized at the corresponding RH and tested at the same RH. Since the samples at dry, RH=33%, RH=55% conditions form Col_{hd} phase and the samples at RH=100% condition form Cub_{bi} phase, the plot of Figure 8 can be divided into 2 regions.

In the Col_{hd}-phase region, both A-Na-Dry and Poly-A-Na-Dry samples exhibit very low ion conductivity below 10^{-8} S/m. After wetting, both the samples before and after the polymerization show the linear dependences of ion conductivity on RH. In detail, the monomer samples increases up to 4 orders of magnitude at RH=55%, while the polymerized samples show a much lower conductivity at RH=55%.

The reason for the decrease of the conductivity after the polymerization in the columnar phase may originate from the highly disordered structure, which may contain an increased amount of "dead ends". Meanwhile, the cross-linked structure my also restrict the water uptake. The evidence is shown in Figure 7b. In the Col_{hd}-phase region, the polymerized samples uptake much less water than the monomer samples.

In the Cub_{bi}-phase region, the polymerization has an opposite effect on the conductive properties.

The ion conductivity of the sample polymerized at RH = 100% (Poly-A-Na-100) is even higher than the monomer A-Na-100 sample, meanwhile, the water uptake is also improved after polymerization (Figure 7) The reason is also supposed to the disordered structures of Cub_{bi} phase. Since the hydrophilic channels are all inter-connected with each other, the disorder in Cub_{bi} phase may add more conductive ionic channels. In addition, a lamellar structure with a 2D ionic channel forms after the polymerization, which might also facilitate the ion transportation and water uptake.

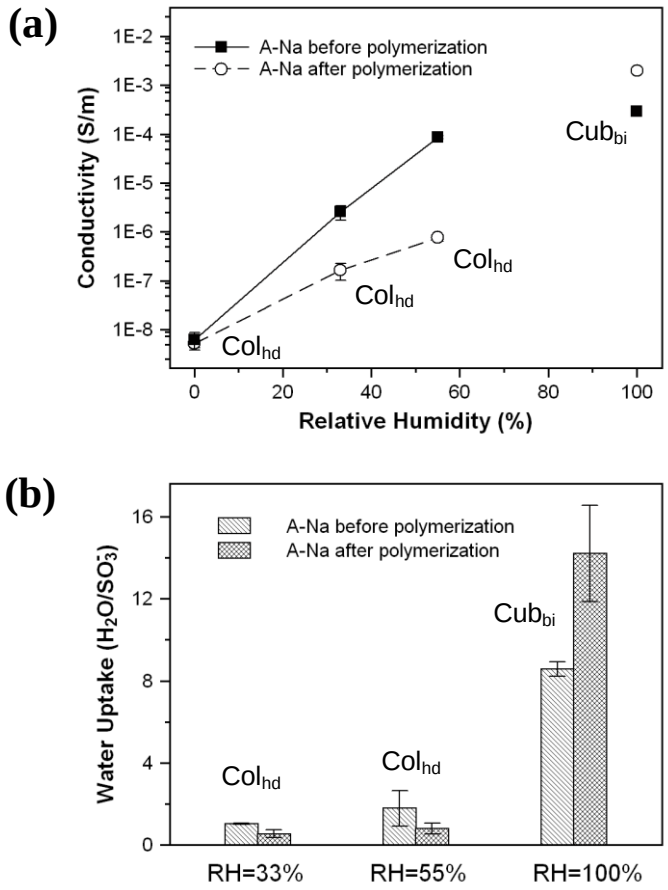

Figure 7. Dependences of (a) ion conductivity and (b) water uptake on relative humidity of A-Na before and after the polymerization.

5.3.5 Conductivity vs. RH for polymer membranes

In contrast to the monomer, the mesostructure of the polymer membranes is no more sensitive to both temperature and humidity due to the cross-linking reaction. The ion conductivity of two polymer membranes prepared under different RH, namely RH = 55% (Poly-A-Na-55) and 100 % (Poly-A-Na-100) is studied as a function of humidity. As mentioned before, Poly-A-Na-55 forms a *Col$_{hd}$* phase, and

Poly-A-Na-100 has Cub_{bi} structures. The results are summarized in Figure 8 and Table 2.

As shown in Figure 8a, the ion conductivity of Poly-A-Na-55 increases with the increase of humidity and reaches plateau at RH = 55 %, meanwhile Poly-A-Na-100 grows an exponentially with RH in the whole humidity range. Such a huge difference indicates that the preparation conditions and consequently the structure of the membranes play a pivotal role in defining the conductivity behaviors.

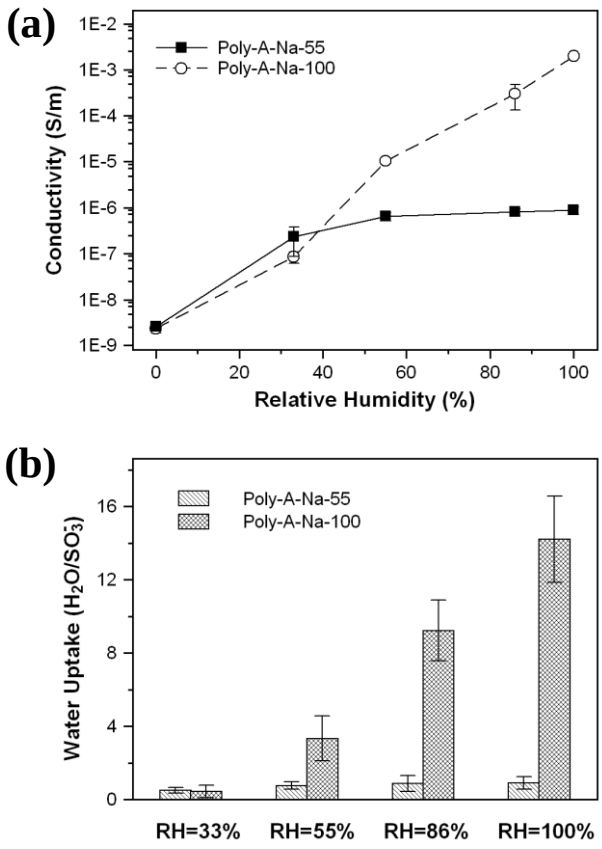

Figure 8. Dependences of (a) ion conductivity and (b) water uptake on relative humidity of Poly-A-Na-55 and Poly-A-Na-100.

Table 2. Ion conductivity of Poly-A-Na-55 and Poly-A-Na-100 at different RH values. The standard deviation is in the brackets with the same order of magnitude.

Sample	Ion Conductivity (S/m)				
	Dry state	RH=33%	RH=55%	RH=86%	RH=100%
Poly-A-Na-55	2.65×10^{-9} (0.24×10^{-9})	2.36×10^{-7} (1.49)	6.56×10^{-7} (1.38)	8.13×10^{-7} (1.47)	8.83×10^{-7} (1.66)
Poly-A-Na-100	2.39×10^{-9} (0.50)	8.67×10^{-8} (2.32)	1.04×10^{-5} (0.12)	3.06×10^{-4} (1.72)	1.99×10^{-3} (0.38)

Table 3. Water uptake of Poly-A-Na-55 and Poly-A-Na-100 at different RH values. The standard deviation is in the brackets.

Sample	Water Uptake (H_2O/SO_3^-)			
	RH=33%	RH=55%	RH=86%	RH=100%
Poly-A-Na-55	0.50 (0.15)	0.76 (0.21)	0.88 (0.43)	0.90 (0.33)
Poly-A-Na-100	0.44 (0.35)	3.33 (1.22)	9.23 (1.65)	14.2 (2.35)

At low humidity (RH=0~33%), both Poly-A-Na-55 and Poly-A-Na-100 membranes exhibit a similar ion conductivity as well as water uptake, however, at high humidity (RH≥55%), Poly-A-Na-100 shows a much higher conductivity and water uptake. For Poly-A-Na-55 both ion conductivity and water uptake reach the plateau. This membrane is prepared by polymerization at RH=55%. Due to the dense cross-linking, the polymer membrane cannot swell further at RH≥55%. The Poly-A-Na-100 membrane is obtained at the highest RH value of 100%, so its conductivity and water uptake can increase with humidity till RH=100%. Figure 9 illustrates the structure and water uptake of the Poly-A-Na-55 and Poly-A-Na-100 membranes in the RH evolution.

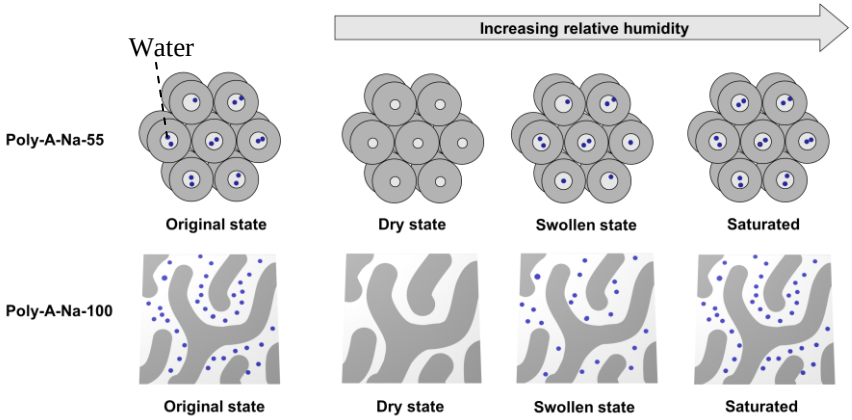

Figure 9. An illustration of the structures and water uptake of Poly-A-Na-55 and Poly-A-Na-100 in the RH evolution.

5.4. Conclusion

Sodium 2,3,4-tris(11'-acryloyloxyundecyl-1'-oxy)benzenesulfonate (A-Na) has been synthesized and polymerized for the preparation of ion conductive membranes. It is found that both Col_{hd} phase (RH=33% and RH=55%) and Cub_{bi} phases (RH=100%) can be arrested by means of photopolymerization under certain humidity, which results in highly disordered structures. Comparing with the monomer, the polymer membranes with the columnar structure shows lower water uptake and consequently lower ion conductivity. In contrast, the structural disordering in the polymer membranes in the Cub_{bi} phases leads to higher water uptake and conductivity, possible due to the formation of a more opened structure with additional conductive channels. Due to the dense cross-linking, the water uptake and ion conductivity of the polymer membranes with the columnar structure reach the plateau

at the humidity, under the polymerization is carried out. However, the water uptake and ion conductivity of the membrane polymerized at RH=100%, which form the Cub_{bi} phases, increase with the increase of humidity in the whole RH range.

5.5. References

[1] Tanaka, Y. *Ion Exchange Membranes: Fundamentals and Applications*, Elsevier, Amsterdam, 2007.

[2] Mauritz, KA; Moore, RB. State of understanding of Nafion, *Chem. Rev.*, **2004**, *104*, (10), 4535-4585.

[3] Curtin, DE; Lousenberg, RD; Henry, TJ; Tangeman, PC; Tisack, ME. Advanced materials for improved PEMFC performance and life, *J. Power Sources*, **2004**, *131*, (1-2), 41-48.

[4] Wang, HS; Li, TH; Jia, WL; Xu, HY. Highly selective and sensitive determination of dopamine using a Nafion/carbon nanotubes coated poly(3-methylthiophene) modified electrode, *Biosens. Bioelectron.*, **2006**, *22*, (5), 664-669.

[5] Iwai, Y; Hiroki, A; Tamada, M; Yamanishi, T. Radiation deterioration in mechanical properties and ion exchange capacity of Nafion n117 swelling in water, *J. Membr. Sci.*, **2008**, *322*, (1), 249-255.

[6] Majsztrik, PW; Bocarsly, AB; Benziger, JB. Viscoelastic response of Nafion. Effects of temperature and hydration on tensile creep, *Macromolecules*, **2008**, *41*, (24), 9849-9862.

[7] Alentiev, A; Kostina, J; Bondarenko, G. *Chemical aging of Nafion: FTIR study*, Conference of the European Membrane Society, Giardini Naxos, Italy, 2006.

[8] Casciola, M; Alberti, G; Sganappa, M; Narducci, R. *Factors affecting the stability of Nafion conductivity at high temperature and relative humidity*, Conference of the European Membrane Society, Giardini Naxos, ITALY, 2006.

[9] Lee, HJ; Nam, EJ; Woo, JJ; Moon, SH; Lee, J. Improved dimensional stability of Nafion membrane modified using a layer by layer self-assembly of biophilic polymers, *Curr. Appl Phys.*, **2012**, *12*, (5), 1235-1238.

[10] Thompson, EL; Capehart, TW; Fuller, TJ; Jorne, J. Investigation of low-temperature proton transport in Nafion using direct current conductivity and differential scanning calorimetry, *J. Electrochem. Soc.*, **2006**, *153*, (12), A2351-A2362.

[11] Schmidt-Rohr, K; Chen, Q. Parallel cylindrical water nanochannels in Nafion fuel-cell membranes, *Nat. Mater.*, **2008**, *7*, (1), 75-83.

[12] Gebel, G. Structural evolution of water swollen perfluorosulfonated ionomers from dry membrane to solution, *Polymer*, **2000**, *41*, (15), 5829-5838.

[13] Weber, AZ; Newman, J. Transport in polymer-electrolyte membranes - I. Physical model, *J. Electrochem. Soc.*, **2003**, *150*, (7), A1008-A1015.

[14] Shimizu, T. *Self-Assembled Nanomaterials I - Nanofibers*, Springer, Berlin, 2008.

[15] Percec, V; Glodde, M; Bera, TK; Miura, Y; Shiyanovskaya, I; Singer, KD; Balagurusamy, VSK; Heiney, PA; Schnell, I; Rapp, A; Spiess, HW; Hudson, SD; Duan, H. Self-organization of supramolecular helical dendrimers into complex electronic materials, *Nature*, **2002**, *419*, (6905), 384-387.

[16] Yoshio, M; Ichikawa, T; Shimura, H; Kagata, T; Hamasaki, A; Mukai, T; Ohno, H; Kato, T. Columnar liquid-crystalline imidazolium salts. Effects of anions and cations on mesomorphic properties and ionic conductivity, *Bull. Chem. Soc. Jpn.*, **2007**, *80*, (9), 1836-1841.

[17] Cho, BK; Jain, A; Gruner, SM; Wiesner, U. Mesophase structure-mechanical and ionic transport correlations in extended amphiphilic dendrons, *Science*, **2004**, *305*, (5690), 1598-1601.

[18] Xiao, SX; Myers, M; Miao, Q; Sanaur, S; Pang, KL; Steigerwald, ML; Nuckolls, C. Molecular wires from contorted aromatic compounds, *Angew. Chem. Int. Ed.*, **2005**, *44*, (45), 7390-7394.

[19] Hirai, Y; Monobe, H; Mizoshita, N; Moriyama, M; Hanabusa, K; Shimizu, Y; Kato, T. Enhanced hole-transporting behavior of discotic liquid-crystalline physical gels, *Adv. Funct. Mater.*, **2008**, *18*, (11), 1668-1675.

[20] Zhou, MJ; Kidd, TJ; Noble, RD; Gin, DL. Supported lyotropic liquid-crystal polymer membranes: Promising materials for molecular-size-selective aqueous nanofiltration, *Adv. Mater.*, **2005**, *17*, (15), 1850-1853.

[21] Ichikawa, T; Yoshio, M; Hamasaki, A; Mukai, T; Ohno, H; Kato, T. Self-organization of room-temperature ionic liquids exhibiting liquid-crystalline bicontinuous cubic phases: Formation of nano-ion channel networks, *J. Am. Chem. Soc.*, **2007**, *129*, (35), 10662-10663.

[22] Frise, AE; Ichikawa, T; Yoshio, M; Ohno, H; Dvinskikh, SV; Kato, T; Furo, I. Ion conductive behaviour in a confined nanostructure: NMR observation of self-diffusion in a liquid-crystalline bicontinuous cubic phase, *Chem. Commun.*, **2010**, *46*, (5), 728-730.

[23] Kerr, RL; Miller, SA; Shoemaker, RK; Elliott, BJ; Gin, DL. New type of Li ion conductor with 3D interconnected nanopores via polymerization of a liquid organic electrolyte-filled lyotropic liquid-crystal assembly, *J. Am. Chem. Soc.*, **2009**, *131*, (44), 15972-15973.

[24] Lu, XY; Nguyen, V; Zhou, MJ; Zeng, XH; Jin, JZ; Elliott, BJ; Gin, DL. Crosslinked bicontinuous cubic lyotropic liquid-crystal/butyl-rubber composites: Highly selective, breathable barrier materials for chemical agent protection, *Adv. Mater.*, **2006**, *18*, (24), 3294-3298.

Chapter 6

Wedge-Shaped Amphiphilic Sulfonate Molecules with Different Counterions: Phase Behavior and Ion Conductivity

In this chapter, a series of wedge-shaped sulfonate amphiphiles with different counterions, namely lithium / sodium / potassium / cesium 2,3,4-tris(11'-acryloyl-oxyundecyl-1'-oxy)benzenesulfonates (A-Li, A-Na, A-K, A-Cs), are studied regarding their phase behavior and ion conductivity. Real-time X-ray measurements are carried out to reveal the detailed phase structures and transitions. It is shown that A-Li and A-Cs are isotropic at room temperature, meanwhile A-Na and A-K form a disordered hexagonal columnar mesophase. By cooling, A-Li and A-Cs undergo a transition from isotropic to lamellar phases at -11 ℃ and -7 ℃, respectively, and both A-Na and A-K are transformed from the hexagonal columnar to a centered rectangular columnar phases at -10 ℃. Model of molecular packing in different mesophases are proposed based on the X-ray data. Furthermore, the conductivity of the sulfonates is determined at room temperature as a function of humidity. It is found that the salts, which form a columnar phase, show a much better water uptake ability, which results in much higher ion conductivity.

6.1. Introduction

Supramolecular assembly is a well-known tool for constructing nanostructured materials [1,2]. The design of self-assembling materials is usually a difficult challenge due to the fact that the structure-property relationship for such molecules has not been completely established yet. It is therefore crucial to investigate the influence of different building blocks of molecules on the structure and properties of the materials [3-8].

This thesis deals with wedge-shaped amphiphilic sulfonate molecules, which can self-assemble into structures with ionic channels. Previously, the synthesis and characterization of two series of such molecules, namely 2,3,4-tris(dodecyl-1'-oxy)benzenesulfonates and 3,4,5-tris(dodecyl-1'-oxy)benzenesulfonates with different counterions, were reported by our group [8]. It is found that the phase occurrence is dominated by the geometric shape of the molecule as well as the radius of the cations rather than by the ionic interactions between cations and anions. In this work, the focus is on the wedge-shaped sulfonate molecules containing polymerizable groups at the periphery, which allow arresting the mesophases by means of polymerization.

In Chapter 2, the synthesis of a series of acrylated wedge-shaped sulfonate molecules with different counterions, namely lithium, sodium, potassium, and cesium 2,3,4-tris(11'-acryloyloxyundecyl-1'-oxy)benzenesulfonates (A-Li, A-Na, A-K, A-Cs) is presented. In Chapter 3 the phase behavior and ion conductivity of the sodium sulfonate A-Na are studied as a function of relative humidity (RH). It is shown that this compound forms a hexagonal columnar mesophase at ambient conditions; and it is transformed into bicontinuous cubic phases by increasing the RH to 86 and 100 %. In this Chapter, the phase behavior of different salts is addressed and their conductivity at room temperature under different RH is measured. The structure-property relationship of these molecules is then discussed.

6.2. Experimental

6.2.1 Synthesis

The synthesis of lithium, sodium, potassium, and cesium 2,3,4-tris(11'-acryloyloxyundecyl-1'-oxy)benzenesulfonates (A-Li, A-Na, A-K, A-Cs) in described in Chapter 2.

6.2.2 Small angle X-ray scattering measurements (SAXS)

Fibers of A-Na and A-K salts are prepared at room temperature by using a home-made micro-extruder with an aperture size of 300 μm. In the case of A-Li and A-Cs salts, due to their low viscosity, samples are just inserted in a capillary of 0.2 μm diameter.

Temperature dependent X-ray scattering measurements in transmission geometry are performed at the BM26 beamline at the ESRF in Grenoble. Real-time X-ray patterns are recorded during a programmed thermo-treatment as follows. (1) Stay at room temperature of 25 ℃ for 5 minutes. (2) Cool to -100 ℃ at a cooling rate of 5 ℃/min. The wavelength used for X-ray measurements is of λ = 1.03 Å. X-ray patterns are recorded by a two-dimensional CCD camera (FReLoN Kodak CCD). The sample detector distance is calibrated by using an AgBe standard.

6.2.3 Other techniques

Differential scanning calorimetry (DSC) measurements, polarized optical microscopy measurements, ion conductivity measurements and water uptakes are all performed according to the descriptions in Part 3.2 Experimental of Chapter 3.

6.3. Results and Discussion

6.3.1 Phase behavior of the four salts

At room temperature, A-Na and A-K are waxy solids, while A-Li and A-Cs are viscous liquids. They are studied by differential scanning calorimetry (DSC), the results of which are presented in Figure 1. Table 1 summarizes the phase transition temperature and transition enthalpy of these compounds determined by DSC.

According to DSC data, both A-Na and A-K salts show clearly an endothermal peak of a small transition enthalpy upon heating. POM investigation demonstrates a transition from a birefringent texture (Figure 2) to an optically isotropic one.

At the same time, A-Li and A-K salts show no clear endothermal peaks in the temperature range from -40 ℃ to 100 ℃, and at room temperature they exhibit an isotropic texture.

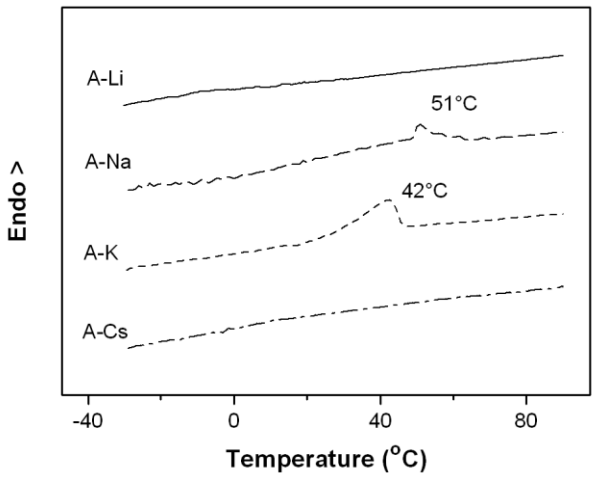

Figure 1. DSC thermograms of A-Li, A-Na, A-K and A-Cs salts obtained from the second heating run with a heating rate of 10 K/min.

Table 1. Phase transition temperature and transition enthalpy calculated from DSC thermograms of A-Na and A-K salts (heating rate 10 K/min). A-Li and A-Cs salts show no endothermal peaks in the experimental temperature range.

Sample	Phase transition temperature range (°C)	ΔH (J/g)
A-Na	51	2.86
A-K	42	1.84

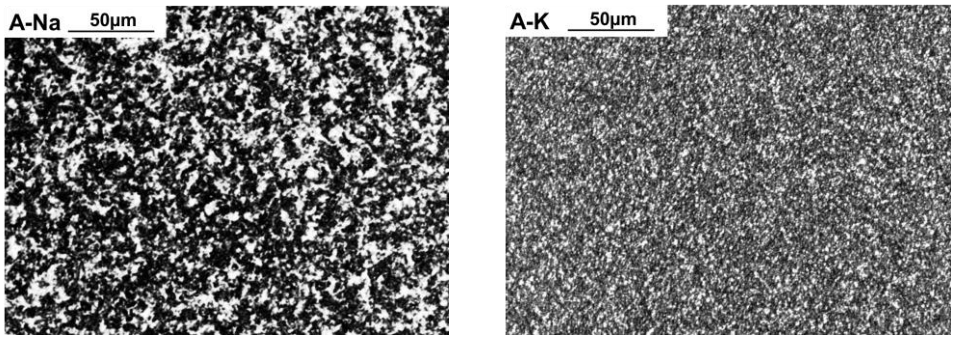

Figure 2. POM images of A-Na and A-K salts at room temperature.

Small-angle X-ray scattering (SAXS) technique is applied to identify the structure of the mesophase formed by each salt. All A-Li, A-Na, A-K and A-Cs samples are performed with a programmed thermo-treatment from 25 ℃ to -100 ℃. Variable-temperature SAXS patterns recorded for all samples are presented in Figure 3.

During the cooling run, there is a change of SAXS patterns observed at -11 ℃ for A-Li, -10 ℃ for A-Na, -10 ℃ for A-K, and -7 ℃ for A-Cs, although DSC does not show any transition at these temperatures. The Miller indices of the reflections are indicated in Figure 3 as well.

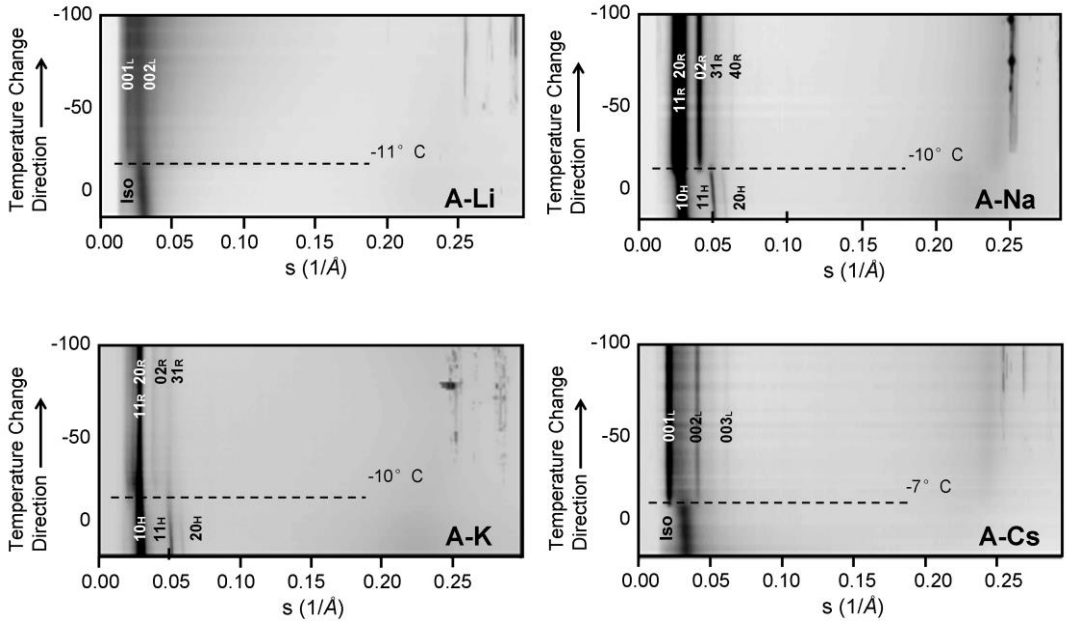

Figure 3. Variable-temperature SAXS patterns of A-Li, A-Na. A-K and A-Cs. At low temperature below 0 ℃, several peaks at high s values around 0.25 are observed for all samples, they can be ascribed to ice, because they disappear when temperature rises above 0 ℃. The Miller indices of the different reflections are indicated (Iso=isotropic, L=lamellar, H=hexagonal and R=centered rectangular).

Table 2. SAXS results obtained at 25 ℃ from A-Na and A-K.

Sample	Mesophase	*hkl*	*d* spacing Experiment (Å)	*d* spacing Calculated (Å)	Lattice parameter (Å)
A-Na	Col_h	*100*	33.8	33.9	*a* = 39.1
		110	19.6	19.6	
		200	17.0	16.9	
A-K	Col_h	*100*	33.6	33.6	*a* = 38.8
		110	19.4	19.4	
		200	16.8	16.8	

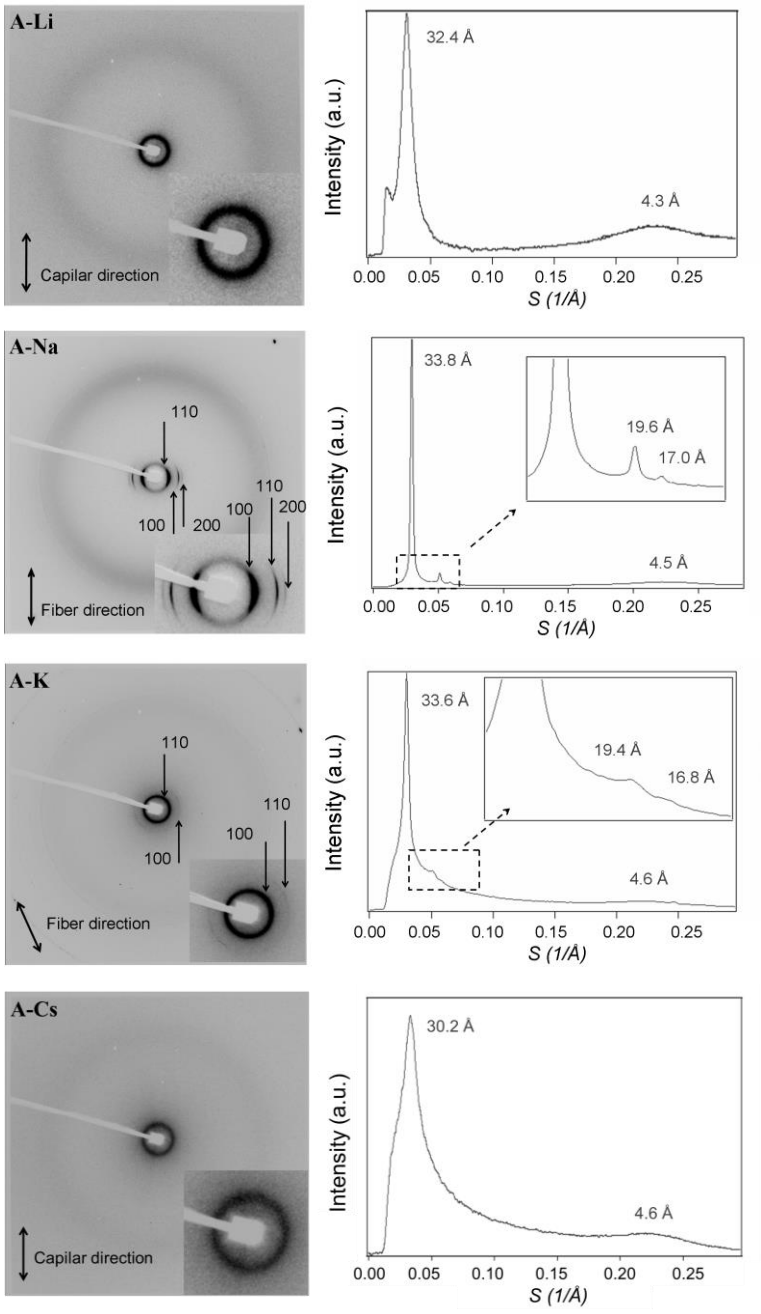

Figure 4. 2D SAXS patterns and corresponding 1D diffractograms of A-Li, A-Na, A-K and A-Cs at room temperature. The *d* spacings corresponding to each peak are indexed in Table 2.

The detailed 2D SAXS patterns and 1D diffractograms obtained from all sulfonates at room temperature (25 ℃) are presented in Figure 4, and the results are listed in Table 2.

According to the SAXS and POM data, A-Li and A-Cs salts show similar phase behavior at 25 ℃. Their SAXS patterns show a peak in the small angle area with an interlayer distance of d = 32.4 Å for A-Li, and d = 30.2 Å for A-Cs. While both of them form an isotropic texture, it can be concluded that they are in an isotropic melt state at room temperature.

Meanwhile, A-Na and A-K salts form a disordered hexagonal columnar (Col_{hd}) phase at 25 ℃, since the ratio of the measured d spacings is 1:1/√3:1/2. They can be attributed to 100, 110 and 200 reflections of a 2D hexagonal lattice with a distance between centers of adjacent columns a = 39.1 Å for A-Na, and a = 38.8 Å for A-K.

Interestingly, when temperature drops to below ca. -10 ℃, all these sulfonates undergo a phase structure, and the low temperature phases remain till -100 ℃ according to the SAXS data. The SAXS patterns measured at -30 ℃ are presented in Figure 5 and the results are also listed in Table 3.

According to Figure 5, A-Li and A-Cs show 001 and 002 reflections with the ratio 1:2 that clearly identifies the existence of a lamellar phase (*Lam*). While A-Na and A-K present the reflections of 110, 200, 020 and 310 from a centered rectangular columnar phase (Col_{cr}). Moreover, the 001 reflection of a lamellar phase can also be seen in the case of A-K, this indicates that A-K forms a mixture of Col_{cr} and *Lam* phases.

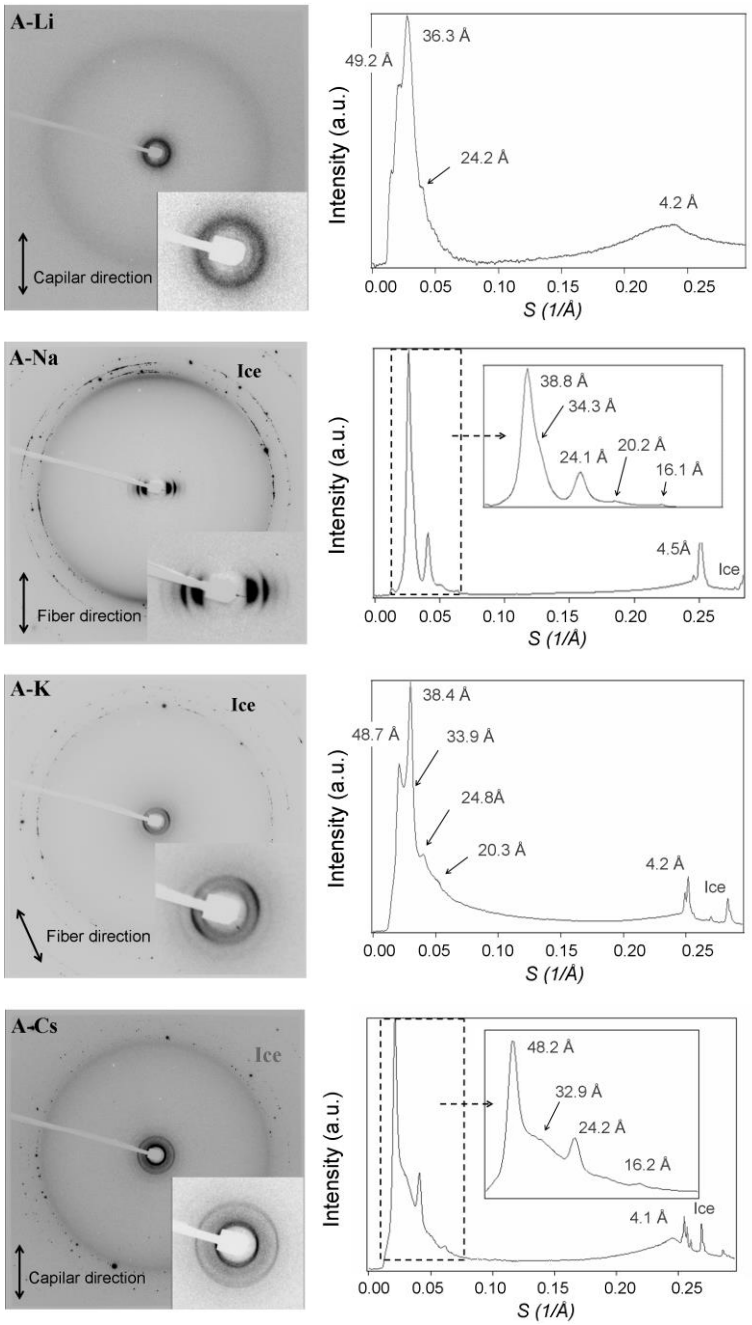

Figure 5. 2D SAXS patterns and 1D diffractograms of A-Li, A-Na, A-K and A-Cs recorded at -30 ℃. The *d* spacings corresponding to each peak are indexed in Table 3.

Table 3. SAXS results of A-Li, A-Na, A-K and A-Cs obtained at -30 ℃.

Sample	Mesophase	*hkl*	*d* spacing Experiment (Å)	*d* spacing Calculated (Å)	Lattice parameter (Å)
A-Li	*Iso*		ca. 36		
	Lam	001	49.2	49.6	
		002	24.2	24.8	
A-Na	Col_{cr}	110	38.8	39.0	a = 67.5 b = 47.8
		200	34.3	33.7	
		020	24.1	23.9	
		310	20.2	20.3	
		400	16.1	16.9	
A-K	Col_{cr}	110	38.4	39.1	a = 67.2 b = 47.1
		200	33.9	33.6	
		020	24.8	24.0	
		310	20.3	20.3	
	Lam	001	48.7	48.7	
A-Cs	*Iso*		ca. 33		
	Lam	001	48.2	48.4	
		002	24.2	24.2	
		003	16.2	16.1	

Phase transition from Col_h to Col_{cr} has been observed in several systems and is featured by the appearance of "biaxiality" and the break of symmetry [10-12], which can be driven by the shape change of the mesogens or by the tilt of discotic units respecting to the column axis. In the case of A-Na, the $Col_h \rightarrow Col_{cr}$ transition starts when the temperature drops below -10 ℃. As shown in Figure 5, the symmetry break occurs and drives the 100 peak of the Col_h split into two peaks indexed as the 110 and 200 of the Col_{cr} phase (Figure 2). The Miller indices of the remaining peaks are

indexed accordingly as 020, 310 and 400. It can be found that the law of the Miller indices of $h+k=2n+1$ identifies the symmetry of the Col_{cr} phase to the c2mm group.

The peak positions of A-Na remain almost unchanged during cooling once the Col_{cr} phase is formed. However, the lattice parameters change from $a = b = 39.1$ Å ($a' = 67.7$ Å, see Figure 6) in Col_h phase to $a = 67.5$ Å and $b = 47.8$ Å in the Col_{cr} phase. This indicates that the supramolecular discs are tilted along *b* axis. The tilt of the mesogens increases the distances between the columns along *b* axis (Figure 6, top), and it is assumed to be the result of the drop of temperature.

While A-K shows almost the same behavior during the phase transition as A-Na, an extra reflection at lower angle at -30 ℃ is however observed. The corresponding *d*-spacing is calculated to be 48.7 Å, which is very close to the 010 spacing of the columnar phase (Figure 2 and 4c). It can be assumed that it corresponds to the first order of a lamellar phase.

Unlike A-Na and A-K showing a transition of $Col_h \rightarrow Col_{cr}$, A-Li and A-Cs show a transition from isotropic to lamellar phase (*Iso*→*Lam*). The ratio between *d*-spacings corresponding to the isotropic rings appeared after phase transition is observed to be 1:2 for A-Li and 1:2:3 for A-Cs, confirming the presence of a layered structure with a layer thickness of ca. 36 and 33 Å for A-Li and A-Cs, respectively. The reason for the formation of lamellar instead of columnar phases may be due to the size of the counterions, it is however in contradictory to our previous study [8], where the size of the counterions is shown to influence only the geometry of the molecules. It can be assumed that the Li^+ is too small and Cs^+ is too large to form the columnar phases. When ionic interactions are dominant in the self assembly process, lamellar phases tend to be stabilized [9].

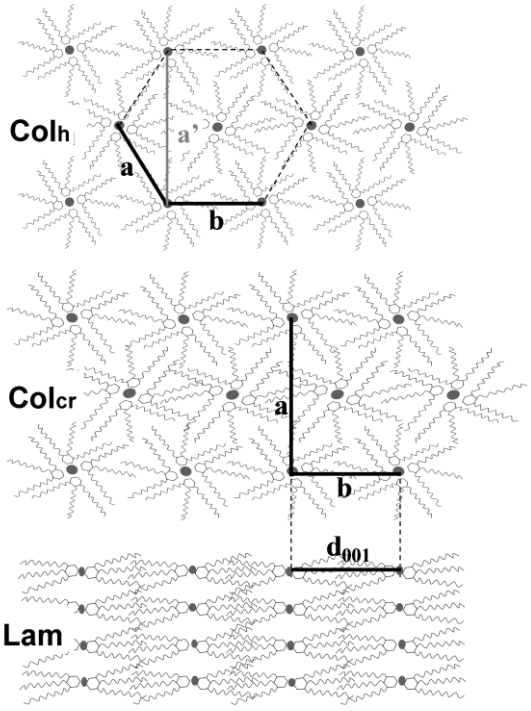

Figure 6. Illustration of hexagonal columnar (Col_h), centered rectangular columnar (Col_{cr}) and Lamellar (*Lam*) lattices for wedge-shaped sulfonate molecules.

The equation below is used to calculate the number of molecules per 2D unit cell in each phase structure of A-Na and A-K, which form columnar phases.

$$N_{EC} = N_A \frac{V \times \rho}{M} \qquad \text{(Eq. 6.1)}$$

where N_{EC} is the number of molecules per 2D unit cell,

N_A is the Avogadro's number,

M is the molecular weight,

V is the average volume of the 2D unit cell (aliphatic chain distances measured by X-ray),

ρ is the density of each molecules.

Table 4. Number of molecules per 2D unit cell (N_{EC}) in each phase structure of A-Na and A-K at 25 ℃ and -30 ℃.

Sample	25 ℃		-30’ ℃	
	Mesophase	N_{EC}	Mesophase	N_{EC}
A-Na	Col_h	4.2 (Tetramer)	Col_{cr}	8.1 (Tetramer)
A-K	Col_h	4.1 (Tetramer)	Col_{cr}	7.9 (Tetramer)

According to Table 4, the N_{EC} of A-Na and A-K molecules in different mesophases are all very close to 4 or 8 (1 or 2 discs in each unit). It can be concluded that the cross section of columns are formed by tetramers of A-Na and A-K molecules. From these results, it can be seen that cooling dose not change the number of molecules forming the columnar cross sections of A-Na and A-K, it only drives the tilt of the supramolecular discs.

6.3.2 Ion conductivities vs. humidity

In Chapter 3 the dependence of ion conductivity on RH of A-Na is studied, and it is related to the swelling of the supramolecular columns and the formation of bicontinuous cubic structures. In this work the through-plane ion conductivity of each sulfonate is measured by impedance spectroscopy at 25 ℃ and different RH. The results are summarized in Table 5 and plotted in Figure 7.

Ion conductivity can be influenced by various factors including type of ions, water content, phase structures, and etc. The ionic and hydrated radii as well as mobility of the alkaline metal ions in aqueous solutions [13] are presented in Table 6. It can be seen that the effective ionic radii in water (so called hydrated ionic radii)

decrease down the group due to the reduction of the degree of hydration. Therefore, the mobility of the alkaline metal ions in water increases with the increase of atomic number.

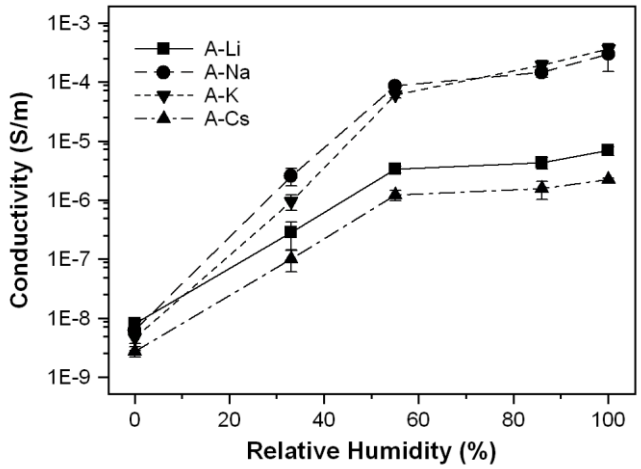

Figure 7. Ion conductivity of A-Li, A-Na, A-K and A-Cs as a function of humidity.

Table 5. The ion conductivities of A-Li, A-Na, A-K and A-Cs. The standard deviations are in the brackets with the same order of magnitude.

Sample	Ion Conductivity (S/m)				
	Dry state	RH=33%	RH=55%	RH=86%	RH=100%
A-Li	8.07×10^{-9} (1.54)	2.84×10^{-7} (1.40)	3.37×10^{-6} (0.46)	4.32×10^{-6} (0.96)	6.87×10^{-6} (1.23)
A-Na	6.22×10^{-9} (2.44)	2.56×10^{-6} (0.83)	8.66×10^{-5} (0.70)	1.45×10^{-4} (0.27)	2.95×10^{-4} (1.45)
A-K	4.69×10^{-9} (1.88)	9.42×10^{-7} (2.67)	6.16×10^{-5} (0.84)	1.95×10^{-4} (0.33)	3.63×10^{-4} (0.62)
A-Cs	2.73×10^{-9} (0.54)	1.01×10^{-7} (0.40)	1.22×10^{-6} (0.24)	1.56×10^{-6} (0.54)	2.21×10^{-6} (1.45)

Table 6. Ionic and hydrated radii as well as mobility of alkaline metal ions in aqueous solutions [13].

Ion	Ionic radius (pm)	Hydrated Radius (pm)	Ionic Mobility ($ohm^{-1}\ cm^2\ mol^{-1}$)
Li^+	76	340	33.5
Na^+	102	276	43.5
K^+	138	232	64.5
Cs^+	167	226	68.0

For this series of sulfonates the ion conductivity behaves completely different from the ions in aqueous solutions. As can be seen in Figure 7 and Table 5, samples with smaller ions show higher ion conductivity in dry states. The conductivity increases significantly with the increase of RH. In particular, the conductivity of A-Na and A-K, which form a Col_{hd} phase, increases much faster than that of A-Li and A-Cs that are in the isotropic state.

In order to clarify the influences of RH, the water uptake λ, which is expresses as the ratio of the number of water molecules per sulfonate group, is determined as a function of RH by means of gravimetric analysis, and calculated according to Equation 6.2 for each sample. The results are summarized in Table 7 and plotted in Figure 8.

$$\lambda = \frac{m(wet) - m(dry)}{m(dry)} \times \frac{M(Sample)}{M(H_2O)} \qquad \text{(Eq. 6.2)}$$

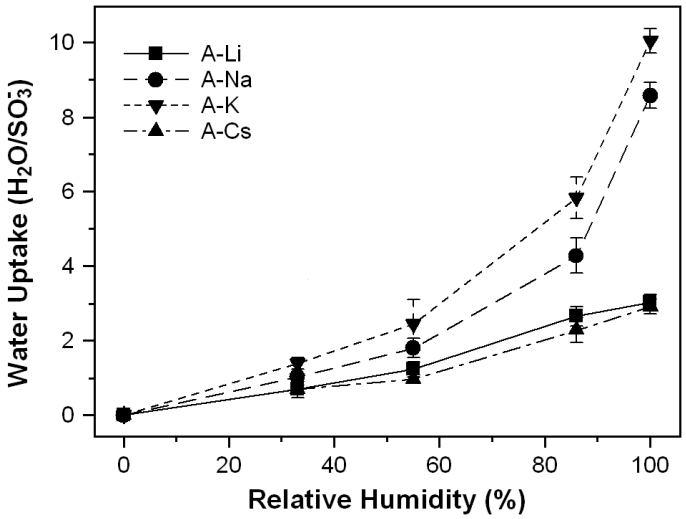

Figure 8. Water uptake of A-Li A-Na, A-K and A-Cs *vs.* relative humidity.

Table 7. The dependence of water uptake of A-Li A-Na, A-K and A-Cs on RH. The standard deviation is in the brackets.

Sample	Water Uptake (H_2O/SO_3^-)				
	Dry state [(a)]	RH=33%	RH=55%	RH=86%	RH=100%
A-Li	0	0.70 (0.11)	1.23 (0.20)	2.66 (0.26)	3.02 (0.22)
A-Na	0	1.03 (0.03)	1.80 (0.26)	4.28 (0.47)	8.58 (0.35)
A-K	0	1.39 (0.15)	2.45 (0.65)	5.83 (0.56)	10.05 (0.33)
A-Cs	0	0.69 (0.22)	0.97 (0.12)	2.29 (0.33)	2.92 (0.21)

(a) At dry state, the λ value is set to be 0.

The dependence of water uptake on RH in Figure 8 shows that A-Na and A-K take up much more water (4 times at most) than A-Li and A-Cs salts at the same RH conditions. It is clear that the higher water uptake accounts for their much faster increase of conductivity.

For A-Na it is already known that in the columnar phase the water molecules penetrate into the center of the columns, creating effective ion channels. At high RH, the columnar structure cannot preserve its cylindrical interface topology anymore and transforms into a bicontinuous 3D water channel structure. The newly formed mesophases generate more conducting pathways, thereby additionally improving the film conductivity, as compared to the swollen columnar structure. A-K behaves quite similarly. However, at room temperature, A-Li and A-Cs do not form any ordered structures. The water uptake in such systems should be quite limited, because the water molecules would create an isolated water domain structure, which has much more interfaces in comparison to the microphase-separated columnar structure. It is clear that such structure does not contain effective ionic pathways. The SAXS measurements on A-Li and A-Cs under different RH are still in progress.

6.4. Conclusion

The temperature dependent phase structures of a series of wedge-shaped sulfonate molecules A-Li, A-Na, A-K and A-Cs are examined by SAXS in the temperature from 25 ℃ to -100 ℃. It is found that A-Li and A-Cs, which are isotropic at room temperature, are transformed to a lamellar phase upon cooling. In contrast, A-Na and A-K that forming a Col_h phase at ambient conditions, undergo a transition to a Col_{cr} phase at -10 ℃, for A-K the columnar phase coexists with a lamellar phase. The

transition from Col_h to Col_{cr} is found to be initiated by the tilt of the supramolecular discs leading to the change of distances between each column in one direction, but the number of molecules forming the columnar cross section remains 4. It is further demonstrated that the ionic channels formed in the columnar phase of A-Na and A-K effectively improve the water uptake and ion conductivity in comparison with the isotropic samples A-Li and A-Cs.

6.5. References

[1] Lehn, JM. Supramolecular Chemistry, Concepts and Perspectives, VCH, Weinheim, **1995**.

[2] Ariga, K; Kunitake, T. Supramolecular Chemistry - Fundamentals and Applications, Springer-Verlag, Berlin Heidelberg, **2006**.

[3] Wiesenauer, BR; Gin, DL. Nanoporous polymer materials based on self-organized, bicontinuous cubic lyotropic liquid crystal assemblies and their applications, *Polym. J.*, **2012**, *44* (6 Special), 461-468.

[4] Desiraju, GR. Prespective in Supramolecular Chemistry: the Crystal as a Supramolecular Entity, John Wiley & Sons, Chichester, **1996**.

[5] Gnanasekaran, K; Daniel, M. Effect of flow on soliton-like director reorientation in a nematic liquid crystal, *Phys. Scr.*, **2012**, *8*6 (1), 015602 (11 pp.).

[6] Yoshizawa, A. Liquid crystal supermolecules stabilizing an optically isotropic phase with frustrated molecular organization, *Polym. J.*, **2012**, *44* (6 Special), 490-502.

[7] Hori, R; Furukawa, D; Yamamoto, K; Kutsumizu, S. Light-driven phase transition in a cubic-phase-forming binary system composed of 4 '-N-docosyloxy-3 '-nitrobiphenyl-4-carboxylic acid and an azobenzene derivative, *Chem. Eur. J.*, **2012**, *1*8 (24), 7346-7350.

[8] Beginn, U; Yan, LL; Chvalun, SN; Shcherbina, MA; Bakirov, A; Moller, M. Thermotropic columnar mesophases of wedge-shaped benzenesulfonic acid mesogens, *Liq. Cryst.*, **2008**, *3*5 (9), 1073-1093.

[9] Binnemans, K. Ionic liquid crystals, *Chem. Rev.*, **2005**, *10*5 (11), 4148-4204.

[10] Safinya, CR; Liang, KS; Varady, WA; Clark, NA; Andersson, G. Synchrotron X-ray study of the orientational ordering d2-d1 structural phase-transition of freely suspended discotic strands in triphenylene hexa-normal-dodecanoate, *Phys. Rev. Lett.*, **1984**, *5*3 (12), 1172-1175.

[11] Gearba, RI; Anokhin, DV; Bondar, AI; Bras, W; Jahr, M; Lehmann, M; Ivanov, DA. Homeotropic alignment of columnar liquid crystals in open films by means of surface nanopatterning, *Adv. Mater.*, **2007**, *1*9 (6), 815-820.

[12] Laschat, S; Baro, A; Steinke, N; Giesselmann, F; Hagele, C; Scalia, G; Judele, R; Kapatsina, E; Sauer, S; Schreivogel, A; Tosoni, M. Discotic liquid crystals: From tailor-made synthesis to plastic electronics, *Angew. Chem. Int. Ed.*, **2007**, *4*6 (26), 4832-4887.

[13] Richens, D. The Chemistry of Aqua Ions: Synthesis, Structure and Reactivity: ATour Through the Periodic Table of the Elements, Wiley, **1997**.

Chapter 7

Synthesis, Phase Behavior and Ion Conductivity of An Azo-Containing Wedge-Shaped Sulfonate Molecule: Sodium 4'-[3'',4'',5''-Tris(11'''-meth-acryloyloxyundecyl-1'''-oxy)benzoyloxy]azobenzene-4-Sulfonate

In this chapter, the synthesis, phase behavior and ion conductivity of a new methacrylated wedge-shaped sulfonate molecule, sodium 4'-[3",4",5"-tris(11"'-meth-acryloyloxyundecyl-1"'-oxy)benzoyloxy]azobenzene-4-sulfonate (Azo-Na), are described. It is found that Azo-Na forms an orthorhombic crystalline phase at low temperature, and by heating it is transformed into a disordered hexagonal columnar (Col_{hd}) phase. The formation of the Col_{hd} mesophase is also observed by water uptake of Azo-Na at RH=100% condition. In this case, according to the X-ray scattering data, very thick supramolecular columns with a diameter of 10.8 nm are formed, and the center of the columns is filled with water molecules. According to gravimetry analysis, at RH=100% condition, Azo-Na uptakes 15.3 water molecules per sulfonate group. At 25 ℃, the dry sample shows a very low conductivity of 7.32×10^{-10} S/m, but at RH=100% condition, the conductivity increases to 0.0103 S/m. The reason for the different behavior of Azo-Na and sodium 2,3,4-tris(11'-acryloyloxyundecyl-1'-oxy)benzenesulfonate (A-Na) is also discussed.

7.1. Introduction

Supremolecular self-assembly offers great avenues for the structural control of materials on the nanoscopic length scale, which plays a pivotal role in the structural design in many applications including nanoporous membranes, lithographic templates, scaffolds, and etc [1-3]. The advantages of self-assembled materials are the large diversity of well-defined structures and easy control of supramolecular structures by applying external fields. In supramolecular chemistry it is a fundamental challenge to use chemical design and external influence as two main tools to address desired functions and applications [4-6].

Our group is interested in the design of wedge-shaped amphiphilic sulfonate molecules as building blocks for the construction of supranolecular membranes with embedded ionic channels [7-14]. Previously, a series of wedge-shaped amphiphilic sulfonates, 2,3,4-tris(11'-acryloyloxyundecyl-1'-oxy)benzenesulfonates, with different counterions were synthesized and systematically studied. In these compounds, the sulfonate group is linked directly to the benzene ring of trialkoxybenzene. It is shown that the humidity has a profound influence on their structure as well as properties. For example, the sodium salt (A-Na) exhibits the formation of a hexagonal columnar (Col_{hd}) phase at low humidity, but with the increase of humidity, a transition to bicontinuous cubic (Cub_{bi}) phases is observed [15].

A question arises here is how the chemical structure of the molecules may influence this transition. In order to address this, a new methacrylated wedge-shaped sulfonate molecule, namely sodium 4'-[3",4",5"-tris(11'"-methacryloyloxyundecyl-1'"-oxy)benzoyloxy]azobenzene-4-sulfonate (Azo-Na) is synthesized. In this molecule, an azobenzene sulfonate group is connected to trialkoxybenzene via an ester group, i.e. a rigid aromatic fragment is introduced. Furthermore, the presence of the azobenzene group offers the possibility to control the supramolecular assembly by

photochemical reactions. The focus of this work is to study the influence of humidity on the mesostructure as well as ion conductivity of this compound. The reason for the different behavior of A-Na and Azo-Na will be discussed.

7.2. Experimental

7.2.1. Materials and Synthesis

Thionyl chloride (reagent grade, 97%, Sigma Aldrich), triethylamine (p.a. grade, Merck), tetrahydrofuran (THF, anhydrous >99.9%, Sigma Aldrich), chloroform (p.a. grade, VWR), benzene (p.a. grade, ≥99.7%, Sigma Aldrich), dimethylformamide (ACS reagent, ≥99.8%, Sigma Aldrich), sodium sulfate (ACS reagent, ≥99.0%, anhydrous, Sigma Aldrich), ethanol (≥99.5%, anhydrous, VWR) are used as received. Other materials are described in the Ref. 10 and 11.

3,4,5-Tris(11'-methacryloyloxyundecyl-1'-oxy)benzoic acid is synthesized according to a literature procedure [10] and it is transformed to 3,4,5-tris(11'-methacryloyloxyundecyl-1'-oxy)benzoyl chloride by reacting with thionyl chloride in benzene. The final product, sodium 4'-[3",4",5"-tris(11'"-methacryloyloxyundecyl-1'"-oxy)benzoyloxy]azobenzene-4-sulfonate (Azo-Na), is prepared as follows. To a well stirred solution of sodium 4'-hydroxyazobenzenesulfonate (1.08 g, 3.6mmol) and triethylamine (0.5 ml, 3.6 mmol) in DMF (20 ml) is slowly added a solution of 3,4,5-tris(11'-methacryloyloxyundecyl-1'-oxy)benzoyl chloride (3.54 g, 2.9 mmol) in dried THF (20 ml) at 0 ℃. Stirring is continued for 12 hours after completing the addition. The reaction mixture is poured to water (400 ml), acidified to pH value 7 and then extracted several times by chloroform. The extract is dried by anhydrous sodium

sulfate and the solvent is removed under reduced pressure. The product is purified by gradient columnar chromatography in THF/ethanol. First, THF is used to wash away all the impurities; subsequently the product is washed out by using a mixture THF/ethanol (1:5). The purified product is then dissolved in dried benzene to prepare a 10 wt% solution, which is filtered through a membrane filter with pore size 5μm. An orange powder was obtained after freeze-drying from benzene. Yield: 2.93 g (68 %). ^{1}H NMR, (DMSO-d6, chemical shift/ppm): 1.27 (m, 30H; PhO-$(CH_2)_3$-$(C\underline{H_2})_5$-$(CH_2)_3$-COO-), 1.47 (m, 12H; PhO-$(CH_2)_2$-$C\underline{H_2}$-, and -$C\underline{H_2}$-$(CH_2)_2$-COO-), 1.67 (m, 6H; -$C\underline{H_2}$-CH_2-COO-), 1.78 (m, 6H; PhO-CH_2-$C\underline{H_2}$-), 2.01 (m, 9H; CH_2=C($C\underline{H_3}$)-COO-), 4.04 (t, 6H; PhO-$C\underline{H_2}$-), 4.18 (t, 6H; $C\underline{H_2}$-COO-), 5.54 (m, 3H; CH$\underline{H}$=C(CH_3)-, E to CH3-), 6.10 (m, 3H; C$\underline{H}$H=C(CH_3)-, Z to CH3-), 7.31 (m, 2H; $H_{aromatic}$ in 2 and 6 positions of -O-Ph-COO-), 7.66 (m, 2H; $H_{aromatic}$ in 2 and 6 positions of -COO-Ph-N=N-), 8.00 (m, 4H; $H_{aromatic}$ in 3 and 5 positions of -COO-Ph-N=N-, and $H_{aromatic}$ in 2 and 6 positions of –N=N-Ph-SO_3Na), 8.50 (m, 2H; $H_{aromatic}$ in 3 and 5 positions of –N=N-Ph-SO_3Na). ^{13}C NMR, (DMSO-d6, chemical shift/ppm): 14.02 (CH_2=C($\underline{C}H_3$)-COO-), 25.95-31.57 (alkyl), 63.65 (-COO-$\underline{C}H_2$-), 69.50 (PhO-$\underline{C}H_2$- in 3 and 5 positions), 73.15 (PhO-$\underline{C}H_2$- in 4 position), 106.4 ($C_{aromatic}$ in 2 and 6 positions of -O-Ph-COO-), 122.1-124.4 ($C_{aromatic}$ in -COO-Ph-N=N-, $C_{aromatic}$ in 1 position of -O-Ph-COO-, and $C_{aromatic}$ in –N=N-Ph-SO_3Na), 127.1 ($\underline{C}H_2$=C(CH_3)-COO-), 138.0 (CH_2=$\underline{C}$(CH_3)-COO-), 145.3 ($C_{aromatic}$ in 4 position of -O-Ph-COO-), 148.2 ($C_{aromatic}$ in 4 position of -COO-Ph-N=N-), 153.4 ppm ($C_{aromatic}$ in 3 and 5 positions of -O-Ph-COO-), 158.2 ($C_{aromatic}$ in 1 position of –N=N-Ph-SO_3Na), 166.1 (-$\underline{C}$OO-Ph-N=N-), 169.5 (CH_2=C(CH_3)-$\underline{C}$OO-).

7.2.2 Differential scanning calorimetry (DSC)

DSC measurements are performed using a Netzsch DSC 204 unit. Samples (typical weight, 8 mg) are enclosed in standard Netzsch 25 μL aluminum crucibles. The measurement steps are (1) heating from 25 ℃ to 200 ℃ at 10 ℃/min, (2)

isothermal process at 200 ℃ for 5 minutes, (3) cooling from 200 ℃ to -100 ℃ at 10 ℃/min, (4) isothermal process at -100 ℃ for 5 minutes, (5) heating from -100 ℃ to 300 ℃ at 10 ℃/min.

7.2.3 Small-angle X-ray scattering (SAXS)

The oriented fibers of Azo-Na are prepared with a home-made micro-extruder having the aperture size of 300 μm. The SAXS experiments are performed in transmission geometry at the BM26 beamline of the European Synchrotron Radiation Facility (ESRF) in Grenoble (France). The wavelength is 1.03 Å. The X-ray patterns are recorded with a Pilatus 1M detector. The norm of the reciprocal space vector *s* is calibrated by silver behenate (AgBe). The patterns are corrected for the air scattering.

7.2.4 Other techniques

The measurements of polarizing optical microscopy (POM), through-plain ion conductivity and water uptake are all performed according to Part 3.2 Experimental in Chapter 3.

7.3. Results and Discussion

7.3.1 Synthesis

Azo-Na is synthesized according to Scheme 1. 3,4,5-Tris(11'-methacryloyl-oxyundecyl-1'-oxy)benzoic acid is synthesized according to a literature procedure [10] and it is transformed to 3,4,5-tris(11'-methacryloyloxyundecyl-1'-oxy)benzoyl chloride by reacting with thionyl chloride in benzene. Using a procedure reported

previously by our group [11], the acid chloride is then coupled with sodium 4'-hydroxyazobenzenesulfonate to yield the final product.

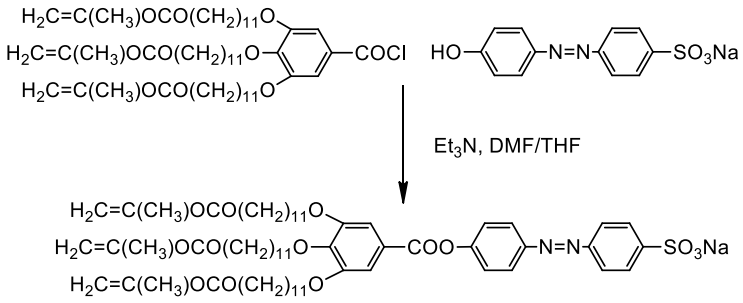

Scheme 1. The synthesis of Azo-Na.

7.3.2 Thermal properties of Azo-Na

The DSC curve of Azo-Na obtained from the second heating run is presented in Figure 1. An endothermal peak with a transition enthalpy of 2.42 J/g is observed at 87.7 ℃. At around 250 ℃, a strong exothermal process starts to take place, which might be related to the decomposition of the compound.

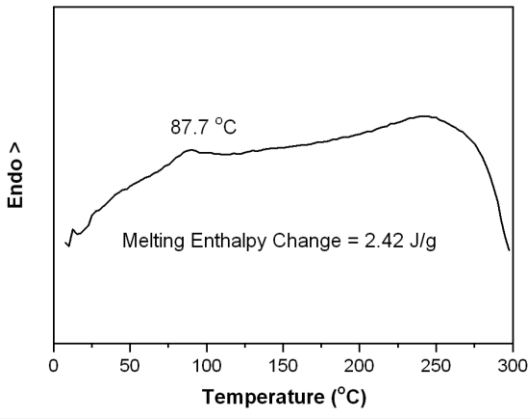

Figure 1. DSC thermogram of Azo-Na on the second heating run.

7.3.3 Thermotropic and lyotropic phase transitions of Azo-Na

For the phase transition study, polarizing optical microscopy (POM) is applied to analyze the textures formed by Azo-Na at different temperature and humidity. Figure 2a and 2b shows the POM images recorded in the dry state at 25 ℃ and 200 ℃, respectively. Figure 2c shows the micrograph obtained at 25 ℃ after equilibration at RH=100% condition. All of the images show birefringent but uncharacteristic textures. In contrast to sodium 2,3,4-tris(11'-acryloyloxyundecyl-1'-oxy)benzenesulfonate (A-Na) that forms bicontinuous cubic phases at high humidity, Azo-Na behaves much differently.

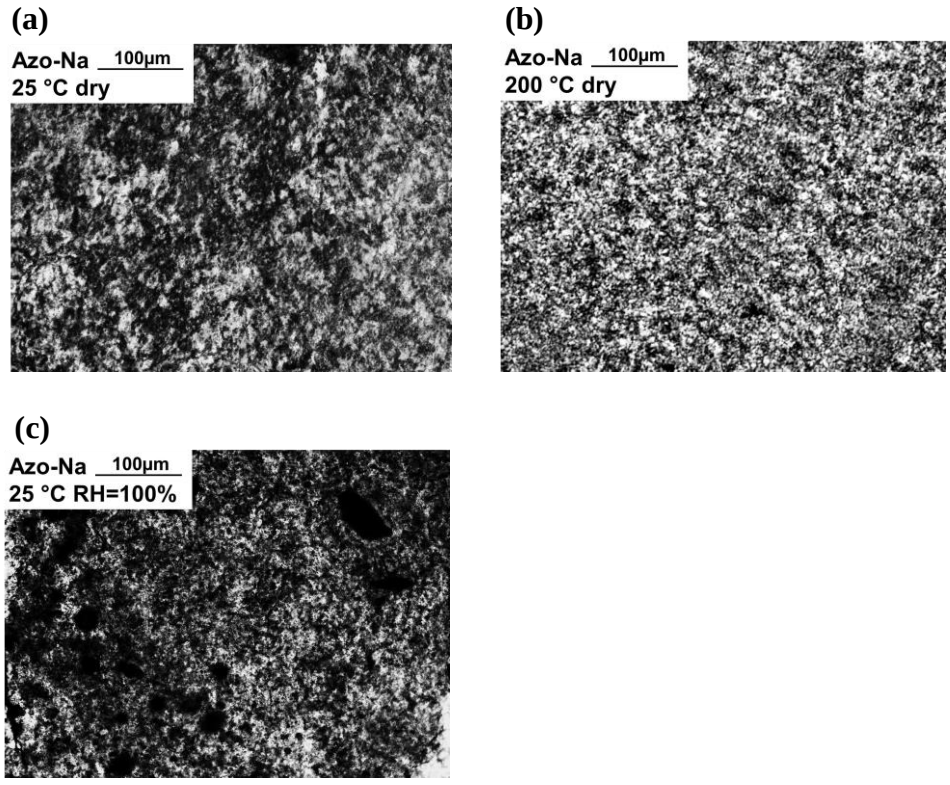

Figure 2. POM images of Azo-Na at (a) 25 ℃ dry state, (b) 200 ℃ dry state, and (c) 25 ℃ after equilibration at RH=100% conditions.

In order to identify the structures at these conditions, small-angle X-ray scattering (SAXS) technique is applied. Figure 3a presents the diffractograms of Azo-Na in the heating run from 25 ℃ to 350 ℃, with the results summarized in Table 1.

In the heating run, it can be seen that there is a phase transition near 85 ℃, which is in accordance with the DSC results showing an endothermic peak at 87.7 ℃. This transition is further demonstrated to be the transition from orthorhombic crystals to a Col_{hd} mesophase. In addition, Figure 3a clearly shows that the mesophase remains till 310 ℃, indicating the good thermal stability of this structure. At around 310 ℃, however, the Col_{hd} mesophase disappears and the sample is completely carbonized.

Table 1. SAXS results of Azo-Na measured at different conditions.

Condition	Mesophase	*d* spacing (Å)	Lattice constant (Å)
25 ℃ Dry	*Cr* *Orthorhombic*	d_{200} = 60.9 d_{020} = 34.7 d_{402} = 22.6 d_{800} = 15.4	*a* = 121.8 *b* = 69.6 *c* = 67.4
200 ℃ Dry	Col_{hd}	d_{100} = 48.5 d_{110} = 28.1 d_{200} = 24.3 d_{210} = 18.4 d_{300} = 16.2	*a* = 56.0
25 ℃ RH=100%	Col_{hd}	d_{100} = 93.2 d_{110} = 53.7 d_{200} = 46.5 d_{210} = 35.4 d_{300} = 31.1	*a* = 107.9

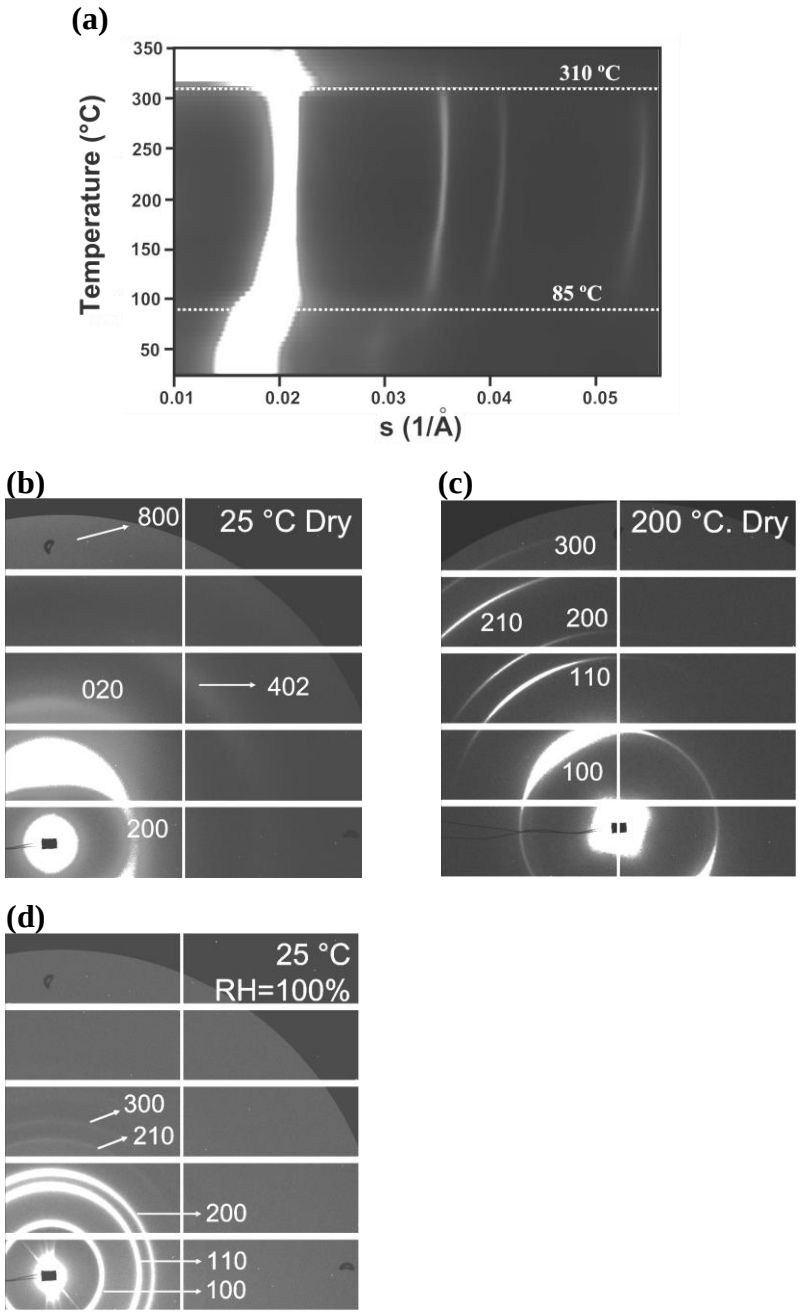

Figure 3. (a) Variable-temperature SAXS patterns of Azo-Na in the heating run. (b) 2D SAXS pattern of Azo-Na at 25 ℃. (c) 2D SAXS pattern of Azo-Na salt at 200 ℃. (d) 2D SAXS pattern of Azo-Na at 25 ℃ after equilibrium at RH=100% condition.

At 25 ℃, four Bragg peaks are visible in the 2D SAXS pattern shown in Figure 3b. From the analysis of the peak positions it can be concluded that at this temperature Azo-Na forms an orthorhombic crystal structure with lattice parameters of a = 121.8 Å, b = 69.6 Å and c = 67.4 Å.

At around 85 ℃, the SAXS pattern starts to change and more peaks appear, from 85 ℃ to 310 ℃, no significant alteration of the SAXS pattern can be observed. The 2D SAXS pattern recorded at 200 ℃ is shown in Figure 2c. Five Bragg peaks with the ratio of s 1:√3:2:√7:3 are visible on the equator of the SAXS pattern. They can be ascribed to the 100, 110, 200, 210 and 300 reflections of a Col_{hd} lattice. During heating from 85 ℃ to 310 ℃, the lattice parameter drops from 57.8 Å to 55.9 Å, i.e. by 3.5 %.

It is worth noticing that in contrast to A-Na which does not crystallize at low temperature, Azo-Na forms an orthorhombic crystalline structure at room temperature. This distinction may originate from the geometry of the molecules. The molecule of Azo-Na is symmetrical; meanwhile the A-Na molecule has an asymmetrical shape that hinders the formation of highly ordered structures. Furthermore, Azo-Na has a much higher isotropization temperature that A-Na, most probably due to the presence of a long rigid aromatic fragment that stabilizes the mesophase.

It is interesting that for Azo-Na the Col_{hd} phase forms not only via heating, but also by increasing RH. On the 2D SAXS pattern of Azo-Na measured at RH=100% shown in Figure 3d, five Bragg peaks are shown with the ratio of s 1:√3:2:√7:3, and they can be ascribed to the 100, 110, 200, 210 and 300 reflections of a Col_{hd} lattice with the lattice parameter of a = 107.9 Å. The diameter of the columns formed in this case is almost twice that of the ones formed by Azo-Na molecules upon heating. By comparing the lattice parameter of the two Col_{hd} phases formed under different conditions, it seems that a water channel with the diameter of more than 5 nm is

present along the axis of the supramolecular column formed at RH=100%. Assuming that the cross section of the thermotropic columns consists of 6 Azo-Na molecules as for most wedge-shaped amphiphilic molecules [16-18] and the conformation of Azo-Na molecule remains unchanged during the swelling, it can calculated as shown in Figure 4 that ca. 18 Azo-Na molecules form a ring surrounded a pool of water molecules in the cross section of the columns.

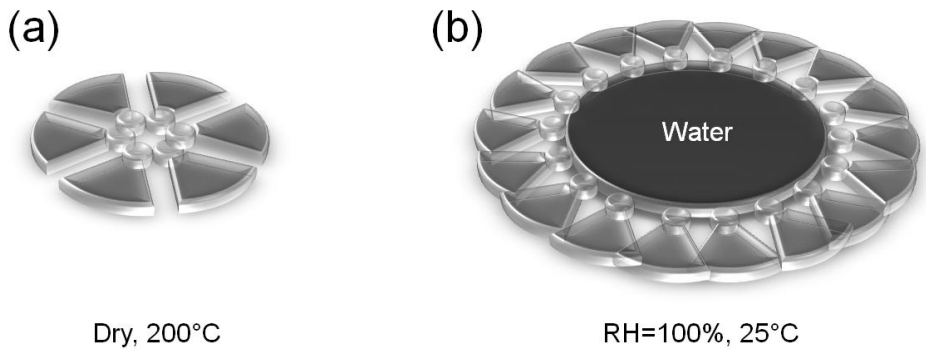

Figure 4. Schematic illustration of molecule packings at (a) dry state at 200 ℃, (b) swollen at RH=100% at 25 ℃.

7.3.4 Ion conductivity and comparison with A-Na

From the analysis of the X-ray data it can be seen that the humidity has a profound influence on the structure of Azo-Na. Further, the ion conductivity and water uptake of this material are studied as a function of RH.

The ion conductivity is measured using AC impedance spectroscopy, at the same time, the water uptake is determined via gravimetric analysis. As shown in Figure 5, at RH ≤ 75%, the impedance of Azo-Na depends strongly on the frequency, and their phases are almost -90 degrees. In contrast, the sample at RH=86% and 100% shows a much weaker dependence of the impedance on frequency, and

meanwhile the phase under these conditions is close to zero. In Figure 4a the ion conductivity calculated from the impedance data versus RH is plotted. It shows that the ion conductivity increases for almost 6 orders of magnitude upon the increase of RH above 75%.

The water uptake of A-Na shows a similar trend as the conductivity (Figure 5a and Table 3). At RH $\leq$ 75%, the water content in A-Na is quite low. When RH increases to 86%, the water uptake increases drastically, and it reaches almost 15 water molecules per sulfonate group. This is in good agreement with the SAXS data, which show the formation of a 5 nm thick water channel inside a supramolecular column.

Table 2. Ion conductivity of Azo-Na at different RH. The standard deviation is in the brackets with the same order of magnitude.

Sample	Ion Conductivity (S/m)					
	Dry state	RH=33%	RH=55%	RH=75%	RH=86%	RH=100%
Azo-Na	7.32×10^{-10} (0.13)	1.52×10^{-9} (0.02)	2.28×10^{-9} (0.09)	9.92×10^{-9} (0.12)	4.24×10^{-3} (0.21)	0.0103 (0.0063)

Table 3. Water uptake of Azo-Na at different RH. The standard deviation is in the brackets.

Sample	Water Uptake (H_2O/SO_3^-)					
	Dry state	RH=33%	RH=55%	RH=75%	RH=86%	RH=100%
Azo-Na	0 [a]	0.35 (0.18)	0.48 (0.08)	1.51 (0.15)	8.28 (0.24)	15.3 (0.12)

[a] The water uptake at dry state is set to be 0.

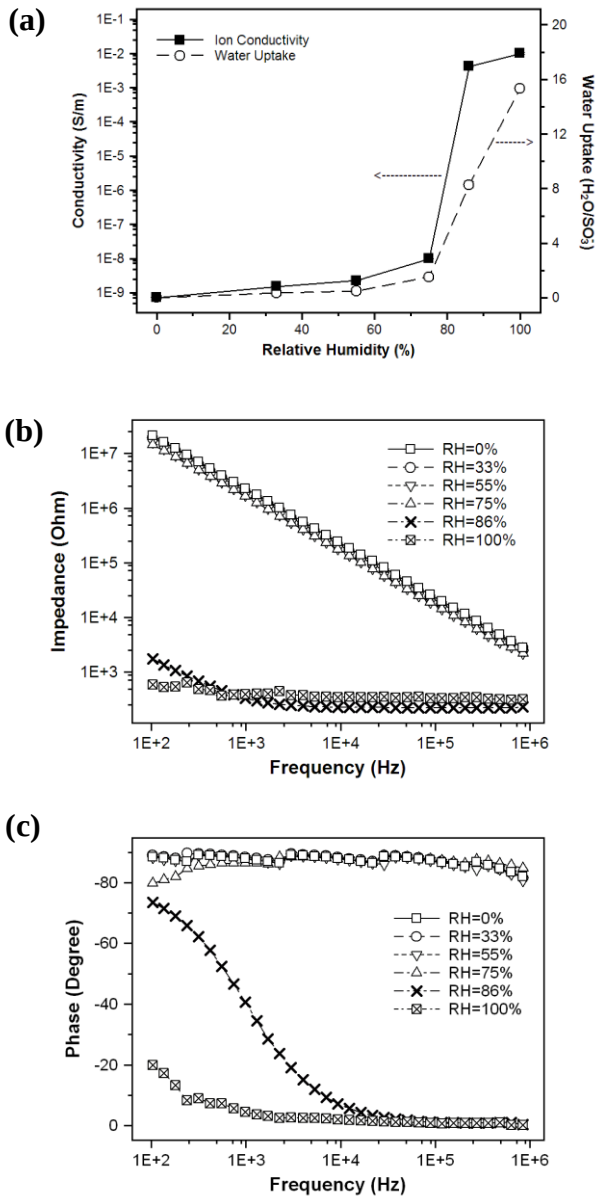

Figure 5. (a) Dependence of conductivity and water uptake λ (water molecules per sulfonate group) on relative humidity. (b) Dependence of impedance on frequency under different RH. (c) Dependence of phase on frequency under different RH.

As shown in Table 2, the dry Azo-Na exhibits very low ion conductivity of 7.32×10^{-10} S/m, which is much lower than that of A-Na which forms a Col_{hd} phase at room temperature. It is possible that in the ordered crystalline phase the sulfonate groups do not form any ionic channels.

By uptaking a big amount of water at high RH, a phase transition takes place and Azo-Na forms a columnar structure containing ionic channels. Due to the huge diameter of the ionic channels (ca. 5 nm at RH = 100%), the ion conductivity reaches a very high value, i.e. 4.24×10^{-3} S/m at RH=86% and 0.0103 S/m at RH=100%, even higher than that of A-Na.

As discussed above, Azo-Na and A-Na behave completely differently upon water uptake by increasing RH. This difference apparently originates from their different chemical structure. In the case of A-Na, the hydrophilic sulfonate groups are always located at the phase boundary because of the molecular structure. The surface energy of the system decreases when the channels are filled with water. Meanwhile, the curvature of the phase boundary increases, which leads to the increase of the conformation energy due to the stretching of the hydrophobic alkyl chains. Therefore, the increase of the number of molecules per cross section would not happen, because it would lead to further stretching of the alkyl chains by keeping the same surface energy and is not energetically favorable. As a result, upon further water uptake, the columns are destructed and become interconnected to form bicontinuous cubic structure.

The Azo-Na molecule contains a long rigid aromatic fragment, which tends to pack parallel to each other to form a liquid crystalline phase. In order to have a dense packing in the crystalline phase, the sulfonate groups should be located inside the aromatic part. This also explains why the conductivity of Azo-Na in the dry state is very low. Upon water uptake, the hydrophilic sulfonate groups move to the phase

boundary and gather together to decrease the energy of the system, resulting in the formation of Col_{hd} phase containing ionic channel structures. Once the ionic channels are constructed, the ion conductivity jumps, up to 6 orders of magnitude in this case.

7.4. Conclusion

A wedge-shaped amphiphilic sulfoante molecule, namely sodium 4'-[3",4",5"-tris(11'"-methacryloyloxyundecyl-1'"-oxy)benzoyloxy]azobenzene-4-sulfonate (Azo-Na), is synthesized and studied regarding the phase behavior and ion conductivity. DSC and SAXS measurements reveal that in the dry state Azo-Na undergoes a phase transition from an orthorhombic crystal structure to a Col_{hd} phase upon heating, and the Col_{hd} phase remains till ca. 310 ℃. The Col_{hd} phase also forms after equilibration at RH=100% condition at 25 ℃. At 25 ℃ the dry Azo-Na sample has shows a very low conductivity of 7.32×10^{-10} S/m, but after equilibration at RH=100% the conductivity jumps to 0.0103 S/m. Such significant increase can be explained by the formation of a 5-nm-wide water channel in the supramolecular column by taking a big amount of water at RH=100%.

7.5. References

[1] Demus, D; Goodby, JWG; Gray, W; Spiess, HW; Vill, L. Handbook of Liquid Crystals, Wiley-VCH, Weinheim, **1998**.

[2] Kato, T; Mizoshita, N; Kishimoto, K. Functional liquid-crystalline assemblies: Self-organized soft materials, *Angew. Chem. Int. Ed.*, **2006**, *45* (1), 38-68.

[3] Shimizu, T. Self-Assembled Nanomaterials I - Nanofibers, Springer, Berlin, **2008**.

[4] Lehn, JM. Supramolecular Chemistry, Concepts and Perspectives, VCH, Weinheim, **1995**.

[5] Ariga, K; Kunitake, T. Supramolecular Chemistry - Fundamentals and Applications, Springer-Verlag, Berlin Heidelberg, **2006**.

[6] Vos, JG; Forster, RJ; Keyes, TE. Interfacial Supramolecular Assemblies, John Wiley & Sons Ltd, Chichester, **2003**.

[7] Beginn, U; Zipp, G; Moller, M. Synthesis and characterization of tris-methacrylated 3,4,5-tris[(alkoxy)benzyloxy]benzoate derivatives, *Chem. Eur. J.*, **2000**, *6* (11), 2016-2023.

[8] Beginn, U; Zipp, G; Mourran, A; Walther, P; Moller, M. Membranes containing oriented supramolecular transport channels, *Adv. Mater.*, **2000**, *12* (7), 513-516.

[9] Beginn, U; Zipp, G; Moller, M. Functional membranes containing ion-selective matrix-fixed supramolecular channels, *Adv. Mater.*, **2000**, *12* (7), 510-513.

[10] Beginn, U; Zipp, G; Moller, M. Self-organization of liquid crystalline 3,4,5-tris[(11-methacryloyl-undecyl-1-oxy)-4-benzyloxy]benzoates in low-shrinkage methacrylate mixtures, *J. Polym. Sci., Part A: Polym. Chem.*, **2000**, *38* (3), 631-640.

[11] Zhu, XM; Tartsch, B; Beginn, U; Moller, M. Wedge-shaped molecules with a sulfonate group at the tip - A new class of self-assembling amphiphiles, *Chem. Eur. J.*, **2004**, *10* (16), 3871-3878.

[12] Zhu, XM; Scherbina, MA; Bakirov, AV; Gorzolnik, B; Chvalun, SN; Beginn, U; Moller, M. Methacrylated self-organizing 2,3,4-tris(alkoxy)benzenesulfonate: A new concept toward ion-selective membranes, *Chem. Mater.*, **2006**, *18* (19), 4667-4673.

[13] Zhu, XM; Beginn, U; Moller, M; Gearba, RI; Anokhin, DV; Ivanov, DA. Self-organization of polybases neutralized with mesogenic wedge-shaped sulfonic acid

molecules: An approach toward supramolecular cylinders, *J. Am. Chem. Soc.*, **2006**, *128* (51), 16928-16937.

[14] Zhu, XM; Mourran, A; Beginn, U; Moller, M; Anokhin, DV; Ivanov, DA. Self-assembled structures formed by a wedge-shaped molecule in 2D and 3D: The role of flexible side chains and polar head groups, *Phys. Chem. Chem. Phys.*, **2010**, *12* (7), 1444-1452.

[15] Zhang, H; Li, Lei; Moller, M; Zhu, X; Rueda, J; Rosenthal, M; Ivanov, D. From channel-forming ionic liquid crystals exhibiting humidity-induced phase transitions to nanostructured ion-conducting polymer membranes, *Adv. Mater.*, **2013**, *25* (26), 3543-3548.

[16] Rosen, BM; Wilson, CJ; Wilson, DA; Peterca, M; Imam, MR; Percec, V. Dendron-mediated self-assembly, disassembly, and self-organization of complex systems, *Chem. Rev.*, **2009**, *109* (11), 6275-6540.

[17] Percec, V; Heck, J; Johansson, G; Tomazos, D; Kawasumi, M; Chu, P. Molecular recognition directed self-assembly of supramolecular liquid-crystals, *Mol. Cryst. Liq. Cryst. Sci. Technol., Sect. A*, **1994**, *254*, 137-196.

[18] Beginn, U. Thermotropic columnar mesophases from N-H center dot center dot center dot O, And N center dot center dot center dot H-O hydrogen bond supramolecular mesogenes, *Prog. Polym. Sci.*, **2003**, *28* (7), 1049-1105.

Chapter 8

Synthesis of Deuterated Wedge-shaped Amphiphilic Sulfonate Molecules: Sodium and Potassium 2,3,4-Tris[(9',9',10',10',11',11',12',12',12'-D_9)dodecyl-1'-oxy]benzenesulfonates

In this chapter, two partially deuterated wedge-shaped amphiphilc sulfonate molecules, namely sodium and potassium 2,3,4-tris[(9',9',10',10',11',11',12',12', 12'-D_9)dodecyl-1'-oxy]benzenesulfonates, are synthesized. The whole synthesis procedure of these compounds consists of 8 steps. All intermediate and final products are characterized by means of ^{1}H NMR and ^{13}C NMR spectroscopy. These compounds will be studied in future by solid state deuterium NMR to elucidate the packing of alkyl groups in different mesophases.

8.1 Introduction

Supramolecular assembly of low molecular weight compounds is known to generate a large diversity of nano-scale structures [1-11]. A full understanding of supramolecular systems, which allows the design of self-assembled structures with desired properties, is always a great challenge since it implies the comprehension of the structure as well as the dynamics at the atomic level. X-ray diffraction measurements are certainly the best choice; however, this technique has certain limitations, especially when dealing with less ordered systems like liquid crystals. Solid state NMR is an alternative method, which is also able to afford structural information [12]. Parameters like chemical shifts, chemical shift tensors, chemical shift anisotropy, homo- and heteronuclear dipolar interactions, relaxation times and line-shape allow the study of short range structural environments and dynamic processes. Among all NMR techniques, deuterium NMR has been proved to as a powerful tool for probing molecular dynamics [13], furthermore, selective deuteration in a supramolecular system enables site-specific investigation.

In this thesis, a series of wedge-shaped amphiphilic sulfonate molecules are proved to form a variety of mesostructures as building blocks for the preparation of supramolecular ion-selective membranes [14]. The understanding of each structural unit on the structure formation is certainly desired for the further design of such molecules. Our previous study shows that the alkyl chains are likely to be responsible for the rich polymorphic behavior of wedge-shaped molecules [15]. However, X-ray crystallography shows only an amorphous halo in such disordered liquid crystalline phases, which does not support the study of the packing of the alkyl chains. In this case, solid state NMR would be appropriate for this purpose. The aim of this work is to synthesize partially deuterated wedge-shaped amphiphilic sulfonate molecules for further investigations by solid state deuterium NMR.

Two compounds, namely sodium and potassium 2,3,4-tris(dodecyl-1'-oxy)benzenesulfonates from a series of wedge-shaped amphiphiles developed in our group [16] (Figure 1), are selected in this work. These two compounds form cubic and hexagonal columnar mesopahses at ambient conditions (Table 1), respectively, and in the case of the potassium salt a rich phase sequence is observed. The alkyl chains of these compounds are partially deuterated, i.e. two deuterated compounds, namely sodium and potassium 2,3,4-tris[(9',9',10',10',11',11',12',12',12'-D_9) dodecyl-1'-oxy]benzenesulfonates, are prepared in this chapter. These compounds will be studied in future by solid state deuterium NMR to elucidate the packing of alkyl groups in different mesophases.

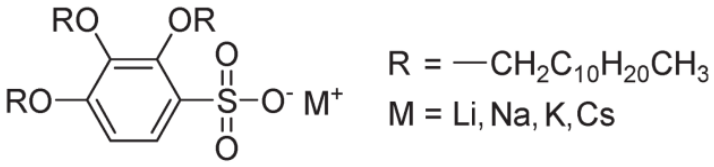

Figure 1. Chemical structure of a series of wedge-shaped sulfonate amphiphiles synthesized in our group [16].

Table 1. Phase sequence of the sodium and potassium compounds shown in Figure 1 [16].

Compounds, M=	Phase sequence
Li	*Cr*, -11 ℃ → *Cub*, 161 ℃ → *Iso*
Na	*Cr*, -3 ℃ → *Cub*, 103 ℃ → *Iso*
K	*Cr*, 18 ℃ → *M1* 47 ℃ → *M2*, 124 ℃ → Col_{hd}, 171 ℃ → *Iso*
Cs	*Cr*, 50 ℃ → Col_{hd}, 193 ℃ → *Iso*

Cr, crystalline phase. ***Cub***, cubic mesophase. ***Col_{hd}***, columnar hexagonal disordered mesophase. ***M***, mesophase type not determined. ***Iso***, isotropic liquid.

8.2. Experimental

8.2.1 Materials

The following materials are all used as received. 1,8-Octanediol (98%, Sigma Aldrich), 1-butanol-d10 (99%, Deutero GmbH), 3,4-dihydro-2H-pyran (97%, Sigma Aldrich), acetone (for analysis, Merck), copper chloride (97%, Sigma Aldrich), dimethyl chloride (for analysis, Merck), ethanol (absolute, for analysis, Merck), ethyl acetate (for analysis, Merck), hexane (for analysis, Merck), hydrobromic acid (puriss. 62%, Sigma Aldrich), hydrochloric acid (>37%, for analysis, Sigma Aldrich), iodine (99.8%, Sigma Aldrich), lithium chloride (anhydrous, >98%, Fluka), N-methyl-2-pyrrolidone (anhydrous, 99.5%, Sigma Aldrich), potassium carbonate (99%, Merck), potassium hydroxide (for analysis, Merck), potassium sulfate (95-97%, Merck), pyridinium p-toluenesulfonate, pyrogallol (puriss. 99%, Riedel-de Haen), sodium chloride (99.99%, Merck), sodium hydrogen carbonate (for analysis, Merck), sodium hydroxide (for analysis, Merck), sodium sulfate (95-97%, Merck), sulphuric acid (95-97%, Merck), tetrabromomethane (99%, Sigma Aldrich), tetrahydrofuran (anhydrous, >99.9%, Sigma Aldrich), toluene (for analysis, Merck), triphenylphosphine (>98.5%, Fluka).

8.2.2. Synthesis

n-Butylbromide-d9 (1): In a flask equipped with a condenser and a magnet stirrer, 12.0 g of 1-butanol-d10 (142.5 mmol) are added into 30.0 mL of hydrobromic acid (62%, 556.2 mmol). The reaction solution is heated at 105 ℃ for 5 hours. Subsequently, 30 ml of dimethyl chloride are added into the mixture and the upper layer is washed with sodium hydrogen carbonate solution and brine, dried over anhydrous sodium sulfate, and then filtered. The final product is purified by distillation at ambient pressure by collecting the fraction in the temperature range

from 98 ℃ to 102 ℃. 12.8 g (87.6 mmol, yield: 61.5 %) of a colorless liquid are obtained. ^{13}C NMR (Chloroform-d1, chemical shift/ppm): 11.8 [$CD_3\underline{C}D_2CD_2CD_2Br$], 15.8 [$\underline{C}D_3CD_2CD_2CD_2Br$], 20.1 [$CD_3CD_2\underline{C}D_2CD_2Br$], 33.0 [$CD_3CD_2CD_2\underline{C}D_2Br$].

8-Bromo-1-octanol (2): In a flask equipped with a condenser and a magnet stirrer, 20.0 g of 1,8-octanediol (136.8 mmol) and 14.0 ml of hydrobromic acid (62%, 259.5 mmol) are added into 500 ml toluene. The reaction suspension is heated at 120 ℃ for 24 hours, and then the upper layer is separated, washed with sodium hydrogen carbonate solution, dried over anhydrous sodium sulfate, filtered and concentrated by a rotary evaporator. The final product is obtained by distillation at $3*10^{-2}$ mbar by collecting the fraction in the temperature range from 80 ℃ to 85 ℃. 26.3 g (125.8 mmol, yield: 92.1 %) of a colorless liquid are obtained. ^{1}H NMR (Chloroform-d1, chemical shift/ppm): 1.33 [m, 6H, $Br(CH_2)_2(C\underline{H_2})_3(CH_2)_3OH$], 1.42 [m, 2H, $Br(CH_2)_5C\underline{H_2}(CH_2)_2OH$], 1.56 [m, 2H, $Br(CH_2)_6C\underline{H_2}CH_2OH$], 1.85 [m, 2H, $BrCH_2C\underline{H_2}(CH_2)_6OH$], 3.40 [t, 2H, $BrC\underline{H_2}(CH_2)_7OH$], 3.63 [t, 2H, $Br(CH_2)_7C\underline{H_2}OH$]. ^{13}C NMR (Chloroform-d1, chemical shift/ppm): 25.6 [$Br(CH_2)_5\underline{C}H_2(CH_2)_2OH$], 28.1-29.2 [3 peaks, $Br(CH_2)_2(\underline{C}H_2)_3(CH_2)_3OH$], 32.6-32.8 [2 peaks, $BrCH_2\underline{C}H_2(CH_2)_6OH$ and $Br(CH_2)_6\underline{C}H_2CH_2OH$], 34.0 [$Br\underline{C}H_2(CH_2)_7OH$], 63.0 [$Br(CH_2)_7\underline{C}H_2OH$].

2-[(8-Bromooctyl)oxy]tetrahydro-2H-pyran (3): Under a nitrogen atmosphere, 15.3 g of 8-bromo-1-octanol (73.2 mmol), 9.0 ml of 3,4-dihydro-2H-pyran (109.6 mmol), and 1.00 g of the catalyst pyridinium p-toluenesulfonate (3.98 mmol) are added into 60 ml of dimethyl chloride in a flask wrapped by aluminum foil. The reaction solution cooled in an ice-water bath is stirred for 30 min and then at room temperature for 3 days. Subsequently, a saturated sodium hydrogen carbonate solution is added into the solution. The upper organic layer is washed with water and brine, dried over anhydrous sodium sulfate, filtered and concentrated by a rotary evaporator. The crude product is purified using silica gel column chromatography with the mobile phase of hexane/ ethyl acetate (13:1 v/v), which affords a colorless

liquid of 19.8 g (67.5 mmol, yield: 92.3 %). ^{1}H NMR (Chloroform-d1, chemical shift/ppm): 1.33 [m, 6H, $Br(CH_2)_2(C\underline{H_2})_3(CH_2)_3OCHO(CH_2)_4$], 1.42 [m, 2H, $Br(CH_2)_5C\underline{H_2}(CH_2)_2OCHO(CH_2)_4$], 1.57 [m, 6H, $Br(CH_2)_6C\underline{H_2}CH_2OCHO(CH_2)_4$ and in 3 and 4 positions of $-O(CH_2)_4$], 1.84 [m, 3H, $BrCH_2C\underline{H_2}(CH_2)_6OCHO(CH_2)_4$ and 1 H atom in 2 position of $-O(CH_2)_4$], 3.40 [m, 4H, $BrC\underline{H_2}(CH_2)_7OCHO(CH_2)_4$ and $Br(CH_2)_7C\underline{H_2}OCHO(CH_2)_4$], 3.51 [t, 1H, 1 H atom in 5 position of $-O(CH_2)_4$], 3.71 [m, 1H, 1 H atom in 5 position of $-O(CH_2)_4$], 3.86 [t, 1H, 1 H atom in 2 position of $-O(CH_2)_4$], 4.57 [t, 1H, $Br(CH_2)_5(CH_2)_3OC\underline{H}O(CH_2)_4$]. ^{13}C NMR (Chloroform-d1, chemical shift/ppm): 19.7 [in 3 position of $-O(CH_2)_4$], 25.5 [in 4 position of $-O(CH_2)_4$], 26.1 [in 2 position of $-O(CH_2)_4$], 28.1-29.7 [4 peaks, $Br(CH_2)_2(\underline{C}H_2)_4(CH_2)_2OCHO(CH_2)_4$], 30.8 [$Br(CH_2)_6\underline{C}H_2CH_2OCHO(CH_2)_4$], 32.8 [$BrCH_2\underline{C}H_2(CH_2)_6OCHO(CH_2)_4$], 34.0 [$Br\underline{C}H_2(CH_2)_7OCHO(CH_2)_4$], 62.4 [$Br(CH_2)_7\ \underline{C}H_2OCHO(CH_2)_4$], 67.6 [in 5 position of $-O(CH_2)_4$], 98.9 [$Br(CH_2)_8O\underline{C}HO(CH_2)_4$].

2-[(9',9',10',10',11',11',12',12',12'-D_9)dodecyl-1'-oxy]tetrahydro-2H-pyran (4): In a three-neck flask which is carefully dried and filled with nitrogen, 1.50 g of magnesium (61.7 mmol) and a grain of iodine are added into 20 ml of anhydrous tetrahydrofuran. To this mixture cooled in an ice-water bath, a solution of 7.90 g of compound **3** (54.1 mmol) in 20 ml of anhydrous tetrahydrofuran is added dropwise. After 2 hours of reaction, the temperature is gradually increased to room temperature. The resulted C_4D_9MgBr is transported into a pre-dried and nitrogen-filled tube and is then added dropwise into a solution of 15.7 g of compound **2** (54.1 mmol), 215.2 mg of anhydrous copper(II) chloride (1.6 mmol), and 67.8 mg of anhydrous lithium chloride (1.6 mmol) in 20 ml of anhydrous N-methyl-2-pyrrolidone and 20 ml of anhydrous tetrahydrofuran. After the reaction solution is stirred at room temperature for 2 hours, 40 ml of hydrochloric acid (5%) is added into the solution. The upper organic layer is added into 50 ml of ethyl acetate, and the resulting solution is then washed with sodium hydrogen carbonate solution, dried over anhydrous sodium

sulfate, filtered and concentrated by a rotary evaporator. The crude product is purified using silica gel column chromatography with the mobile phase of hexane/ ethyl acetate (1:1 v/v), which affords a light yellow liquid of 10.5 g (37.6 mmol, yield: 72.4 %). ^{1}H NMR (Chloroform-d1, chemical shift/ppm): 1.27 [m, 10H, $C_4D_9(C\underline{H}_2)_5(CH_2)_3OCHO(CH_2)_4$], 1.36 [m, 2H, $C_4D_9(CH_2)_5C\underline{H}_2$-$(CH_2)_2OCHO(CH_2)_4$], 1.52 [m, 6H, $C_4D_9(CH_2)_6C\underline{H}_2CH_2OCHO(CH_2)_4$ and in 3 and 4 positions of -$O(CH_2)_4$], 1.64 [m, 1 H in 2 position of -$O(CH_2)_4$], 1.78 [m, 2H, $C_4D_9CH_2C\underline{H}_2(CH_2)_6OCHO(CH_2)_4$], 3.33 [m, 2 H, $C_4D_9(CH_2)_7C\underline{H}_2OCHO(CH_2)_4$], 3.44 [t, 1H, 1 H atom in 5 position of -$O(CH_2)_4$], 3.65 [m, 1H, 1 H atom in 5 position of -$O(CH_2)_4$], 3.80 [t, 1H, in 2 position of -$O(CH_2)_4$], 4.51 [t, 1H, $C_4D_9(CH_2)_5(CH_2)_3OC\underline{H}O(CH_2)_4$].

(9,9,10,10,11,11,12,12,12-D_9)Dodecanol-1 (5): Under a nitrogen atmosphere, 10.5 g of compound **4** (37.6 mmol) and 1.00 g of the catalyst pyridinium p-toluenesulfonate (3.98 mmol) are added into 60 ml of ethanol in a flask equipped with a condenser and a magnetic stirrer. The reaction solution is heated at 70 ℃ for 2 days and is subsequently concentrated by a rotary evaporator. The crude product is purified using silica gel column chromatography with the mobile phase of chloroform, which afforded a light yellow liquid of 5.51 g (28.2 mmol, yield: 74.9 %). ^{1}H NMR (Chloroform-d1, chemical shift/ppm): 1.25 [m, 10H, $C_4D_9(C\underline{H}_2)_5(CH_2)_3OH$], 1.32 [m, 2H, $C_4D_9(CH_2)_5C\underline{H}_2(CH_2)_2OH$], 1.56 [m, 2H, $C_4D_9(CH_2)_5CH_2C\underline{H}_2CH_2OH$], 3.63 [t, 2H, $C_4D_9(CH_2)_5CH_2CH_2C\underline{H}_2OH$]. ^{13}C NMR (Chloroform-d1, chemical shift/ppm): 25.6 [$C_4D_9(CH_2)_5\underline{C}H_2(CH_2)_2OH$], 29.4-29.6 [3 peaks, $C_4D_9(CH_2)_2(\underline{C}H_2)_3$-$(CH_2)_3OH$], 32.8 [$C_4D_9(CH_2)_6\underline{C}H_2CH_2OH$], 63.1 [$C_4D_9(CH_2)_7\underline{C}H_2OH$].

1-Bromo(9,9,10,10,11,11,12,12,12-D_9)dodecane (6): Under a nitrogen atmosphere, 5.51 g of compound **5** (28.1 mmol), 13.1 g of tetrabromomethane (39.4 mmol) and 10.3 g of triphenylphosphine (39.4 mmol) are added into 100 ml anhydrous dimethyl chloride in a flask equipped with a magnetic stirrer. After being stirred in an ice-water bath for 30 min and then at room temperature for 2 days, the

reaction solution is washed with brine, dried over anhydrous sodium sulfate and concentrated by a rotary evaporator. Subsequently, the residue is added into 20 ml of hexane and the resulting mixture is kept at ice-water bath for 2 hours. After the precipitate is removed by filtration, the final product is obtained by removal of hexane in vacuum as a light yellow liquid. Yield: 5.30 g (20.5 mmol, 72.9 %). ^{1}H NMR (Chloroform-d1, chemical shift/ppm): 1.19 [m, 10H, $C_4D_9(C\underline{H}_2)_5(CH_2)_3Br$], 1.36 [m, 2H, $C_4D_9(CH_2)_5C\underline{H}_2(CH_2)_2Br$], 1.79 [m, 2H, $C_4D_9(CH_2)_5CH_2C\underline{H}_2CH_2Br$], 3.33 [t, 2H, $C_4D_9(CH_2)_5CH_2CH_2C\underline{H}_2Br$]. ^{13}C NMR (Chloroform-d1, chemical shift/ppm): 25.6 [$C_4D_9(CH_2)_5\underline{C}H_2(CH_2)_2Br$], 28.1-29.2 [3 peaks, $C_4D_9(CH_2)_2(\underline{C}H_2)_3$-$(CH_2)_3Br$], 32.8 [$C_4D_9(CH_2)_6\underline{C}H_2CH_2Br$], 34.0 [$C_4D_9(CH_2)_7\underline{C}H_2Br$].

1,2,3-Tris[(9',9',10',10',11',11',12',12',12'-D$_9$)dodecyl-1'-oxy]benzene (7): Under a nitrogen atmosphere, 3.12 g of compound **6** (12.1 mmol), 0.431 g of pyrogallol (3.42 mmol) and 5.60 g of potassium carbonate (40.3 mmol) are added into 100 ml anhydrous dimethylformamide in a three-neck flask equipped with a condenser and a magnetic stirrer. The reaction mixture is heated at 90 ℃ for 5 hours, then filtered and concentrated by a rotary evaporator. The crude product is recrystallized twice from 30 ml of acetone at -18 ℃ to afford a white powder of 1.55 g (2.35 mmol, yield: 69.2 %). ^{1}H NMR (Chloroform-d1, chemical shifts/ppm): 1.28 [m, 30H, $C_4D_9(C\underline{H}_2)_5(CH_2)_3O$-], 1.45 [m, 6H, $C_4D_9(CH_2)_5C\underline{H}_2(CH_2)_2O$-], 1.65 [m, 6H, $C_4D_9(CH_2)_5CH_2C\underline{H}_2CH_2O$-], 3.95 [t, 2H, PhOC$\underline{H}_2$- in 3 position], 4.11 [m, 4H, PhOC$\underline{H}_2$- in 2 and 4 positions], 6.54 [d, 2H, $H_{aromatic}$, in 5 position], 6.87 [d,1H, $H_{aromatic}$, in 6 position]. ^{13}C NMR (Chloroform-d1, chemical shifts/ppm): 11.6 [$CD_3\underline{C}D_2CD_2CD_2$-], 14.0 [$\underline{C}D_3CD_2CD_2CD_2$-], 20.5 [$CD_3CD_2\underline{C}D_2CD_2$-], 22.5 [$CD_3CD_2CD_2\underline{C}D_2$-], 25.7 [$C_4D_9(CH_2)_5\underline{C}H_2(CH_2)_2O$-], 28.5-30.1 [multiple peaks, $C_4D_9(\underline{C}H_2)_5CH_2(CH_2)_2O$- and $C_4D_9(CH_2)_5CH_2\underline{C}H_2CH_2O$-], 68.0 [PhOC$\underline{H}_2$- in 2 position], 72.5-73.1 [PhOC$\underline{H}_2$- in 1 and 3 positions], 106.6 [$C_{aromatic}$, in 4 and 6

positions], 122.7 [$C_{aromatic}$, in 5 position], 134.8 [$C_{aromatic}$, in 2 position], 153.4 [$C_{aromatic}$, in 1 and 3 positions].

Sodium / potassium 2,3,4-tris[(9',9',10',10',11',11',12',12',12'-D_9)dodecyl-1'-oxy]benzenesulfonate (D-Na and D-K, 8 and 9): Under intensive stirring, 1.50 ml of concentrated sulphuric acid (95-97%) are added into a solution of 0.500 g of compound **7** (0.760 mmol) in 20 ml of dimethyl chloride. The reaction suspension is stirred at room temperature for 24 hours and subsequently is slowly poured into 30 ml of ice water. The aqueous solution is adjusted to pH 12 by adding a solution of sodium hydroxide or potassium hydroxide, respectively. The resulting suspension is stirred for another 1 hour and afterwards is extracted by ethyl acetate three times. The organic phase is then dried over anhydrous sodium sulfate or potassium sulfate and concentrated by a rotary evaporator. The crude product is purified using silica gel column chromatography. Firstly, ethyl acetate is applied to wash away organic impurities, secondly ethanol is used to wash out the product. 0.320g of compound **8** (0.421 mmol, yield: 55.4 %) or 0.276 g of compound **9** (0.317 mmol, yield: 41.7 %) are obtained as yellowish solids. ^{1}H NMR (DMSO-d6, chemical shifts/ppm. D-Na and D-K are the same): 1.24 [m, 30H, $C_4D_9(C\underline{H}_2)_5(CH_2)_3O$-], 1.43 [m, 6H, $C_4D_9(CH_2)_5C\underline{H}_2(CH_2)_2O$-], 1.70 [m, 6H, $C_4D_9(CH_2)_5CH_2C\underline{H}_2CH_2O$-], 3.83 [t, 2H, PhOC$\underline{H}_2$- in 3 position], 3.92 [m, 4H, PhOC$\underline{H}_2$- in 2 and 4 positions], 6.63 [d, 1H, $H_{aromatic}$, in 5 position], 7.31 [d,1H, $H_{aromatic}$, in 6 position]. ^{13}C NMR (DMSO-d6, chemical shifts/ppm. Na and K salts are the same): 11.5 [$CD_3\underline{C}D_2CD_2CD_2$-], 13.8 [$\underline{C}D_3CD_2CD_2CD_2$-], 20.3 [$CD_3CD_2\underline{C}D_2CD_2$-], 22.1 [$CD_3CD_2CD_2\underline{C}D_2$-], 25.7 [$C_4D_9(CH_2)_5\underline{C}H_2(CH_2)_2O$-], 28.8-29.9 [multiple peaks, $C_4D_9(\underline{C}H_2)_5CH_2(CH_2)_2O$- and $C_4D_9(CH_2)_5CH_2\underline{C}H_2CH_2O$-], 68.0 [PhOC$\underline{H}_2$- in 3 position], 72.5-73.2 [PhOC$\underline{H}_2$- in 2 and 4 positions], 106.6 [$C_{aromatic}$, in 5 position], 122.7 [$C_{aromatic}$, in 1 position], 134.5 [$C_{aromatic}$, in 3 position], 141.8 [$C_{aromatic}$, in 2 position], 150.2 [$C_{aromatic}$, in 6 position], 153.5 [$C_{aromatic}$, in 4 position].

8.3. Results and Discussion

The whole synthesis route is presented in Scheme 1. Each product is numbered sequentially from ***1*** to ***9***. The NMR spectra of each product are recorded and then analyzed to prove the purity of each product.

A commercially available fully deuterated compound 1-butanol-d10 is used as the deuterium source, is brominated by reacting with HBr. The resulting bromide (compound ***1***) is then reacted with magnesium to yield the Grignard reagent.

The compound 1,8-octanediol is first monobrominated by HBr by continuous extraction of the monobrominated product 8-bromo-1-octanol (compound ***2***) from the aqueous phase by toluene. For the Grignard coupling reaction, the hydroxyl group of compound ***2*** should be protected, since the active hydrogen atom in the hydroxyl group terminates the Grignard reaction. The remaining is protected by reacting with 3,4-dihydro-2H-pyran group to result in compound ***3*** with a tetrahydropyranyl ether group, which can remain intact in the Grignard reaction.

In the following step, the Grignard reagent of compound ***1*** is coupled to compound ***3*** under anhydrous conditions. After termination with HCl, compound ***4*** is yielded. Further, the compound ***5*** is obtained by deprotection in a mild acidic condition. The further bromination yields compound ***6***, which is the deuterated alkyl chain for the preparation of the target wedge-shaped sulfonate molecules.

The alkylation of pyrogallol (1,2,3-trihydroxybenzene) by compound ***6*** is a type of Williamson ether synthesis and is carried out in the presence of K_2CO_3 in anhydrous dimethylformamide to yield compound ***7***. The final products, D-Na and D-K (compounds ***8*** and ***9***) are then synthesized via sulfonation of compound ***7*** with concentrated sulfuric acid and subsequent neutralization with corresponding alkaline hydroxide.

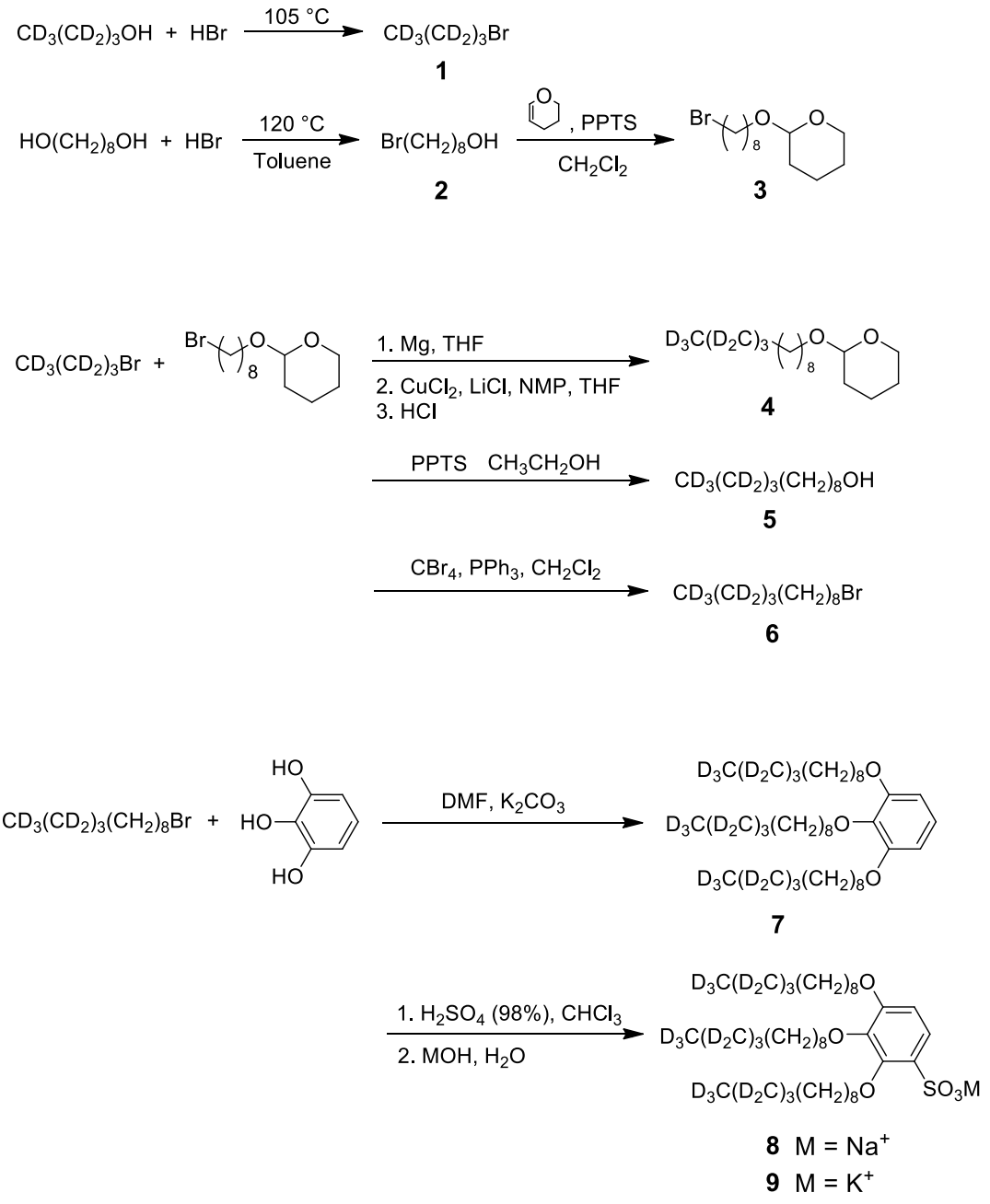

Scheme 1. Synthesis of sodium / potassium 2,3,4-tris[(9',9',10',10',11',11',12',12', 12'-D_9)dodecyl-1'-oxy]benzenesulfonates (D-Na and D-K).

The intermediate and final products are characterized by means of ^{1}H and ^{13}C NMR spectroscopy. Figure 2a shows the ^{1}H NMR spectrum of compound ***3***, which identifies the protection tetrahydropyranyl ether group by the signals with chemical shifts δ at 4.5, 3.9, 3.7, 3.5 and 3.4. After Grignard reaction, the signal at these chemical shifts can still be observed in the ^{1}H NMR spectrum of compound ***4*** shown in Figure 2b. Actually the spectra of compounds ***3*** and ***4*** look identical except the integral intensity of the peak at δ = 3.4, since the bromide group is replaced by the deuterated butyl group. After deprotection, as can be seen in the ^{1}H NMR spectrum of compound 5 (Figure 2c), the signals corresponding to the protection group disappear, and a signal at δ = 3.6, which can be attributed to the protons of the methylene unit linked to the hydroxyl groups.

Figure 3 shows both the ^{1}H NMR and ^{13}C NMR spectra of one of the final products D-Na in DMSO-d6. It is important to note that in ^{1}H NMR spectra two peaks with the chemical shift of 7.31 and 6.63 with the ratio of integral intensity close to 1:1 are observed. They are ascribed to the aromatic protons, and indicate that the sulfonate group is grafted asymmetrically to the benzene ring relative to the alkoxy groups. The reason can be explained according to Figure 4. In compound ***7***, both 4 and 6 positions on the benzene ring are activated by the alkoxy chains in 1 and 3 positions, At the same time, the 5 position on the benzene ring is activated only by the alkoxy chain in the 2 position, so the position 4 or 6 is much more active in the sulfonation reaction than the position 5. Both the ^{1}H and ^{13}C NMR spectra show the high purity of the final products. These compounds exhibit a similar phase behavior as the protonated counterparts. These compounds will be studied in future by solid state deuterium NMR to elucidate the packing of alkyl groups in different mesophases.

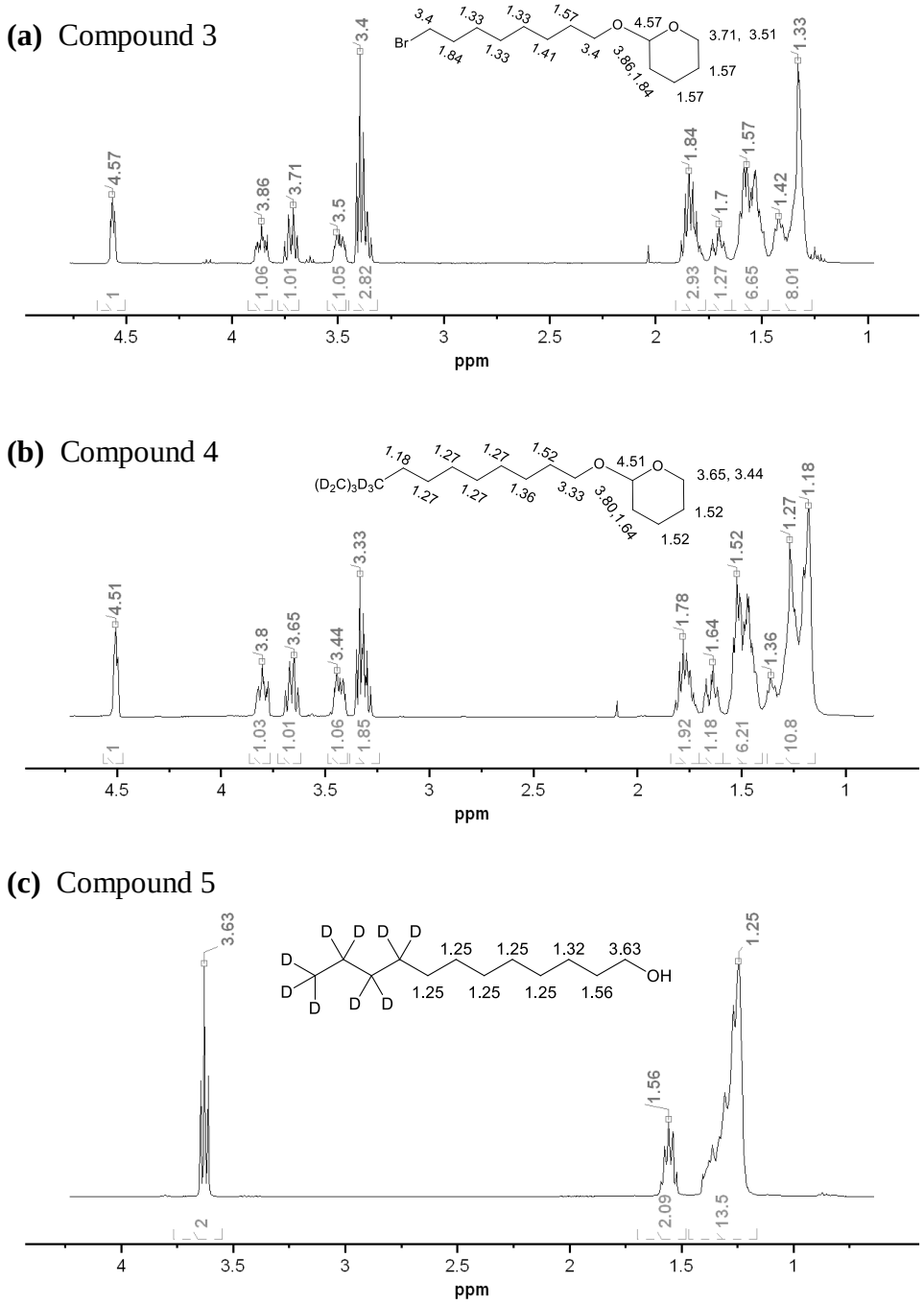

Figure 2. ^{1}H NMR spectra of (a) compound ***3***, (b) compound ***4*** and (c) compound ***5*** measured in $CDCl_3$.

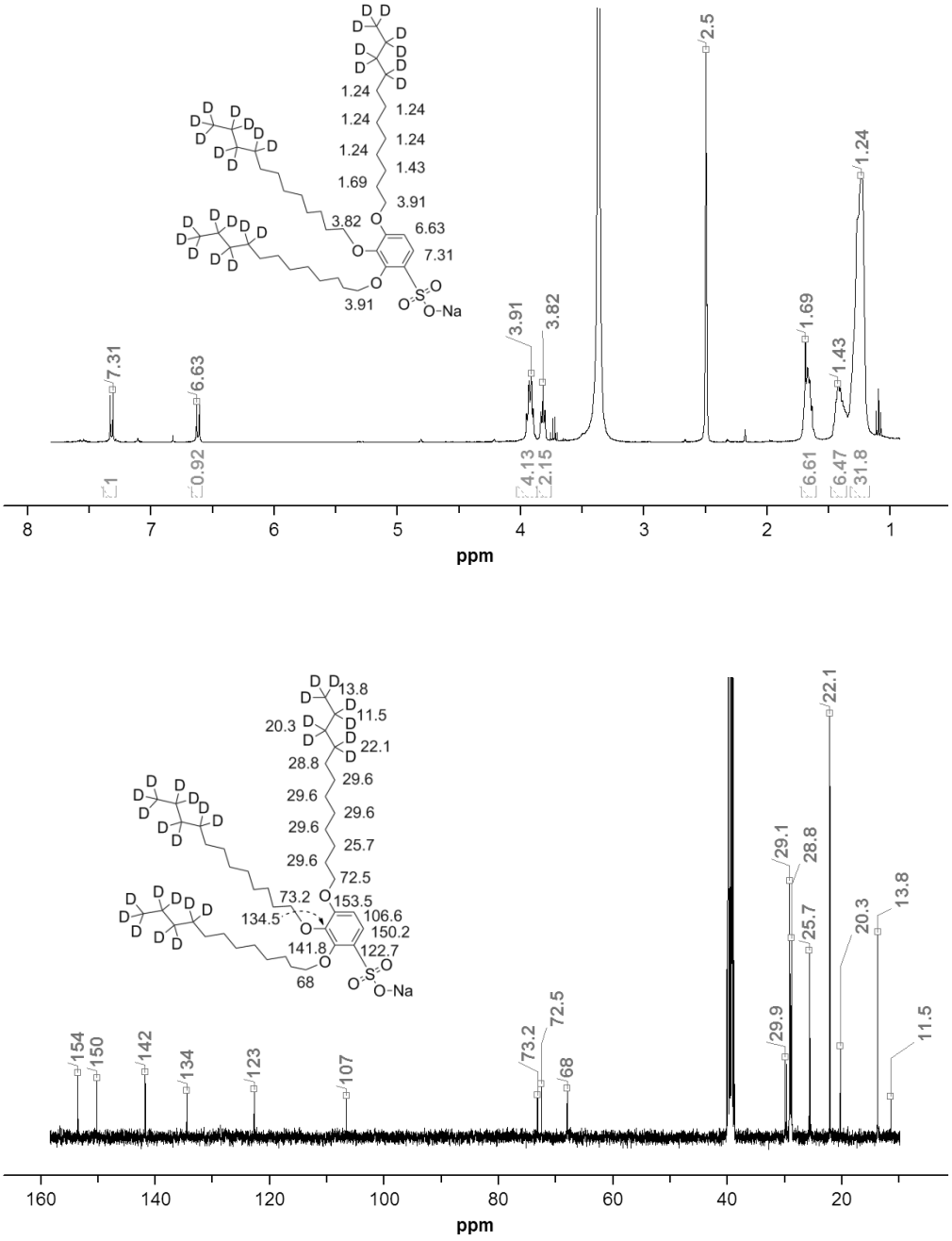

Figure 3. ^{1}H NMR (top) and ^{13}C NMR (bottom) spectra of D-Na in DMSO-d6.

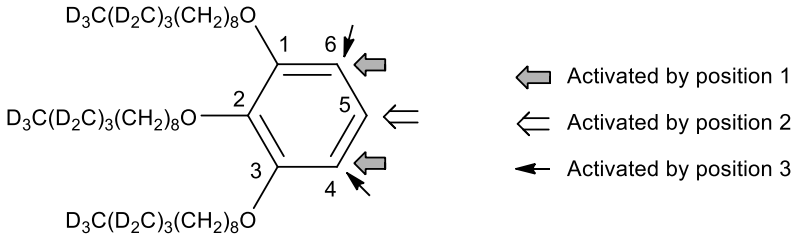

Figure 4. Activated positions on the benzene ring of compound ***7***.

8.4. Conclusion

Via a multistep synthetic route, two partially deuterated wedge-shaped amphiphilic sulfonate molecules: sodium and potassium 2,3,4-tris[(9',9',10',10',11', 11',12',12',12'-D_9)dodecyl-1'-oxy]benzenesulfonates are successfully synthesized. The purity of the final products is confirmed by means of ^{1}H and ^{13}C NMR spectroscopy.

8.5. References

[1] Demus, D; Goodby, JWG; Gray, W; Spiess, HW; Vill, L. Handbook of Liquid Crystals, *Wiley-VCH*, Weinheim, **1998**.

[2] Kato, T; Mizoshita, N; Kishimoto, K. Functional liquid-crystalline assemblies: Self-organized soft materials, *Angew. Chem. Int. Ed.*, **2006**, *45* (1), 38-68.

[3] Sergeyev, S; Pisula, W; Geerts, YH. Discotic liquid crystals: A new generation of organic semiconductors, *Chem. Soc. Rev.*, **2007**, *36* (12), 1902-1929.

[4] Ikeda, T; Mamiya, J; Yu, YL. Photomechanics of liquid-crystalline elastomers and other polymers, *Angew. Chem. Int. Ed.*, **2007**, *46* (4), 506-528.

[5] Hori, R; Furukawa, D; Yamamoto, K; Kutsumizu, S. Light-driven phase transition in a cubic-phase-forming binary system composed of 4 '-N-docosyloxy-3 '-nitrobiphenyl-4-carboxylic acid and an azobenzene derivative, *Chem. Eur. J.*, **2012**, *18* (24), 7346-7350.

[6] Yoshio, M; Mukai, T; Ohno, H; Kato, T. One-dimensional ion transport in self-organized columnar ionic liquids, *J. Am. Chem. Soc.*, **2004**, *126* (4), 994-995.

[7] Yoshizawa, A. Liquid crystal supermolecules stabilizing an optically isotropic phase with frustrated molecular organization, *Polym. J.*, **2012**, *44* (6 Special), 490-502.

[8] Wiesenauer, BR; Gin, DL. Nanoporous polymer materials based on self-organized, bicontinuous cubic lyotropic liquid crystal assemblies and their applications, *Polym. J.*, **2012**, *44* (6 Special), 461-468.

[9] Zhu, XM; Tartsch, B; Beginn, U; Moeller, M. Wedge-shaped molecules with a sulfonate group at the tip - A new class of self-assembling amphiphiles, *Chem. Eur. J.*, **2004**, *10* (16), 3871-3878.

[10] Zhu, XM; Beginn, U; Moeller, M; Gearba, RI; Anokhin, DV; Ivanov, DA. Self-organization of polybases neutralized with mesogenic wedge-shaped sulfonic acid molecules: An approach toward supramolecular cylinders, *J. Am. Chem. Soc.*, **2006**, *128* (51), 16928-16937.

[11] Beginn, U; Zipp, G; Mourran, A; Walther, P; Moeller, M. Membranes containing oriented supramolecular transport channels, *Adv. Mater.*, **2000**, *12* (7), 513-516.

[12] Duer, MJ. Solid State NMR Spectroscopy: Principles and Applications, *Blackwell Science Ltd*, USA, **2002**.

[13] Vold, RR; Tycko, R. Deuterium NMR Studies of Dynamics in Solids and Liquid Crystals, in Nuclear Magnetic Resonance Probes of Molecular Dynamics, *Kluwer Academic Publishers*, Dordrecht, **1994**.

[14] Zhang, H; Li, L; Moeller, M; Zhu, X; Rueda, J; Rosenthal, M; Ivanov, D. From channel-forming ionic liquid crystals exhibiting humidity-induced phase transitions to

nanostructured ion-conducting polymer membranes, *Adv. Mater.*, **2013**, *25* (26), 3543-3548.

[15] Zhu, XM; Mourran, A; Beginn, U; Moeller, M; Anokhin, DV; Ivanov, DA. Self-assembled structures formed by a wedge-shaped molecule in 2D and 3D: The role of flexible side chains and polar head groups, *Phys. Chem. Chem. Phys.*, **2010**, *12* (7), 1444-1452.

[16] Beginn, U; Yan, LL; Chvalun, SN; Shcherbina, MA; Bakirov, A; Moeller, M. Thermotropic columnar mesophases of wedge-shaped benzenesulfonic acid mesogens, *Liq. Cryst.*, **2008**, *35* (9), 1073-1093.

Acknowledgements

I deeply express my acknowledgements to those who have assisted in the work of this thesis, without your kindly help, it would not be possible to finish this thesis. Especially, I would like to extremely appreciate my parents to their warmest encouragement, understanding, patience and support to my PhD study and my daily life. I love my parents forever and ever.

I would like to thank my supervisor, Prof. Dr. Martin Möller, for his kind guidance and support during my PhD study. I feel quite fortunate and happy to work in an international environment with outstanding working conditions.

I would like to thank Mr. Dr. Xiaomin Zhu for his direct supervision of my PhD work. He provided me a big freedom and a lot of training opportunities, which were of great help to me for the development of scientific knowledge, hand-on laboratory skills, communications and presentation skills, paper-writing skills, and etc.

I would like to thank Mr. Dr. Dimitri A. Ivanov, Mr. Dr. Martin Rosenthal and Mr. Jaime J. Hernandez Rueda from the Institut de Sciences des Matériaux de Mulhouse, France, for their practical help of the X-ray measurements and the invaluable advices and discussions about X-ray.

I would like to thank Prof. Dr. Christian Bahr and Mr. Dr. Xunda Feng from Max Planck Institute for Dynamics of Complex Fluids, Göttingen, for their great help of my secondment assessment.

I would like to thank my group members of Ms. Dr. Lei Li, Ms. Manisha Gupta, Ms. Carmen Ioana Filipoi, for their discussions and cooperation in my PhD. And also

I would like to thank my colleagues of Mr. Dr. Ahmed Mourran, Mr. Dr. Ning Sun, Mr. Rainer Haas, Ms. Nebia Greving, for their great help on my PhD experiments.

Finally, I would like to thank all my Chinese friends of Mr. Yaodong Wu, Mr. Qingxin Zhao, Mr. Chao Liang, Mr. Yongliang Zhao, Mr. Hailin Wang, Mr. Zhirong Fan, Mr. Jingbo Wang, Mr. Qizheng Dou, Ms. Lei Li, Ms. Yanqing Li, Ms. Fei Ni, Ms. Yuting Zhao, Ms. Yunfei Jia, Ms. Huihui Wang, Ms. Yanlan Zheng, Ms. Helin Li, Ms. Yinchun He, Ms. Cheng Cheng, Ms. Chi Zhang, Ms. Qianjie Zhang. We are so good friends that we do not even notice that one day we would be apart. They provide me strong and warm support in my work and we share all the happiness and joy in the spare-time activities.

Heng Zhang

29.07.2013

Curriculum Vitae

Personal Details

Family Name:	Zhang
Given Name:	Heng
Birth Date:	14 May, 1984
Birth Place:	Chongqing, China
Nationality:	Chinese

Education

09/2002 – 07/2006

Bachelor's Degree of Macromolecular Science & Engineering

Fudan University, Shanghai, China

09/2006 – 07/2009

Master's Degree of Macromolecular Chemistry & Physics

Fudan University, Shanghai, China

08/2009 – 10/2013

Doctor Study of Macromolecular Chemistry.

RWTH Aachen University, Aachen, Germany

List of Publications (during PhD Study)

1. **Zhang, H**; Zhao, YL; Wang, HT; Zhong, W; Du, QG; Zhu, XM. Phase behavior of polyetherimide /benzophenone/triethylene glycol ternary system and its application for the preparation of microporous membranes, *Journal of Membrane Science*, **2010**, *354* (1-2), 101-107.

2. **Zhang, H**; Hernandez Reuda, JJ; Ivanov, DA; Zhu, XM; Möller, M. Wedge-shaped acrylated sulfonate molecules: Morphology and ion conductivity. *American Chemistry Society Annual Conference*, **2012**, San Diego, USA. **(*)**

3. Li, L; Rosenthal, M; **Zhang, H**; Hernandez, JJ; Drechsler, M; Phan, KH; Rutten, S; Zhu, XM; Ivanov, DA; Moller, M. Light-switchable vesicles from liquid-crystalline homopolymer-surfactant complexes, *Angew. Chem. Int. Ed.*, **2012**, *51* (46), 11616-11619.

4. **Zhang, H**; Chen Z; Zheng, Z; Zhu, XM; Wang, HT. Shape memory polymer hybrids of SBS/*dl*-PLA and their shape memory effects. *Mater. Chem. Phys.*, **2013**, *137* (3), 750-755.

5. **Zhang, H**; Li, Lei; Moeller, M; Zhu, X; Rueda, J; Rosenthal, M; Ivanov, D. From channel-forming ionic liquid crystals exhibiting humidity-induced phase transitions to nanostructured ion-conducting polymer membranes, *Adv. Mater.*, **2013**, *25* (26), 3543-3548. **(*)**

(*) The descriptions of the results in this publication are part of this thesis and are not marked by quotation marks.